TWO-PHASE FLOW PRESSURE DROP IN A TEE JUNCTION

By

"Ala'Aldeen" Tawfeek Saleem Al-Halhouli

Supervisor

Prof. Mahmoud Hammad

Co-Supervisor

Prof. Mahmoud Alhusein

Submitted in Partial Fulfillment of the Requirements for the

Degree of Master of Science in

Mechanical Engineering

Faculty of Graduate Studies

University of Jordan

August 2001

COMMITTEE DECISION

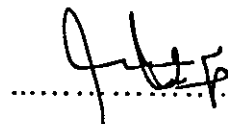This thesis was defended successfully on 16, august, 2001
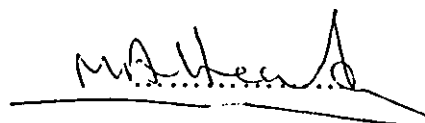
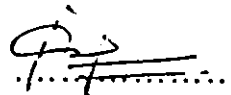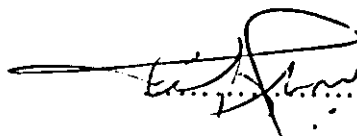| COMMITTEE MEMBERS	SIGNATURE
Prof. Mahmoud Hammad, Chairman.	
Prof. Mahmoud Alhusein, Member.	
Prof. Mohammad Hamdan, Member.	
Prof. Saad Habali, Member.	
Dr. 'Benbella' Al-Shannak, external examiner.	

DEDICATION

To the loving memory of my grandfather, who I shall always remember. To my father and mother who gave me love and support. To my wife, daughter, sister and brothers who gave me hope and love.

Contents

List of Figures

viii

List of Tables

xi

Nomenclature

A	cross sectional area; (m^2)
D	diameter; (mm)
f	friction factor
G	mass flux; ($kg/s.m^2$)
H	head loss; (mm Hg)
J_L	superficial liquid velocity; (m/s)
J_G	superficial gas velocity; (m/s)
K	single-phase loss coefficient
ℓ	length; (m)
$\dot{m}$	mass flow rate; (kg/s)
P	average pressure; (Pa)
ΔP	pressure difference; (Pa)
s	system
S	velocity ratio
T_1	temperature at the inlet of the T-junction; ($^\circ$C)
V	average velocity; (m/s)
$\dot{V}$	volumetric flow rate; (ℓ/hr)
W	mass flow rate; (kg/s)
X	quality
ω	mass flow ratio

Greek symbols

α	void fraction
ϕ	two-phase flow loss multiplier
ρ	density; (kg/m^3)
σ	surface tension; (N/m)

subscripts

a	air
d	dynamic
E	energy
G	gas
H	homogeneous
i	test number
ℓ	liquid
M	momentum
P	pipe
s	system
t	tap
w	water
1	inlet test leg
2	branch two
3	branch three

ABSTRACT

"Two-phase flow pressure drop in a tee-junction"

By

"Ala' Aldeen" Tawfeek Saleem Al-Halhouli

Supervisor

Prof. Mahmoud Hammad

Co-Supervisor

Prof. Mahmoud Alhusein

In this work an experimental test loop system was designed, constructed and investigated using horizontal inlet and branches orientation, equal sided inner diameter (25.4 mm), sharp edge T-junction using PVC pipes at a system pressure of 1 bar.

The experimental set up includes: centrifugal water pump, air compressor, pipe connection, mixer, air-water separator, valves and T-junction, pressure gauge and taps and pressure holder.

Experiments were performed in fluid mechanics laboratory of the engineering faculty of Mu'tah University, by the aid of an instrumentation system consisting of pressure bourdon gauge, Rotometers, Thermocouples and digital thermometer, pitot tube and U-manometer. Experimental observations of pressure differences at various positions for single-phase flow and two-phase flow, and measurements of air and water mass flow rates and temperatures are presented.

Single-phase loss coefficient, single phase and two-phase flow pressure difference values were determined.

The results show that the two-phase flow pressure difference depends on the inlet mass flux, inlet quality, and extraction rate. Pressure difference increases with increasing these parameters. Comparisons show good agreement, with some existing models.

Several conclusions and recommendations were drawn to enhance research in two-phase flow field.

1. INTRODUCTION

1.1 Introduction

Phase is simply one of the states of matter and can be either a gas, a liquid or a solid. Two-phase flow is the simultaneous flow of two phases within the piping system and it obeys all the basic laws of fluid mechanics. The equations associated with two-phase flow are merely more complicated than those of single-phase flows, the major complications in comparing two-phase flow with single-phase flow is the variety of flow patterns that can be . produced in a gas-liquid system.

Branching junctions are common features of the piping networks used for single-phase flow and two-phase flow distribution systems. These networks are essential components for many facilities in the power and process industries, such as boilers, condensers, refrigerators, air-lift pumps, natural gas pipelines and nuclear reactors. Knowledge of the phase separation and pressure drop in two-phase flow systems are of primary important to the system designer to select pumps minimize pressure losses in the system piping, since they have a significant effects on the operation and efficiency of all components downstream of the junction and it leads to safe the labors and industrial fluid dynamic systems.

547467

I

1.2 Literature Review

The phenomenon of two-phase flow is important in the fields of mechanical, chemical and aerospace engineering. Owing to the inherent complexities of the physical process of two-phase flow only simplified analytical and experimental studies have had some success. Most investigations, among that available in the literature, have been experimented in nature because of the limitations of existing theoretical models.

Seeger *et al.* (1986) and Reimann *et al.* (1986) investigated the phase separation and pressure drop of two-phase flow in a T-junction with horizontal inlet, equal pipe diameters (d=50 mm) for air-water and steam-water flow at a horizontal, vertical upward or downward branch orientations. Their experiments were performed with air-water flow (maximum pressure $p_1 <$ 1MPa), steam-water flow ($p_{max} <$ 10 MPa) and an inlet mass flux range $500 < G_1 < 7000$ kg/m^2.s.

From plotting the ratio of branch to inlet qualities (x_3/x_1) versus their mass flux ratio (G_3/G_1), they found that their results are very close to the total separation curve for upward branch orientation. In horizontal orientation, all curves are quite close to the total separation curve for high values of G_3/G_1 as shown in figure (1.1). A maximum of vicinity at $G_3/G_1 = 0.3$ and then decreases quite rapidly with decreasing G_3/G_1. Downward branch results showed that there is a range where only liquid enters the branch and this range increases the more stratified the flow pattern is. At constant superficial gas velocity, they found that the branch to inlet quality (x_3/x_1) increases with increasing the superficial liquid velocity. Their results were compared with other works, showed good agreement with Saba & Lahey (1982), Honan & Lahey (1981), Zotzmann (1982) and McCreery (1984) at high mass flux ratios

and lacking in the lower parameter range, at which Azzopardi & Whalley (1982) and Azzopardi and Backer (1981) proposed a model based on void fraction and phase velocity distribution in the cross section together with local momentum flux that agree well at these low values.

An improved model for two-phase flow pressure difference in a T-junction was proposed. Comparing their results with other known models such as Saba & Lahey slip and homogeneous models (1984), Chisholm model (1967) and the homogeneous model, shows good agreement with superior results in air-water data for horizontal and downward branches, but fail for the case of · upward branch due to the separation effects on the branch which increases with decreasing mass flux.

They suggested further investigations to include global or local void fraction measurements, in order to obtain suitable model for upward branch. They also influenced clarifying the dependency of the results on the system pressure through increasing number of experiments at each pressure level.

Ballyk et al. (1988) investigated separation phenomena and pressure drop of a steam-water annular flow in equal leg flow areas, horizontal dividing T-junction covering a range of operating conditions of $400< G_1< 1200$ kg/m^2.s, $0<x_1<0.15$ and $0.0<m_3/m_1<1$. They measured pressure and void fraction distributions as well as the total flow rates and quality along the inlet and branching legs in order to determine the phase separation and pressure characteristics. They also improved the mechanical energy based model for calculating the branch pressure drop to be able to account for the inlet dynamic head of the branching flow. They found that at low branch flow

splits ($\dot{m}_3 / \dot{m}_1$), the branch quality (x_3) increases very rapidly with

increasing flow splits crossing the equal phase distribution line at close to 90°. This supports the finding of Azzopardi & Whalley (1982) and Henry (1981) and suggests that the liquid is first removed from the low velocity film flowing at the tube wall in the line with the branching port. The effect of inlet mass flux variation on the branch phase separation ratio is found to be less significant than that of inlet quality, where the point of total separation is some what independent of mass flux. And there is a strong interdependence between separation phenomenon and pressure distribution, where it was clear that as the total phase separation was approached a significant increase in the run pressure recovery was encountered. This was referred to flow regime transition from annular to plug flow in the run of the T-junction. Their axial pressure recovery data obtained in their work demonstrated similar trends as Shoukri *et al.* (1987) and poor agreement with Riemann & Seeger (1986) particularly for low split ratios. Based on their results they recommended their model for evaluating the branch pressure changes.

Rubel *et al.* (1988) investigates phase distribution of low pressure steam-water mixture in a horizontal T-junction with equal sided (37.6 mm) inner diameters, the purpose of there investigation is to develop new phase distribution data under certain operating conditions and enhancing the current understanding of the phenomenon. The range of conditions is of low inlet mass flux $15 < G < 50$ kg / m^2.s and low pressure of $100 < p < 250$ kPa, wide range of inlet qualities ($20 < x_1 < 90$ %) were used and extraction rates of $0.15 < w_3/w_1 < 0.8$. The operating conditions corresponding to their test groups were plotted on the flow pattern map of Mandhane *et al.* (1974) from which their visual observations of inlet flow patterns are in good agreement with Mandhane predictions. Rubel and his colleagues found that as a general rule, there is uneven phase distribution at the junction where preferential

4

liquid flow into the branch occurred for all the data of stratified flow, while most of wavy flow data showed preferential vapor flow into the branch. They also studied the individual effects of important independent parameters such as inlet quality, inlet mass flux and the inlet superficial liquid velocity on the phase distribution. They found that at the same high mass flux and different inlet qualities the ratio of branch to inlet qualities (x_3/x_1) decreases with x_1 increasing, while an opposite trend were obtained at the lowest mass flux. At the same inlet quality but different inlet mass flux (G_1), G_1 doesn't appear to influence (x_3/x_1) within the same inlet flow pattern but the main influence is related to the inlet flow pattern transitions.

At fixed values of inlet superficial gas velocities (J_{Gs}) the effect of inlet superficial liquid velocity (J_{Ls}) indicates that the ratio of the branch to inlet liquid extraction rates (W_{L3}/W_{L1}) decreases continuously with increasing (J_{Ls}), and shows an important effect of the velocity ratio on phase distribution irrespective of flow pattern.

Comparisons with other models show a remarkable agreement with Seeger *et al.* (1986) for the data corresponding to $G_3/G_1 \geq$ 0.4 and $x_1 \geq 40\%$ and encouraging results for other ranges. Azzopardi & whalley (1982) model is based on annular flow shows that the data is generally out side $\pm 20\%$ prediction accuracy and it becomes increasingly better as x_1 and J_{Gs}/J_{Ls} increase, which moves the flow to fully-established annular flow. Hwang *et al.*(1988) developed his model based on a dividing streamline concept shows that the predicted values of x_3/x_1 are within $\pm 30\%$ of the corresponding measured values for all points .

Buell *et al.* (1994) investigated two-phase pressure drop and phase distribution at a horizontal T-junction of low pressure (1.5 bar) air-water

mixture and equal sided (37.6mm) inner diameters. Inlet flow regimes of stratified, wavy, slug and annular with inlet liquid velocities $J_{L1} < 0.2$ m/s at which limited pressure drop information is available. Data consist of both phase distribution and pressure drop at different extraction rates and a wide range of inlet condition is obtained. The effect of superficial liquid velocity J_{L1} on the phase distribution for annular flow was found that the preference of gas to exit through the branch increases as J_{L1} increases at a fixed super facial gas velocity J_{G1}. This explained using the ideas suggested by Hwang *et al.* (1988) and Azzopardi *et al.* (1988), whereby an increase in J_{L1} results in an increase in the average axial momentum of the liquid phase as consequently, a · decrease in the probability of the liquid to enter the branch. But the effect of varying J_{G1} at fixed J_{L1} failed to produce consistent trends due to flow regime transition encountered with changing J_{G1}. Good agreement for the phase distribution of $\dot{m}_3/\dot{m}_1 \geq 0.3$ has been demonstrated against the analytical models of Hwang *et al.* (1988), empirical correlation of Seeger *et al.* (1986) and Azzopardi & Whally (1982).

Comparisons of pressure differences ΔP_{12} (inlet-run) and ΔP_{1-3} (inlet-branch) of their data with different empirical models, developed for significantly higher values of J_{L1}, showed that best prediction of ΔP_{12} data was produced by a separated flow model, originally proposed by Fouda & Rhodes (1974) and less satisfactory predictions were obtained for ΔP_{13}. For high extraction rates $\dot{m}_3/\dot{m}_1 \geq 0.3$ separated flow model recommended by Saba & Lahey (1984) gave the best prediction while for $\dot{m}_3/\dot{m}_1 < 0.3$ the model recommended by Reimann & Seeger (1986) gave better predictions. They expected that obtained results could guide the future search for generalized methods of correlation the pressure results. The performance of the above

6

models in predicting the pressure drop in slug flow regime is summarized and given in table (1.1)

Table (1.1) Summary of model performance for branch pressure drop

Model	Interval	%of data predicted correctly
		Slug flow regime(inlet)
Homogeneous Flow Model (HFM)	±50%	0
	±30%	0
	±20%	0
Separated Flow Model (SFM)	±50%	62
	±30%	31
	±20%	8
Reimann and Seeger Model (RSM)	±50%	62
	±30%	39
	±20%	31
Ballyk Model (BM)	±50%	39
	±30% □	15
	±20%	8
Hwang and Lahey Model (HLM)	±50%	0
	±30%	0
	±20%	0

Schmidt and Loth (1994) discuss several predictive methods for two-phase flow pressure loss calculation in T-junctions with combining conduits. Based on known methods, three predictive methods for pressure loss were developed; these are "loss coefficient model", "contraction coefficient model" and "momentum coefficient model". The flow loop is shown in

annular for both test sections plus slug for the larger branch test section. The objective of their investigation is to generate data concerning the effects of branch diameter using two sets of data where the branch-to-inlet diameter ratios (D_3/D_1) were 0.206 and 0.5.

They found that data of stratified flow regimes for D_3/D_1=0.5 shows greater tendency for the gas to enter the branch than for D_3/D_1=1.0 as in Buell *et al.* (1994). That it is reasonable to expect that smaller fraction of liquid could be taken off into the branch as the branch diameter decreases. But the trends for D_3/D_1=0.206 is not as consistent, because at high extraction rates the tendency · for liquid preferentially to enter the branch begins to increase and the phase distribution data approach the case of (D_3/D_1=1.0), this related to the fact that the branch of D_3/D_1=0.206 is much smaller than that of D_3/D_1=0.5. Therefore, for similar values of fraction of gas entering the branch F_{BG}, the branch gas superficial velocity of D_3/D_1=0.206 is considerably larger than that for D_3/D_1=0.5. Due to Bernoulli effect, it is possible that liquid entrainment into the branch is responsible for this phenomenon. These trends are consistent in the stratified wavy, wavy, semi annular and annular flow regimes.

Comparison with other phase distribution models showed that the geometrically based model by Azzopardi (1988), using the correlation of Kataoka and Ishii(1983) for entrainment, gave the best results for both diameter ratio for annular flow, and the deviation between data and any of the models is highest at two extraction rates, and this deviation decreases as the extraction rate increases. The effect of D_3/D_1 on ΔP_{12}(inlet-run) pressure drop is minimal while ΔP_{13} (inlet-branch) pressure drop increase significantly with a decrease in D_3/D_1, these results are consistent with the single-phase flow.

9

Their results were compared against homogeneous flow model by Saba & Lahey (1984), the separated flow model by Fouda & Rhodes (1974), the model by Riemann & Seeger (1986) and the model by Hwang and Lahey (1988). The performance of the various ΔP_{12}, ΔP_{13} models showed that the separated flow model (SFM) has the best over all predictive capabilities and the lowest deviations for both diameter ratios. However, in the semi-annular and annular flow regimes the models by Reimann & Seeger (1986), Hwang & Lahey (1988) and the homogeneous flow model all perform better than the separated flow model.

Despite the above studies related to two-phase flow discussed in the literature survey, which intensively covered phase distribution in a T-junction at different flow regimes, test leg diameters, inlet qualities and extraction rates, a lack in pressure differences studies were observed. Only limited pressure drop data for slug flow regime is available. All models presented were failed in obtaining a model describes this pressure difference through a T-junction generally. They referred this to the lack of pressure drop data and the number of parameters affect their values.

1.3 Objective of the present work

This study aimed at the following objectives:
1. to build a two-phase flow facility that participates in the research in the two-phase flow field.
2. to study the two-phase flow pressure differences through a T-junction of air and water mixture in slug flow regime with equal sided diameters, at different inlet qualities and extraction rates.

3. to provide new pressure differences experimental data to the researchers, helping them in their efforts to obtain a general model describes the two-phase flow pressure differences through the T-junction.

1.4 Out line of the Report

Following this introduction, a theory is presented in chapte two. Chapter three is a description of experimental setup and procedure. The results and discussion of the pressure difference in a T-junction are presented in chapter four.

Finally conclusions and recommendations are summarized in chapter five.
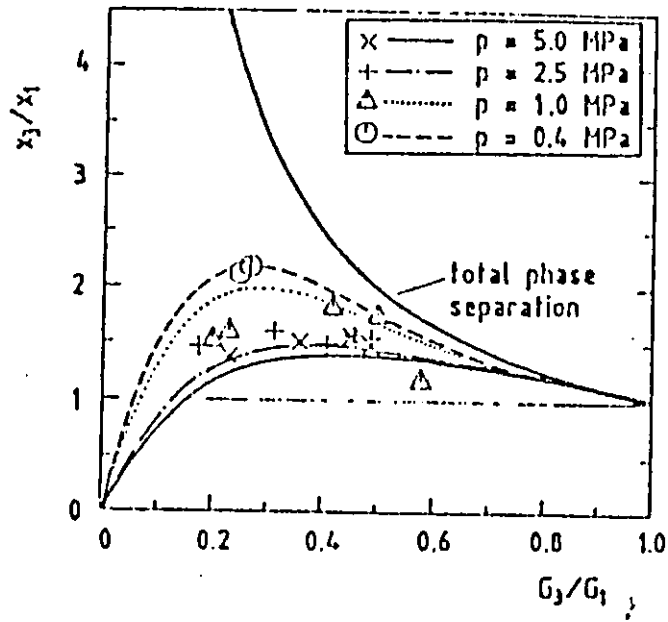
Figure (1.1) Phase separation for horizontal branch (Seeger, 1986).
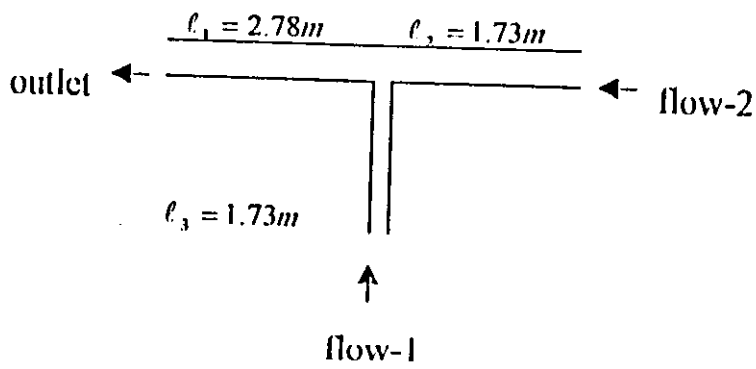
Figure (1.2) T-junction with combining conduits.(Schmidt, 1994) .

2. THEORY

2.1 Introduction

A phase is simply one of the states of matter and can be either a gas, a liquid or a solid. Multiphase flow is the simultaneous flow of several phases.

The term two component is sometimes used to describe flows in which the phases do not consist of the same chemical substance. For example, steam-water flows are two-phase, while air-water are two component. Since the mathematics which describe two-phase or two- component flows are identical, it doesn't really matter which definitions are chosen. The two expressions will therefore be treated as synonyms. (Wallis, 1969)

Two-phase flow obey all the basic laws of fluid mechanics, the equations associated with two-phase flow are merely more complicated than those of single-phase flow. The major complications in comparing two-phase flow to single-phase flow is the variety of flow patterns, that can be produced in a gas-liquid system. In an attempt to simplify these complexities researchers have conducted empirical testing in an effort to develop correlations that are easy for the average design engineer to utilize in solving practical problems. Other than correlation method, researchers have developed additional techniques to predict flow patterns and quantify pressure drops.

2.2 Flow Regimes

There are various flow regimes or "patterns" that are common in any two-phase flow system, each having different characteristics and associated pressure drops. The flow patterns also vary between horizontal and vertical piping runs.

In horizontal pipe, the flow regimes are (in order of lowest gas velocities to highest) bubble flow, plug flow, stratified flow, wavy flow, slug flow, annular flow and mist flow. In vertical pipe there are bubble, slug, churn, ripple, annular and mist flow.

2.2.1 Horizontal flow regimes

For two-phase flow in horizontal pipes, the flow patterns shown in figure (2.1) classified as bubble, plug, stratified, wavy, slug, annular and mist flow these patterns can be clarified as follow:

Bubble flow: - This flow is prevalent at high ratios of liquid to gas flow rates. The gas is dispersed as bubbles that flow along the upper surface of the pipe at approximately the same velocity as the liquid. At high liquid rates, bubbles may be dispersed throughout the liquid, a pattern referred to as froth flow.

Plug flow: - Plug flow describes a pattern in which alternates plugs of gas and liquid move along the upper part of the pipe. This pattern develops when the gas bubbles coalesce due to gas flow rate increases.

Stratified flow: - This flow pattern is very common in typical multi-phase systems. In stratified flow, the liquid flows along the bottom of the pipe and

14

the gas flows at the top of the pipe over a smooth liquid/gas interface. This pattern occurs at lower liquid flow rates than bubble or plug flow.

Wave flow: - This flow pattern is also very common in typical multi-phase systems. Similar to stratified flow, the liquid flows along the bottom of the pipe. However, increased gas velocities above the liquid produce waves on the liquid/gas interface. Increasing gas flow rates produce waves of increasing amplitude.

Slug flow: - This flow pattern is also common in typical multi-phase systems. When the wavy flow wave crests become sufficiently high to bridge the pipe, they form frothy slugs which move much faster than the average liquid velocity. Slug flow is also formed from plug flow as the gas flow rate is increased at a constant liquid flow rate. Slug flow can cause severe and sometimes dangerous vibrations in piping and equipment because of the impact of the high velocity slugs against bends and other fittings.

Annular flow: - In annular flow, the liquid flows as a thin film along the pipe wall and gas flows in the core. The gas moves at high velocity in the core and carries with it some of the liquid as a spray.

Mist flow: - This flow pattern occurs at very high gas velocities at which nearly all of the liquid in the pipe is entrained as small droplets. More and more liquid is carried in the gaseous core at the expense of the annular film, until nearly all of the liquid is entrained in the gas. (Peramaki, m. p., 2001)
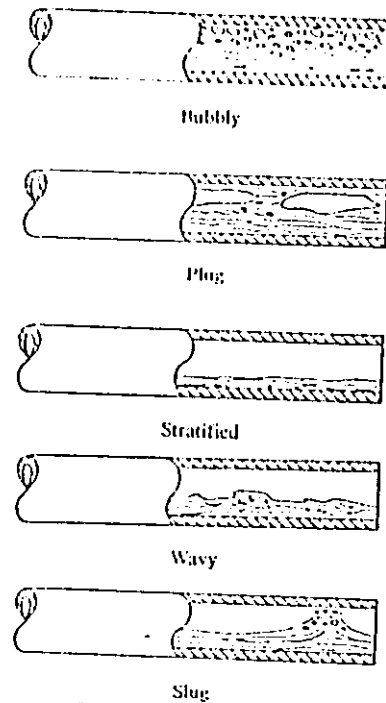
Figure (2.1) Flow patterns for horizontal flow of a liquid and a
gas.(Mills, 1995)

2.2.2 Vertical flow regimes

Visual definitions of flow patterns in vertical flow appear to cause more difficulty than do those in horizontal flow. Figure (2.2) illustrates the vertical flow patterns and they can be described as follow:

Bubble flow: - In bubble flow pattern the gas phase is nearly uniformly distributed in the form of bubbles in a continuous liquid phase with some tendency to concentrate toward the center of the pipe. As the gas flow rate increases the bubbles steadily increase in size and numbers. This flow pattern has a high relative pressure drop due to the hydrostatic losses resulting from very low air to water ratios.

Slug flow: - In this pattern gas bubbles coalesce to form larger bullet shaped bubbles. Most of the gas is contained in large bullet shaped bubbles which

have a diameter nearly equal to the pipe diameter. These bubbles are commonly called "Taylor Bubbles". Taylor bubbles move uniformly upward and are separated by slugs of liquid which bridge the pipe and contain small gas bubbles. Between the Taylor bubbles and the pipe wall, liquid flows downward in the form of a thin falling film. Taylor bubbles increase in length and diameter and their upward velocity increases with an increasing gas flow rate.

Churn flow: - Churn flow is similar to slug flow, although much more chaotic and disorderly. The Taylor bubbles narrow and become distorted. The continuity of the liquid in the slug between bubbles is repeatedly destroyed by a high local gas concentration within the slug. As the liquid slug is destroyed, it falls. This liquid accumulates, forms a bridge and is again lifted by the gas. The elements of this structure are in a continual process of collapse and reformation. This activity results in a pattern-less turbulent mixture. Churn flow is characterized by strong intermittent and intense mixing, with neither phase easily described as continuous or dispersed.

Churn flow at low air to water ratios has the highest relative pressure drops common to multi-phase systems. The interaction between the gas and liquid phases increases the pressure drop compared to other flow patterns. For this reason this flow pattern should be avoided. Additionally, the slugging produces strong vibrations in piping.

Ripple flow: - Ripple flow is characterized by an upwards-moving, wavy or ripply layer of liquid on the piping wall, far less chaotic that of churn flow. The zone of ripple flow is narrow and actually forms a transition region between churn and annular flow. The pressure drop associated with this

17

transition is a relative low and if possible, designers should attempt to produce this flow pattern in vertical pipe runs and drop tubes.

Annular (film) flow: - The annular flow pattern consists of an annular liquid layer moving on the pipe wall with a gas core moving at much higher velocities. This flow pattern results from the smoothing out of the waves and ripples of Ripple flow by the attrition of higher gas flow rates. Some liquid is entrained as droplets within the gas core. Gravitational (hydrostatic) forces become less important than interphase forces, and the liquid is mainly carried as a thin film a long the pipe wall.

Mist flow: - Annular flow becomes mist flow when the gas flow rate becomes high enough to capture the water droplets from the gas liquid interface, removing the annular liquid layer. Mist flow occurs when all the liquid is carried as fine drops within the gas phase. (Peramaki, m. p., 2001)

Bubbly   Slug   Churn   Wispy Annular   , Annular
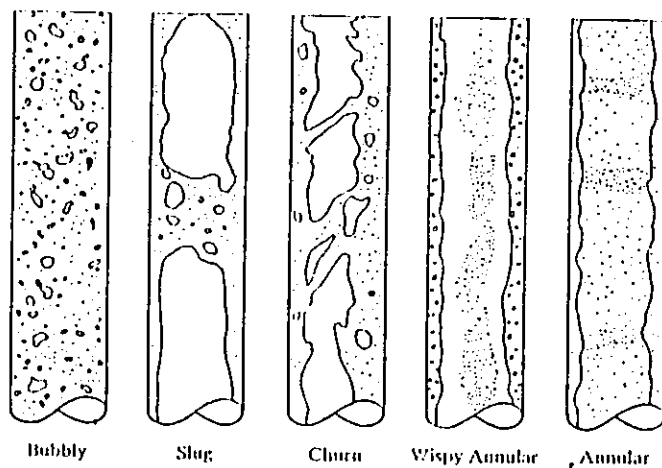
Figure (2.2) Flow patterns for vertical flow of a liquid and a gas.
(Mills, 1995).

2.2.3 Flow Patterns Maps

Numerous authors have presented flow-regime maps in which various areas are indicated on the graph for which there are two independent coordinates.

The two-phase flow pattern map such as Mandhane shown in figure (2.3) serve a very useful purpose in allowing designers to predict the nature of the flow pattern that might be expected in a given case. This can assist in selecting the most suitable correlation for calculating the pressure drops. Otherwise, this information can be used to avoid slug flow in the horizontal piping and early churn flow in the vertical piping.
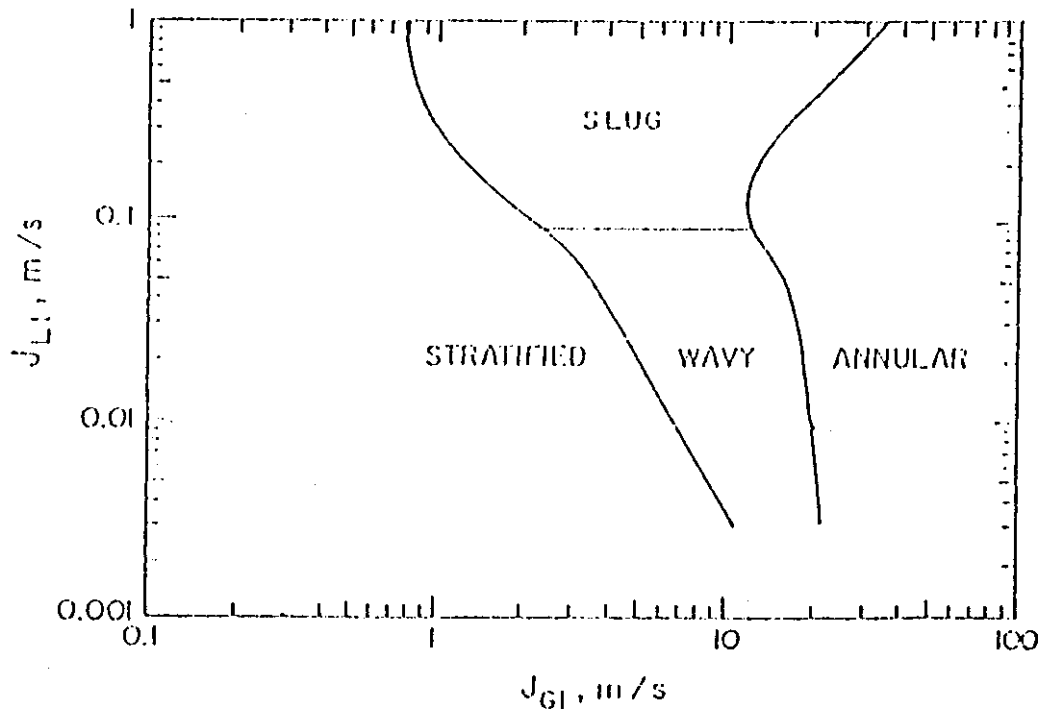
Figure (2.3) flow regime map showing inlet conditions. (Mandhane, 1974)

2.3 Method Of Analysis

Two phase flow obey all the basic laws of fluid mechanics, the equations are merely more complicated or more numerous than those of single-phase flow.

Several characteristics make them more complicated, such as: the difference in the fluid characteristics (especially the phase density difference) create flow patterns that can be dramatically different when only the pipe orientation changes. In addition to the fact that flow pattern description is not merely an identification of laminar, transitional or turbulent flow.

2.3.1 Simple Definitions

The two phase are distinguished by subscripts 1 and 2 in general, or by ℓ and g for a liquid-gas system or ℓ and s for a liquid-solid system.

The total mass flow rate is represented by the symbol W or $\dot{m}$. The total flow is the sum of the component flows:

$$\dot{m}_{2ph} = \dot{m}_g + \dot{m}_\ell \tag{2.1}$$

the ratio of gas flow to total flow x ,

$$x = \dot{m}_g / \dot{m}_{2ph} \tag{2.2}$$

is sometimes called the dryness fraction or the quality .

For a channel with cross sectional area A, the mass flux or mass velocity G is defined as,

$$G = \dot{m}_{2ph} / A_{2ph} \tag{2.3}$$

The void fraction α is defined as the ratio of the gas-flow cross-sectional area A_g to the total cross sectional area,

$$\alpha = A_g / A_{2ph} \tag{2.4}$$

where A_{2ph} must equal the sum of the cross sectional areas occupied by the two phases :

$$A_{2ph} = A_g + A_\ell \tag{2.5}$$

It follows that the liquid volume fraction α_ℓ is given by,

$$\alpha_\ell = 1 - \alpha = A_\ell / A_{2ph} \tag{2.6}$$

20

It is also useful to define superficial gas and liquid fluxes, J_ℓ and J_G respectively as,

$$J_G = Gx / \rho_g \qquad (2.7)$$

$$J_\ell = G(1-x) / \rho_\ell \qquad (2.8)$$

Although these parameters have units of velocity, they can also be thought of as the volume flux of each phase through the channel. Numerically they are equal to the velocity that each phase would have if it flowed at its specified mass flow rate through the channel alone.

Simple analytical models can be quite successful, both for organizing experimental results and for predicting design parameters. For example, homogeneous flow theory provides the simplest technique for analyzing two-phase (or multiphase) flows. Suitable average properties are determined and the mixture is treated as a pseudofluid that obeys the usual equations of single-phase flow. All of standard methods of fluid mechanics can then be applied. But separation flow theory takes the account of the fact that the two phases can have differing properties and different velocities. Separate equations are written for each phase and the interaction between the phases is also considered. Drift flux model is essentially a separated-flow model in which attention is focused on the relative motion rather than on the motion of the individual phases. (Wallis, 1969)

2.3.2 Two Phase Pressure Drop Fundamentals

Two-phase flows obey all the basic laws of fluid mechanics, the equations associated with two-phase flow are merely more complicated or more numerous than those of single-phase flows. In an attempt to simplify these complexities researchers have conducted empirical testing in an effort to

develop correlations that are easy for the average design engineer to utilize in solving practical problems. Other than the correlation method researchers have developed additional techniques to predict flow patterns and quantify pressure drops.

Pressure drop calculations for two-phase flow are more complex than for single-phase flow. The introduction of a second phase causes a sharp rise in pressure drop due to the following:

1) the cross-sectional area available for the flow of one phase is reduced by the introduction of the second.

2) the flow boundary is no longer a relatively smooth pipe was, but is a rough, irregular, mobile interface between phases.

3) the introduction of a second phase can cause a very unsteady flow accompanied by intense turbulence.

Powers, 1992 states that the actual pressure drop in horizontal construction dewatering pipe containing both water and air can be from 150 to 200 percent of the drop due to water flowing in the pipe a lone. (Peramaki, 2001)

2.3.2.1 Single Phase Flow

For single-phase incompressible flow in a T-junction, a correlation for the inlet-to-run pressure difference is normally derived from a momentum approach as follows:

Branch 3

Inlet 1   Run 2
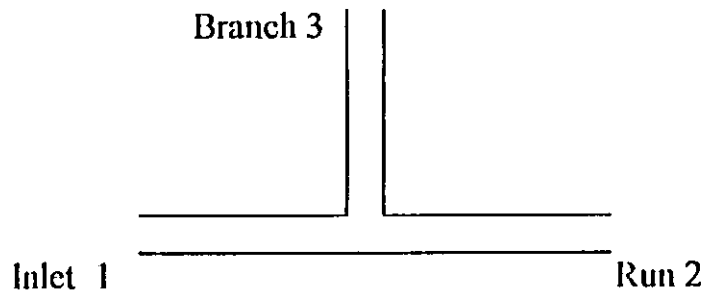
Figure (2.4) Test section shape of the T-junction considered in Theory.

22

$$\Delta p_{12} = p_1 - p_2 = k_{12} (G_2^2 - G_1^2) / \rho \qquad (2.9)$$

Where P_1 and P_2 are the average pressures at the junction from the inlet and run sides. G_1 and G_2 are the inlet and run mass fluxes, k_{12} is the momentum correction factor and ρ is the density.

An energy approach has been frequently adopted for the inlet-to-branch pressure difference, subdividing Δp_{13} into a reversible component $(\Delta P_{13})_{rev}$ and an irreversible component $(\Delta P_{13})_{irr}$, thus

$$\Delta P_{13} = P_1 - P_3 = (\Delta P_{13})_{rev} + (\Delta P_{13})_{irr} \qquad (2.10)$$

where, $(\Delta P_{13})_{rev} = (G_3^2 - G_1^2) / 2\rho \qquad (2.10.1)$

$\qquad (\Delta P_{13})_{irr} = K_{13} G_1^2 / 2 \rho \qquad (2.10.2)$

P_3 is the pressure at the junction from the branch side, G_3 is the branch mass flux and K_{13} is a loss coefficient. (Buell, et al., 1994, Reimann and Seeger, 1986, Walters, et al. 1997)

The loss coefficient were correlated by many authors, their results gives different correlations summarized as follow

- Buell et al.(1994) correlation:

$$K_{13} = 1 - 0.982(G_3/G_1) + 1.843 (G_3/G_1)^2 - 0.717 (G_3/G_1)^3 \qquad (2.11)$$

- Ballyk, et al.(1988) correlation:

$$K_{13} = 1.081 - 0.914 (\dot{m}_3/\dot{m}_1) + 1.05 (\dot{m}_3/\dot{m}_1)^2 \qquad (2.12)$$

- Reimann and Seeger (1986) correlation:

$$K_{13} = 1.036 - 0.9546(G_3/G_1) + 1.2123(G_3/G_1)^2 \qquad (2.13)$$

- Saba and Lahey curve obtained from Buell, et al., 1994.

23

2.3.2.2 Two-Phase flow

The available correlations for ΔP_{12} and ΔP_{13} during two-phase flow are mostly modifications of the single-phase flow correlations. In general, most of these correlations can be agglomerated into these forms:

$$\Delta P_{12} = K_{12} ((G_2^2/\rho_2) - (G_1^2/\rho_1))$$ (2.14)

and

$$\Delta P_{13} = \frac{\rho_{H3}}{2} ((G_3^2/\rho_3^2) - (G_1^2/\rho_1^2)) + K_{13} \frac{G_1^2}{2\rho_t} \phi$$ (2.15)

Where ρ_1, ρ_2 and ρ_3 are mixture densities in the inlet, run and branch sides respectively, ρ_{H3} is the homogeneous density in the branch, ϕ is a two-phase loss multiplier and ρ_t is the liquid density. (Buell et al., 1994, Reimann and Seeger, 1986, Walters et al. 1997)

Different models were computed, the particular specifications some of these models are as follow:

- Homogeneous flow model (HFM): the two-phase loss multiplier, as suggested by saba & Lahey (1984), was correlated by

$$\phi = \rho_t/\rho_{in}$$ (2.16)

K_{12} and K_{13} estimated from single phase flow experiments, and the homogeneous densities were determined from:

$$\rho_{Hi} = [\frac{(1-x_i)}{\rho_t} + \frac{x_i}{\rho_g}]^{-1}$$ (2.17)

Where ρ_g is the gas density and $i = 1, 2$ and 3 for the inlet, run and branch respectively.

- Separated flow model (SFM): the momentum-weighted densities were used for ρ_1 and ρ_2 in equation (2.14), as proposed by Fouda & Rhodes (1974), where

$$\rho_{Mi} = [\frac{(1-x_i)^2}{\rho_t(1-\alpha_i)} + \frac{x_i^2}{\alpha_i \rho_g}]^{-1} \quad i=1,2,3 \tag{2.18}$$

where ρ_M is the momentum density and α is the void fraction evaluated from the correlation of Rouhani (1969), $\phi = \frac{\rho_t}{\rho_{Mi}}$, and the energy weighted densities were used for ρ_1 and ρ_3 in equation (2.15), as proposed by Saba & Lahey (1984), where

$$\rho_{Ei} = [\frac{(1-x_i)3}{\rho^2_t(1-\alpha_i)^2} + \frac{x_i^3}{\alpha_i^2 \rho^2_g}]^{-0.5} \quad i=1,2,3 \tag{2.19}$$

where ρ_E is the energy density and α is the void fraction calculated from the Rouhani's (1969) correlations, as

$$\alpha_i = \frac{x_i}{x_i + (S_i/R)(1-x_i)} \tag{2.20}$$

where, S_i is the velocity ratio and $R = \rho_t/\rho_g$.

$$S_i = \frac{\rho_t}{(1-x_i)}(\frac{(1+0.12(1-x_i))}{\rho_{li}} + \frac{(\frac{1.18}{\sqrt{\rho_l}}(g \times \sigma \times (\rho_l - \rho_{Gi}))^{1/4}}{G_i} - \frac{x_i}{\rho_{Gi}})(2.21)$$

as g is the acceleration due to gravity and σ is the surface tension.

- Hwang & Lahey (1988) model (HLM): in equation (2.14), this model employs $\rho_1 = \rho_{M1}$, $\rho_2 = \rho_{II2}$. The correlation of Zuber & Frindlay (1965) was used in calculating the void fraction, as recommended by Hwang & Lahey. In equation (2.15), the HLM specifies $\rho_1 = \rho_{E1}$, $\rho_3 = \rho_{II3}$ and $\phi = \rho_t\rho_{II3}/\rho_{III}^2$.

- Ballyk et al., (1988) model (BM): in equation (2.14) this model specifies $\rho_1 = \rho_{M1}$, $\rho_3 = \rho_{II3}$ and $K_{12} = 1$. In equation (2.15), the BM specifies $\rho_3 = \rho_{E3}$, an equivalent density for ρ_1 and an empirical formulation for ϕ as a function of extraction rate.

- Reimann & Seeger (1986)model (RSM) : for ΔP_{13} , this model uses equation (2.15) with $\rho_1 = \rho_{II1}$, $\rho_3 = \rho_{II3}$ and $\phi = \rho_l \rho_{II3} / \rho_{In}^2$. A different method was proposed for ΔP_{12} by splitting it into a reversible pressure difference between the inlet and the throat of a venacontracta in the run and a second pressure difference between the venacontracta and a position down stream in the run.

3. EXPERIMENTAL SET UP AND PROCEDURE

3.1 Introduction

The two-phase flow test loop has a lot of connections using different type of fittings (tee, bend, elbow, valve...) at different branch orientations (horizontal, vertical upward and down ward), and different flow entrance positions or may be more than one inlet. For the purpose of the present study, a two-phase flow test loop was designed and built using a T-junction oriented horizontally, this loop is shown in figure (3.1).

This chapter is divided into five sections. Section (3.2) describes the experimental set up. Section (3.3) describes the building steps of the test loop. The instruments used in the measurements was described In section (3.4). Lastly, section (3.5) presents the experimental procedure. Two tests were carried out, these include: single-phase flow and two-phase flow.
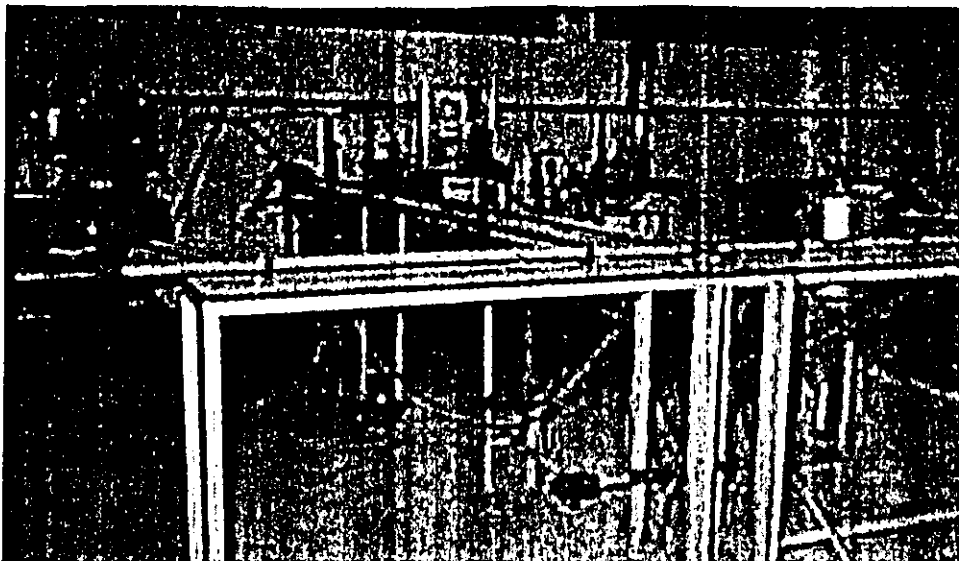
Figure (3.1) The experimental test system.

3.2 Experimental set up

The test loop shown in figure (3.2) was designed and constructed in order to be used in the present experimental program involving a T-junction with a horizontal inlet and branches orientation. The test loop consists of water filter, centrifugal pump, mixer, air compressor, way valves, PVC pipes and T-junction, pressure taps and one pressure gauge, air-water separator and water tank.

The following sections will describe the components of the test loop and summarize the manufacturing processes that were applied to build them.

3.2.1 Water pump

A centrifugal pump (type 2CPm, 2900 rpm) with the following specifications 10-80 ℓ/min flow rate, 40-15 m head, $H_{max}=41m$, $Q_{max}=80$ ℓ/min has been used to supply water to the test loop. The inlet duct conducts the fluid into the center of the impeller, due to impeller rotation, the fluid is centrifuged outwards, towards the outside diameter of the impeller.

The high velocity of the fluid at the exit from the impeller is converted into pressure energy by velocity reduction in the volute, which acts basically as a fluid collection channel, the high pressure fluid that passes through the pump discharged to the test loop.

28

Compressed Air · **Test Section** · **FM** · **ST** · **M** · **FM** · **WF** · **P** · **WT**
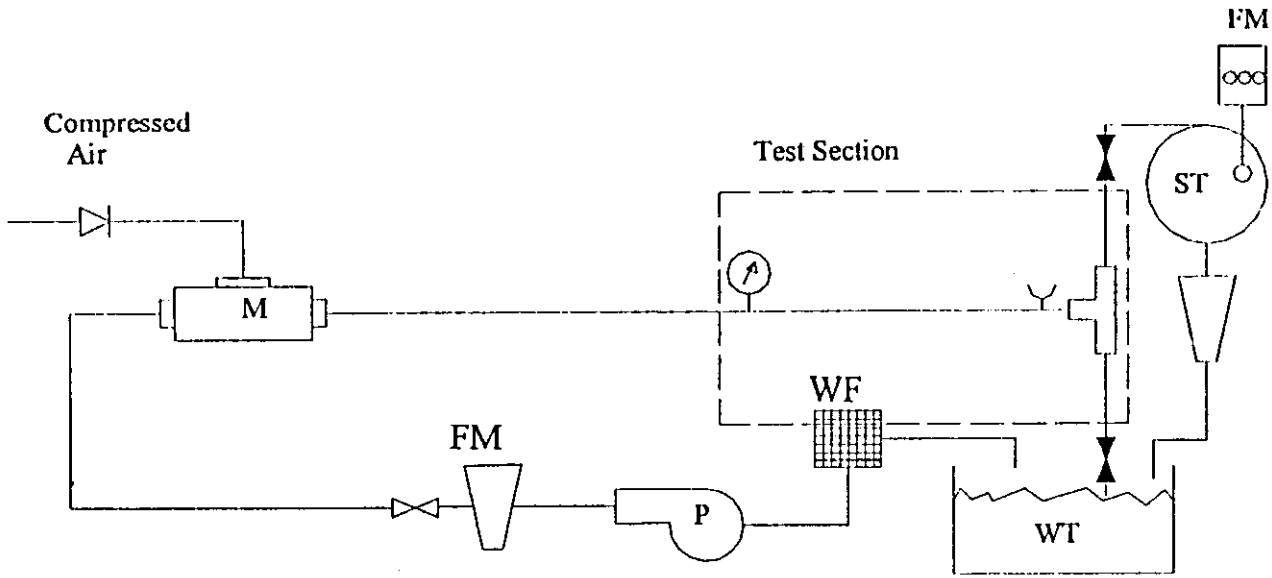
Legend

FM	Flow meter	⋈	Way valve
P	Pump	⋈	Control valve
ST	Separation tank	▷	Non-return valve
WF	water filter	Y	Thermocouple
WT	Water tank	⊘	Pressure gauge
M	Mixer		

Figure (3.2) Experimental test facility.

3.2.2 Air compressor

"Gilkes tutor reciprocating air compressor" used in this study which is basically a simple mechanical device, that supplies air to the test loop. It can be operated at a maximum pressure of 10.3 bar nominal, 425 rpm minimum speed and 850 rpm as a maximum speed.

29

shown in figure (3.3), a photograph for the mixer is also shown in figure (3.4).
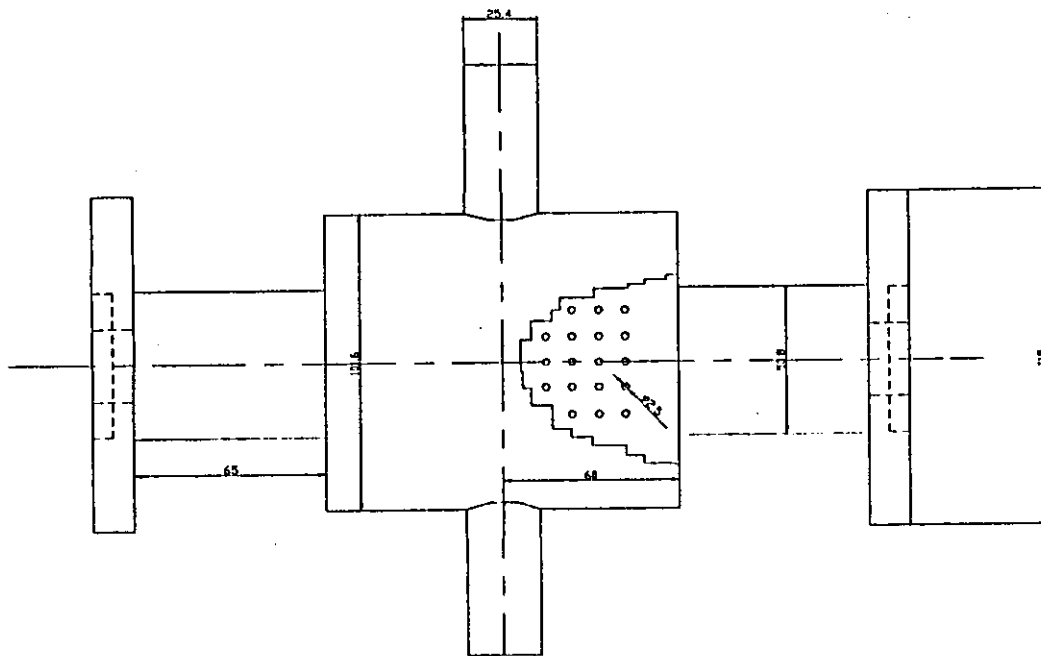
Figure (3.3) A schematic plot of the Mixer.
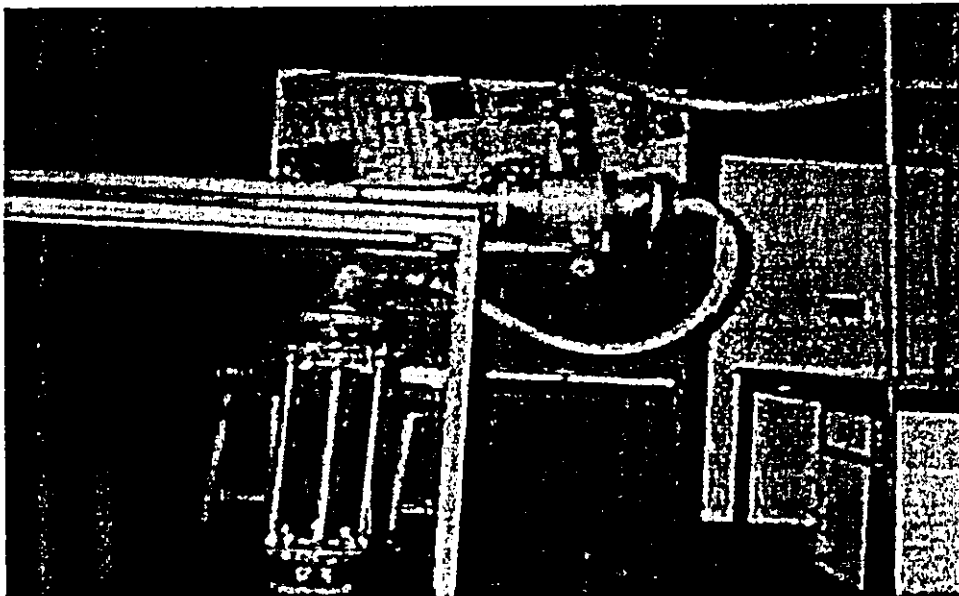
Figure (3.4) Photograph of the mixer.

31

3.2.5 Air-Water Separator

An air-water separator was designed and manufactured from 1.25mm thickness galvanized metal sheet as shown in figure (3.5). It is an essential element that enables us to separate air from water at outlets. It has simply a sink at the lower end and a vent at the upper one. The sink was connected to the rotometer, where the outlet water mass flow rate was measured, while the air velocity was measured by a pitot tube placed at the vent. Separation phenomena depends on a free vortex principle. Photogrph of the air-water separator is shown in figue (3.6)
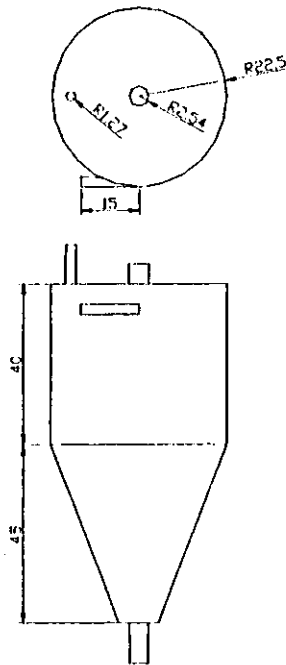
Figure (3.5) A schematic plot of air-water separator.

3.2.6 Valves and T-Junction:

Two valves and a sharp edge T-junction that made from PVC 32-1", UNE 53112 and PN-1.6 were used to control the flow rates and the system

pressure. The T-junction is the vital element at which the pressure drop within is studied. A non-return valve was set in the compressor supply line to avoid water entering to the compressor.
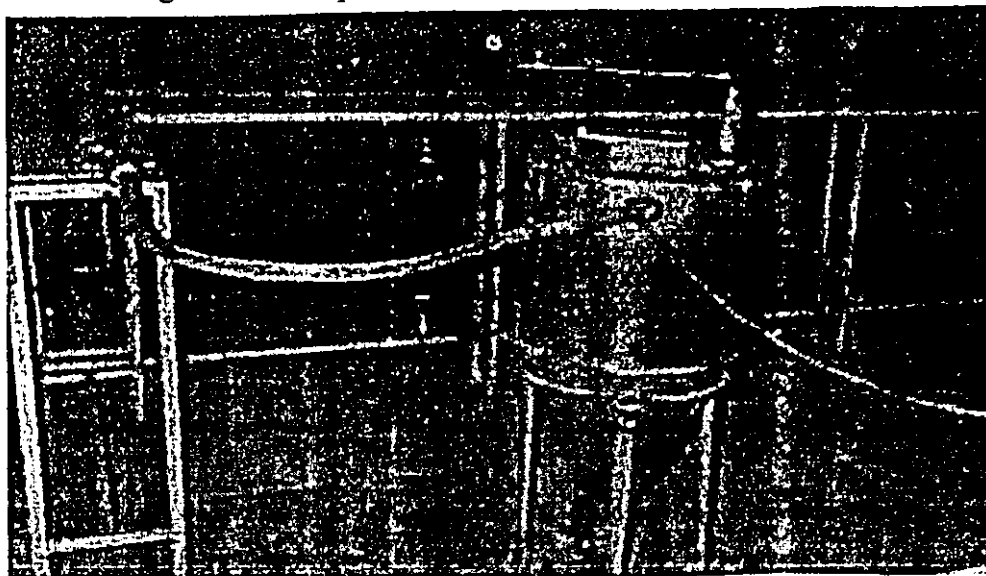
Figure (3.6) Photograph of the air-water separator.

3.2.7 Pressure Gauge and Taps

A 1 bar scale bourdon gauge, figure (3.10), is used to justify the system pressure, placed at a distance of (60×diameter)from the center of the T-junction. Thirty two pressure taps were manufactured from copper, with 1.5mm inner diameter distributed regularly at (2d, 5d, 10d, 20d and 40d) from the center of the T-junction, at the inlet and the branches as shown in figure (3.7). A schematic plot of the pressure tap is also shown in also shown.

3.2.8 Pressure taps holder:

This device was designed and manufactured in order to measure the pressure drop through the 15 taps. A pressure holder as shown in fig(3.8), was manufactured from a 60cm long PVC pipe closed from one end and have a valve from the other. 15 drills (6mm diameter) were arranged on the upper

33

face, connected to the pressure taps at the test loop and one on the other face connected to the U-manometer
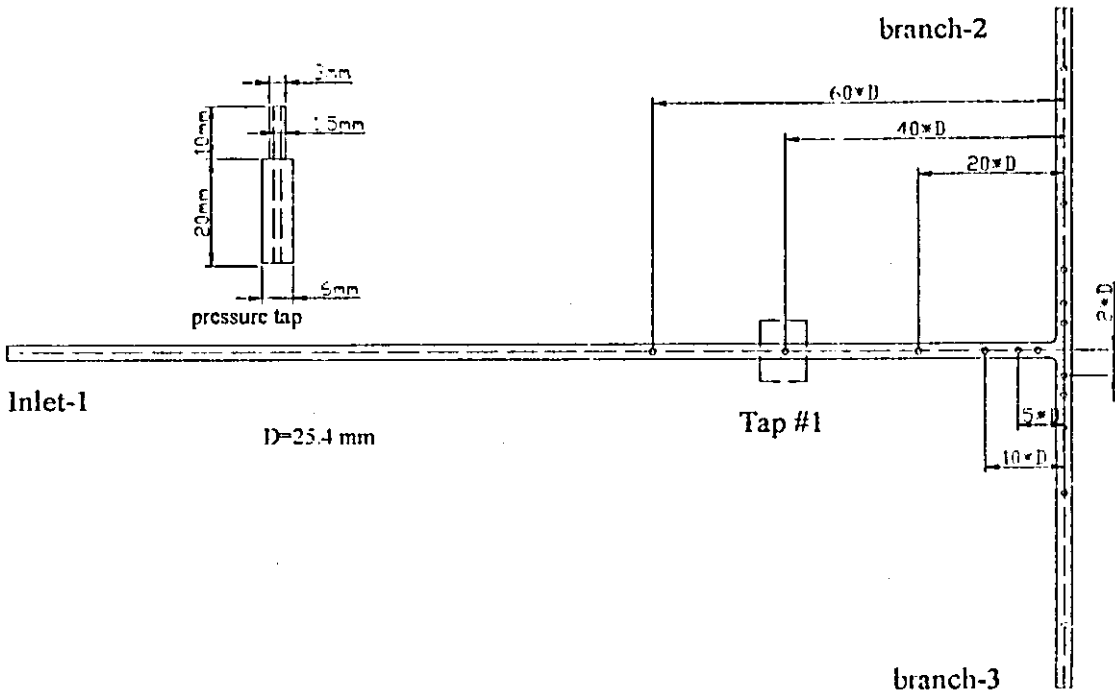
Figure (3.7) Layout of pressure taps.
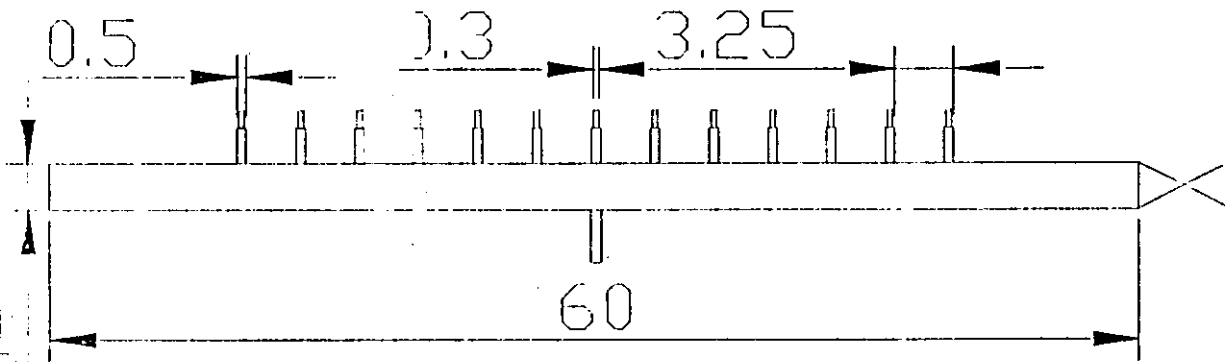
Figure (3.8) Layout of the pressure taps holder.

3.3 Building the test loop

The following steps were followed to build the test section shown in figure (3.1), used in this study :

1. three stands ($420 \times 30 \times 120, 120 \times 30 \times 120, 120 \times 30 \times 120$) length, width and height, were manufactured and fixed to the ground.

2. thirty two pressure taps were manufactured from copper and placed at regular displacements at the PVC pipes and holder.

3. Two rotometers were placed at the stand legs.

4. PVC pipes were connected and glued with the T-junction and placed at the stands.

5. two way valves were connected to the ends of the branches to control the mass flow rates.

6. The pressure taps holder was fixed at the branch stand legs.

7. Silicon pipes with 1.5 mm inner diameter were connected to the pressure taps at the PVC pipes with the pressure taps holder, as shown in figure (3.9).

8. a 1bar pressure gauge was placed at the stand and connected with the system pressure tap through a tee, while the other side of the tee were connected with the U-manometer.

35

9. the mixer was placed at the inlet to the test section.

10. a centrifugal pump was placed to supply the system with water from the water tank.

11. a rotometer was set at the stand legs after the pump to measure the inlet mass flow rate.

12. a way valve was placed at the rotometer outlet to control the inlet mass flow rate and connected with the mixer.

13. the air compressor was connected with the mixer by hose of one inch diameter having non-return valve at its end to avoid water entering to the compressor.

14. one of the branches returns water to the tank directly, while the other connected to the air-water separator.

15. air-water separator was manufactured from 1.25mm thickness, galvanized metal sheet, and connected to another rotometer to measure the outlet water mass flow rate. While the outlet of the rotometer returns water to the tank directly.

16. Pitot tube connected with the manometer was set at the air-water separator vent to measure air mass flow rate.

17. a digital thermometer was used to measure the temperature at the inlet to the T-junction.

18. a $5\mu m$ water filter was connected to the pump inlet, to assure pure water entering to the loop.
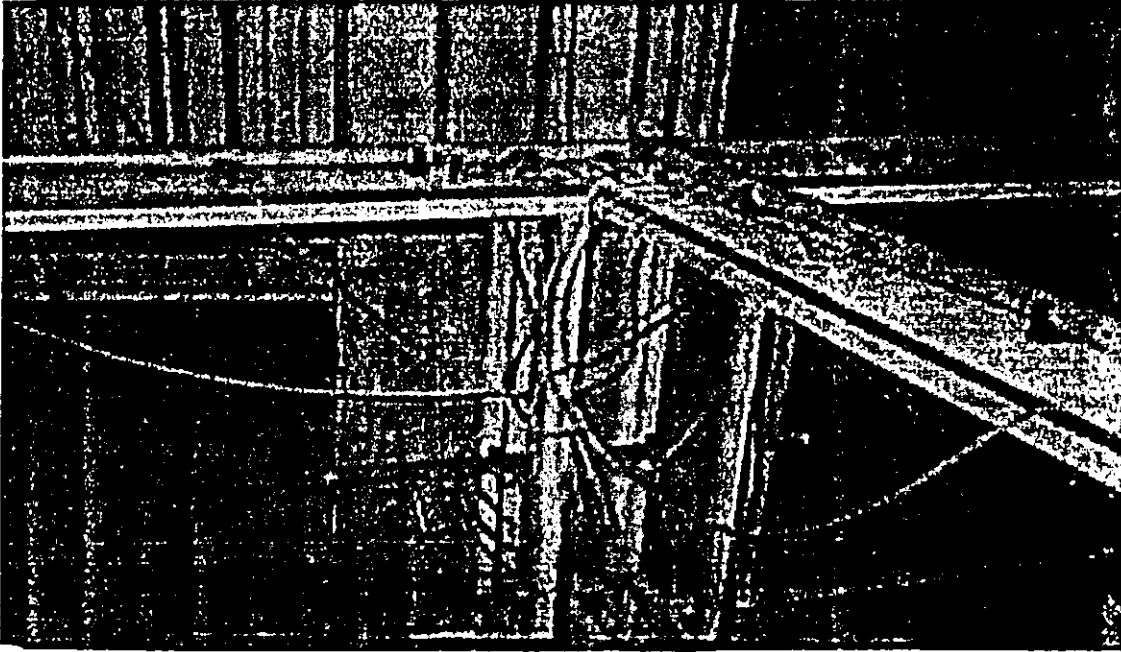
Figure (3.9) Photograph of the test section.

3.4 Measuring instrumentation

The instrumentation used during the test are introduced briefly in the following :

1. Pressure bourdon gauge: Bourdon gauge shown in figure (3.10) is typical of the devices used for measuring gauge pressures. The pressure element is a hollow, curved, flat metallic tube, closed at one end with the other end connected to the pressure to be measured. When the internal pressure is increased, the tube tends to straighten, pulling on a linkage to which is attached a pointer and causing the pointer to move. The dial reads zero when inside and outside of the tube are at the same pressure, regardless of its particular value. A 1bar scale gauge was used to measure the system

37

pressure, set at the inlet pipe at (60 × d) from the centerline of the T-junction, the minimum reading of the gauge is 10 Pa.
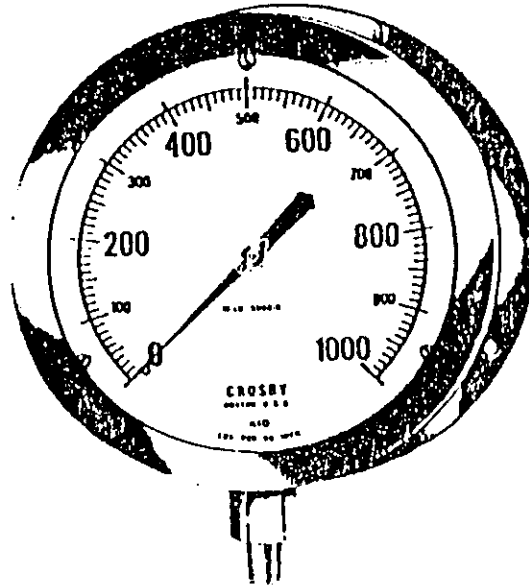
Figure (3.10) Bourdon gauge

2. Rotometers: Two rotometers were used, the first measures the inlet mass flow rate of water to the mixer, with a range of (900-9000L/hr), with minimum reading of 100 L/hr. And the other measures the water flow out from the separator with a range of (180-1800L/hr) with minimum reading of 20 L/hr. The principle of rotometers as shown in figure (3.11), is to maintain the float in equilibrium and as it is of constant weight, the pressure difference is independent of discharge. The cause of the pressure difference is the head loss associated with the high velocity of water around the float periphery. Since this head loss is constant then the peripheral velocity is constant. To maintain a constant velocity with a varying discharge rate, the cross-sectional area through which this high velocity occurs must vary. This variation of cross sectional area will increase as the float moves up and down the tapered rotometer tube.
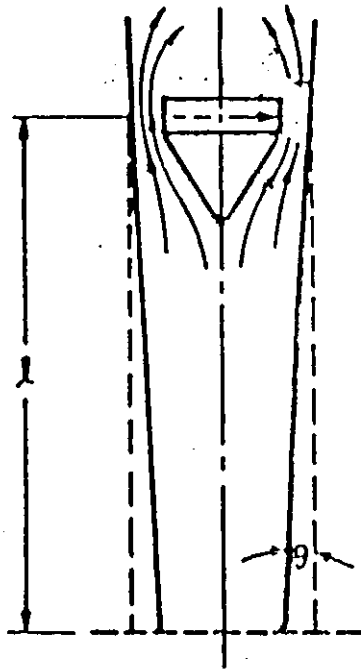
Figure (3.11) Principle of the rotometer

3. Thermocouple and digital thermometer: One copper constantan thermocouple wire type was used to measure the temperature at the inlet to the T-junction. It was connected to a digital thermometer (305) type with 0.1°high resolution, maximum record and offset adjest.

4. Orifice : It is used to measure the inlet mass flow rate according to BS 1042 with d_1=12.7mm and D=25.4mm :

$$\dot{m} = 6.574 \times 10^{-3} \sqrt{\frac{\Delta P.P_3}{T_3}} \qquad \text{Kg/s} \qquad\qquad [3.1]$$

where ΔP= orifice differential head   mm wg

   P_3 = orifice plate down stream pressure bar abs

   $= P_3' + P_0$ bar abs

where P_3'= pressure gauge reading bar abs

   P_0 = atmospheric pressure bar abs

And $T_3 = T_3' + 273.15$ K

5. Pitot tube: The outlet air mass flow rate at the separator was calculated from the air velocity measured by means of a pitot tube. If h is the liquid dynamic head in mm then the velocity is given by :

$$V = \sqrt{\frac{2.\rho_\ell.g.h}{\rho_a}} \quad \text{m/s} \tag{3.2}$$

then the mass flow rate, $\dot{m}$, is given by

$$\dot{m} = \rho_a. V. A_p \tag{3.3}$$

where, A_p is the air-water separator vent cross sectional area.

6. U-manometer: U-tube containing mercury was used to measure the pressure loss across the test section points. Considering fig.(3.12) since the pressure difference was taken at the same elevation and pipe diameter then from Bernoulli's equation :

$$\frac{P_1 - P_2}{\rho_{H_2O}g} = h_L \tag{3.4}$$

pressure in both limbs of the U-tube are equal at level 00. Therefore equating pressures at 00:

$$P_2 - \rho_{H_2O}g(X+Y) + \rho_{Hg}gX = P_1 - \rho_{H_2O}(gY_1) \tag{3.5}$$

arrange above equations taking the specific gravity of mercury as 13.6 gives:

$$h_L = 12.6X \tag{3.6}$$

$$\Delta P_{1x} = 12.6g\rho_{H_2O}X \tag{3.7}$$

where X = Head loss at the inlet or branches taps

40

WATER

MERCURY

P_2 P_1
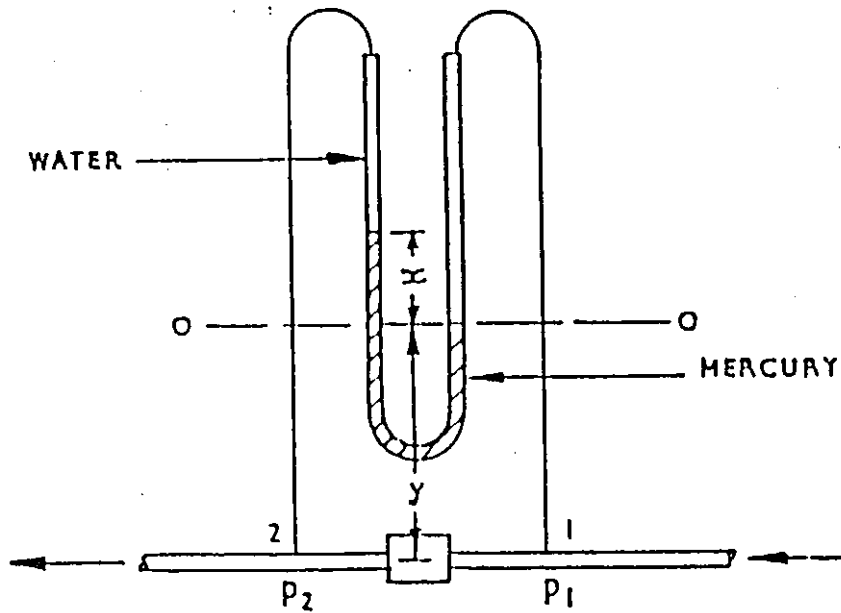
Figure (3.12) mercury U-tube manometer used to measure the pressure loss.

3.5 Experimental tests and procedure

The experimental test facility used in this study was placed in the Fluid Mechanics Laboratory of Mechanical Engineering department of Mu'tah University. The test facility was allowed to operate at different air and water mass flow rates. The data collected are:

1. Inlet and outlet water mass flow rates.

2. Inlet and outlet air mass flow rates.

3. System pressure (P_s).

4. Temperature at the inlet of the T-junction (T_1).

5. Pressure difference values at the fifteen pressure tap locations.

3.5.1 Single-Phase Flow Test

The objective of this test is to obtain the loss coefficient (K) for the material (PVC) used in this study.

Single-phase (liquid) pressure drop data were obtained in this investigation using seven test runs, corresponding to a mass flux of 709.8 $Kg/s.m^2$ and $0.0 \leq G_2/G_1 \leq 1.0$. Magnitudes of the loss coefficient (K) were calculated from the measured values of ΔP_{12}.

Obtained results are tabulated in table (B$_1$-B$_3$), at which pressure differences at different extraction rates were taken from the U-manometer. The inlet and outlet water mass fluxes were taken from rotometers. Details of procedure is the same as in section (3.5.2) except that there is no air flow.

3.5.2 Two-Phase Flow Test

The objective of this investigation is to find the pressure difference across the T-junction.

The test system shown in figure (3.2) consists of a 5 μm water filter that filters the water enters to the system. A rotometer was set after the pump to measure the water flow rates (1000, 1100, 1200, 1300, 1400 and 1500)L/hr entering the mixer. Air compressor supplies air to the system at which an orifice is used to measure the air mass flow rates. A non-return valve was set on the compressor supply line to avoid water entering to the compressor.

42

Mixer was used to mix air with water, and supply regular stream lines of the mixture (air & water) to the inlet of the test loop. This flow is divided into the two branches, during the flow the pressure difference was measured by using pressure taps at 15 points along the inlet and branches with respect to the system pressure, which was measured by a pressure gauge.. The 15 pressure taps were connected to the U-manometer through a pressure holder. In order to read the pressure difference directly from the U-manometer a line from the system pressure was connected to the other edge of the U-manometer. The outlet air and water mass flow rates were measured by a means of a pitot tube and a rotometer at the outlets of the air-water separator, The data collected are tabulated in tables (A.2.1-A.3).

4. RESULTS AND DISCUSSION

4.1 Introduction

In this chapter, the pressure differences are studied with detailed analysis. This study is based on the experimental results, obtained from the performed tests.

Results and sample calculation are presented in section (4.2), and the final part deals with the discussion and analysis of the results obtained.

4.2 Calculations and Results

The calculations and curves presented in this study were performed by using Excel package.

The data collected during all tests are tabulated in appendix A. All measured pressure difference values (four to six readings within one minute) at each tap location were averaged to ensure low errors due to fluctuations in head measurements. The calculations are based on the equations presented previously in chapters two and three. The results and sample calculation of all tests are presented in the following sub-sections.

547467

4.2.1 Single-Phase Flow Test

This test was performed at inlet mass flux of 709.8 kg/s.m² and extraction rates of $0.0 \leq G_2/G_1 \leq 1.0$. The data collected during the test are presented in tables (A.1) in appendix A. From obtained data the pressure difference (ΔP_{12}) and the loss coefficient (K) were obtained and listed in tables (B.1-B.3) in appendix B.

At each extraction rate (G_2/G_1), the U-manometer heads of the taps at the inlet and at branch-2 (H_1, H_2) in mmHg and the inlet temperature to the T-junction (T_1) were recorded. Each head measurement is a group of five readings for the taps distributed along each test leg. The pressure differences ($\Delta P_{st}^2)_i$ was estimated from equation (3.7), where subscripts s, t and i are representing system pressure, tap pressure and test leg number, respectively. For the purpose of simplifying calculations in order to be consistent with others data, the pressure differences were transformed to be ($\Delta P_{1t}^2)_i$, which is the pressure difference between each tap against tap#1 as indicated in the sample calculation. The values of ($\Delta P_{1t}^2)_i$ were plotted against tap position as shown in figure (4.1), the average pressures and then the pressure differences across the T-junction can be taken by extrapolating the fully developed values to the centerline of the T-junction.

From obtained results the loss coefficient values (K) can be calculated from equation (2.10) and plotted against the extraction rates (G_2/G_1) as shown in figure (4.2). The equation that represents the loss coefficient as a function of extraction rates can be obtained from the available Excel polynomial curve fitting as:

$$K=1.0799(G_2/G_1)^2-0.6686(G_2/G_1)+1.1321 \qquad (4.1)$$

45

This relation was compared with previous results as shown in figure (4.3). The values of water density and the acceleration due to gravity were assumed to be constant at given temperatures as $(996\ \text{kg/m}^3, 9.81\ \text{m/s}^2)$ Mills, 1995, respectively, since the variation of temperatures is relatively small. The inlet volumetric flow rates (ℓ/hr) were taken in term of mass flux directly in the calculations according to the following relation:

$$G = \dot{V}(L/hr) * \frac{1hr}{3600\sec} * \frac{1m^3}{1000L} * \rho_{H_2O}(\frac{kg}{m^3}) * \frac{1}{A}(m^2) \qquad (4.2)$$

$$= 0.546 * \dot{V} \qquad (4.3)$$

Sample calculation

Referring to table (A.1)the measured values of average pressure heads (H_1, H_2) at each pressure location for the extraction rate $G_2/G_1 = 0.3846$ are tabulated in table (4.1)

Table (4.1) average pressure head for extraction rate $G_2/G_1 = 0.3846$

G_2 (kg/s.m²)	G_2/G_1	Distance at inlet (m)	H_1 (mm Hg)	Distance at branch-2 (m)	H_2 (mm Hg)
273	0.3846	-1.016	1.5	0.0508	4
		-0.508	2.75	0.127	4.25
		-0.254	3.5	0.254	4.5
		-0.127	3.75	0.508	4.75
		-0.0508	3.5	1.016	5

The pressure difference values (ΔP_{st}) can be calculated from equation (3.7):

$(\Delta P_{s1})_1 = 12.6 g \rho_{H_2O} X$, where $X = H_1$ or H_2

$= 12.6 * 9.81 * 996 * 0.0015$

$= 184.6674$ Pa

$(\Delta P_{s2})_1 = 12.6 g \rho_{H_2O} X$

$= 12.6 * 9.81 * 996 * 0.00275$

$= 338.5568$ Pa

This value is used to find the pressure difference with respect to tap #1 as follows:

$(\Delta P_{1t})_1 = (\Delta P_{s1})_1 - (\Delta P_{st})_2$ (4.4)

$(\Delta P_{12})_1 = 184.6674 - 338.5568$

$= -153.887$ Pa

Results are presented in table (4.2)

Table (4.2) pressure differences for $G_2/G_1 = 0.3846$

Distance at inlet (m)	$(\Delta P_{st})_1$ bar	$(\Delta P_{1t})_1$ bar	Distance at branch-2 (m)	$(\Delta P_{st})_2$ bar	$(\Delta P_{1t})_2$ bar
-1.016	184.6674	0.0	0.0508	492.4463	-307.776
-0.508	338.5568	-153.887	0.127	523.2242	-338.554
-0.254	430.8905	-246.221	0.254	554.0021	-369.332
-0.127	461.6684	-276.998	0.508	584.78	-400.11
-0.0508	430.8905	-246.221	1.016	615.5579	-430.888

The values of pressure difference with respect to tap #1 (ΔP_{1t}) were plotted against taps positions, as shown in figure (4.1) and the pressure difference across the T-junction can be obtained directly from the plot at this extraction rate to be

$\Delta P_{12} = 55$ Pa

Rearranging equation (2.10) gives the loss coefficient value as:

$$K = \frac{2\rho_{H_2O}\Delta P}{G_1^2} - (\frac{G_2}{G_1})^2 + 1 \qquad (4.5)$$

$$= \frac{2*996*55}{709.8^2} - 0.3846^2 + 1$$

$$= 1.069553$$

The loss coefficient values (K) were computed for each extraction rate and plotted against it, as shown in figure (4.2). For the purpose of comparison, the loss coefficient values (K) from previous works are also estimated using equations (2.11-2.13) and plotted against extraction rates as shown in figure (4.3). Results obtained are listed in table (B.1-B.3).

4.2.2 Two- phase Flow Tests

These tests were performed at different inlet water mass fluxes of (547, 601, 656, 710, 820) kg/s.m^2 and air mass flow rates of (0.000452, 0.000586, 0.000641, 0.000642, 0.000786)kg/s, respectively.

The data collected during the tests are shown in table (A.2, A.3) in appendix A. The average pressures (P$_1$, P$_2$ and P$_3$) and the pressure difference values across the T-junction ($\Delta P_{12}, \Delta P_{13}$) were obtained. These results are shown in table (B.7)in appendix B.

Five tests were carried out with constant air mass flow rate and different water mass fluxes for each test. During each test, the U-manometer heads of the taps at the inlet and branches (H$_1$, H$_2$ and H$_3$), the inlet temperature to the T-junction (T$_1$), the orifice differential head ΔP, the orifice plate downstream

48

pressure, the atmospheric pressure, the dynamic pressure at the air-water separator vent and the inlet and outlet water volume flow rates were recorded.

The values of the pressure heads were substituted in equation (3.7) to obtain the pressure differences $(\Delta P_{st})_i$ and then the pressure differences against tap#1 $(\Delta P_{1r})_i$ from equations (4.4). Results were plotted against measurement positions as shown in figures (4.4-4.32). The average pressures (P_1, P_2 and P_3) and the pressure differences (ΔP_{12}, ΔP_{13}) were obtained from these figures for all tests.

The total (air and water) mass fluxes (G_1, G_2 and G_3) and the qualities (x_1, x_2 and x_3) were estimated from equations (2.2, 2.3). The pressure differences (ΔP_{12}, ΔP_{13}) were plotted against inlet mass flux (G_1) and extraction rates(G_2/G_1, G_3/G_1) at constant inlet qualities, and against inlet quality(x_1) at constant inlet mass flux, as shown in figures (4.33-4.38). Here, due to the lack of repeatability of the same values of inlet mass flux and inlet quality, values within $\pm 5\%$ error were taken the same. The superficial gas and liquid velocities are also estimated and used to determine the flow regime caused due to two-phase flow according to Mandhane, 1974.

For the purpose of comparison with other models, the reproductive accuracy (Schmidt, 1997) of obtained results is found on the basis of dimensionless statistical number: standard deviation S_{ln} of the logarithmic ratios of measured (subscript meas.) and predicted (subscript SFM or RSM) pressure differences and ploted on the parity plot as shown in figure (4.39), according to the following definitions

The logarithmic ratio between measured and predicted pressure difference
($X_{ln,i}$)

$$X_{ln,i} = ln \left(\frac{\Delta P_{i,meas.}}{\Delta P_{i,pred.}} \right) \tag{4.6}$$

The standard deviation of logarithmic ratios (S_{ln})

$$S_{ln} = exp\left\{ \sqrt{\frac{\sum_{i=1}^{n} X_{ln,i}^2}{(n-f-1)}} \right\} - 1 \tag{4.7}$$

Where n = number of experimental values, f = number of variables

Sample calculation

Referring to table (A.2.1-A.2.5), the measured values of average pressure heads (H_1, H_2 and H_3) for each pressure tap on the test leg, at inlet water volume flow rate of 1000 ℓ/hr and inlet air mass flow rate of 0.000641 kg/s at system pressure P_s of 1 bar are listed in table (4.3).

Table (4.3) Average pressure heads for $\dot{V}_1$ =1000 ℓ/hr, $\dot{m}_a$ =0.000641 kg/s

$\dot{V}_1$ (ℓ/hr)	$\dot{V}_2$ (ℓ/hr)	Measurement positions (m)	H_1 (mm Hg)	Measurement positions (m)	H_2 (mm Hg)	H_3 (mm Hg)
1000	370	-1.016	3.83	0.0508	7.33	9
		-0.508	6	0.127	8	10.67
		-0.254	6.67	0.254	8.67	11.33
		-0.127	7	0.508	9	11.67
		-0.0508	6.67	1.016	9.33	12.33

The pressure difference values $(\Delta P_{st})_i$ can be calculated from equation (3.7) as:

$$(\Delta P_{st})_i = 12.6 g \rho_{H_2O} X$$

where, $X = H_1, H_2$ and H_3

$(\Delta P_{st})_1 = 12.6 * 9.81 * 996 * 0.00383$

$\qquad = 471.5173$ Pa

$(\Delta P_{s2})_1 = 12.6 * 9.81 * 996 * 0.006$

$\qquad = 738.6692$ Pa

These values are used to find out the pressure difference with respect to tap #1 from equation (4.4) as follows :

$(\Delta P_{1r})_1 = (\Delta P_{st})_1 - (\Delta P_{s2})_1$

$(\Delta P_{12})_1 = 471.5173 - 738.6692$

$\qquad = -267.1521$ Pa

Results are shown in table (4.4)

Table (4.4) Pressure differences for $\dot{V}_1 = 1000 \, \ell/hr$,

$\dot{m}_a = 0.00064$ kg/s

$(\Delta P_{st})_1$ bar	$(\Delta P_{1r})_1$ bar	$(\Delta P_{st})_2$ bar	$(\Delta P_{1r})_2$ bar	$(\Delta P_{st})_3$ bar	$(\Delta P_{1r})_3$ bar
471.5173	0.0	902.4079	-430.8905	1108.004	-636.4869
738.6695	-267.1521	984.8926	-513.3753	1313.601	-842.0832
821.1542	-349.6369	1067.377	-595.86	1394.854	-923.3369
861.781	-390.2637	1108.004	-636.4868	1436.712	-965.1948
821.1542	-349.6369	1148.631	-677.1137	1517.966	-1046.4484

51

The values of pressure difference with respect to tap #1 ($\Delta P_{1i}'$) were plotted against the tap positions, as shown in figures(4.4-4.32). The pressure difference across the T-junction can be obtained directly from the plot as :

$\Delta P_{12} = 95$ Pa

$\Delta P_{13} = 390$ Pa

Results are tabulated in table (B.7)

For the purpose of comparison with other models, number of parameters (homogeneous, momentum, energy densities and two-phase loss multiplier) must be estimated first. The parameters are calculated in the followings. From table (A.2, A.3), the inlet and outlets air mass flow rates can be calculated using equations (3.1, 3.2, 3.3), given in table (B.4.1-B.4.5). From equation (3.1) the inlet air mass flow rate is:

$P_3 = P_o + P_3'$

$\qquad = 0.942 + 0.058$

$\qquad = 1$ bar

$$\dot{m}_{a1} = 6.574 \times 10^{-3} \sqrt{\frac{\Delta P.P_3}{T_3}}$$

$$= 6.574 \times 10^{-3} \sqrt{\frac{3 \times 1}{315.15}}$$

$\qquad = 0.000641$ kg/s

The air mass flow rate of branch-2 is found from equations(3.2, 3.3)

$$V = \sqrt{\frac{2.\rho_\ell.g.h}{\rho_a}} \quad \text{m/s}$$

$$= \sqrt{\frac{2 \times 787 \times 9.81 \times 1 \times 10^{-3}}{1.177}}$$

$\qquad = 3.622$ m/s

then the mass flow rate, $\dot{m}_{a2}$, is given by

$\dot{m}_{a2} = \rho_a. \text{V}. \text{A}_p,$ where, A_p is the vent pipe cross sectional area.

$$= 1.177 \times 3.622 \times \frac{\pi}{4} \times (8 \times 10^{-3})^2$$

$$= 0.000214 \text{ kg/s}$$

$\dot{m}_{a3} = \dot{m}_{a1} - \dot{m}_{a2}$

$$= 0.000641 - 0.000214$$

$$= 0.000427 \text{ kg/s}$$

The water mass flow rate can be found from the following equation

$$\dot{m}_{wi} = V(L/hr) * \frac{1hr}{3600\sec} * \frac{1m^3}{1000L} * \rho_{H_2O}(\frac{kg}{m^3})$$

where, $\rho_{H_2O} = 996 kg/m^3$

$\dot{m}_{wi} = 0.000276666 * V_1$

$$= 0.000276666 * 1000$$

$$= 0.276666 \text{ kg/s}$$

Equation (2.3) is used to find out the total mass flux as :

$G_i = G_{iw} + G_{ia}$ $i = 1,2,...$

where subscript w represents for water

$$= 0.546 \times \dot{V}_i + \frac{\dot{m}_{ia}}{A} \qquad \text{for } i = 1$$

$$G_1 = 0.546 \times 1000 + \frac{0.000214}{(\frac{\pi}{4} \times 8 \times 10^{-3})^2}$$

$$= 547.2658 \text{ kg/s.m}^2$$

The same is done for G_2, G_3 at the outlets, results are shown in table (B.5.1-B.5.5).

The inlet and outlet qualities can be obtained from equation (2.2) as follow

$$x = \frac{\dot{m}_a}{\dot{m}_a + \dot{m}_w}$$

$$x_1 = \frac{0.00641}{0.00641 + 0.276666}$$

$$= 0.002313$$

and the same procedure is followed for the remain qualities. Results are listed in table(B.7).

The homogeneous densities ($\rho_{H_1}, \rho_{H_2}, \rho_{H_3}$) can be estimated from equation (2.17)

$$\rho_{Hi} = [\frac{(1-x_i)}{\rho_t} + \frac{x_i}{\rho_g}]^{-1}$$

$$= [\frac{(1 - 0.002313\ )}{996} + \frac{0.002313}{1.177}]^{-1}$$

$$= 344.8235 \ \ \text{kg/m}^3$$

the results are given in table (B.8).

In order to evaluate momentum density values the void fraction should be estimated first. The velocity ratio (S_i) and then the void fraction (α_i) were obtained using equations (2.20,2.21). Results substituted in equation (2.18) in order to obtain the momentum density values that shown in table (B.8).

$$S_i = \frac{\rho_t}{(1-x_i)}(\frac{(1+0.12(1-x_i))}{\rho_{Hi}} + \frac{(\frac{1.18}{\sqrt{\rho_t}}(g \times \sigma \times (\rho_t - \rho_G)))^{1/4}}{G_i} - \frac{x_i}{\rho_G})$$

$$x_i = 0.002313, \rho_{Hi} = 337.0609 kg/m^3, \rho_t = 996, \sigma = 0.0819 N/m$$

For

$$G_1 = 547.2658 kg/s.m^2, \rho_G = 1.177 kg/m^3, g = 9.81 m/s^2$$

$S_i = 1.705633$

$$\alpha_i = \frac{x_i}{x_i + (S_i/R)(1-x_i)} \quad ,$$

$$R = \frac{\rho_l}{\rho_G} = 846.22$$

$$\alpha_1 = \frac{0.002313}{0.002313 + (\frac{1.705633}{846.22})(1-0.002313)}$$

$\alpha_1 = 0.534926$

$$\rho_{Mi} = [\frac{(1-x_i)^2}{\rho_l(1-\alpha_i)} + \frac{x_i^2}{\alpha_i \rho_g}]^{-1}$$

$$\rho_{M1} = [\frac{(1-0.002313)^2}{996(1-0.534926)} + \frac{0.002313^2}{0.534926 \times 1.177}]$$

$\rho_{M1} = 463.5315$ kg/m^3

Equation (2.19) is used to find another term called Energy density, which is also required in calculations. Results are tabulated in table (B.9).

$$\rho_{Ei} = [\frac{(1-x_i)3}{\rho^2_l(1-\alpha_i)^2} + \frac{x_i^3}{\alpha_i^2 \rho^2_g}]^{-1}$$

$$\rho_{E1} = [\frac{(1-0.002313)^3}{996^2(1-0.534926)^2} + \frac{0.002313^3}{0.534926^2 \times 1.177^2}]^{-0.5}$$

$= 463.2663$ kg/m^3

the two-phase loss multiplier ϕ has different correlations, results shown in table(B.9). According to the separated flow model (SFM) and the Riemann & Seeger model (RSM) the values of ϕ can be estimated as follow

55

$$\phi_{SFM} = \frac{\rho_l}{\rho_{M1}} \quad \text{this valid for the two branches (2,3)}$$

$$= \frac{996}{463.6893}$$

$$= 2.14799$$

$$(\phi_{RSM})_i = \frac{\rho_l \times \rho_{IIi}}{\rho_{H1}}$$

$$(\phi_{RSM})_2 = \frac{996 \times 360.4426}{337.0609}$$

$$= 3.159939$$

$$(\phi_{RSM})_3 = \frac{996 \times 324.6952}{337.0609}$$

$$= 2.846547$$

After these calculations, the pressure differences ($\Delta P_{12}, \Delta P_{13}$) for the above models are :

$$(\Delta P_{12})_{SFM} = \frac{\rho_{II2}}{2}[(G_2^2/\rho_{E2}^2) - (G_1^2/\rho_{E1}^2)] + K_{12} \frac{G_1^2}{2\rho_l} \phi_{SFM}$$

$$= \frac{360.4426}{2}[\frac{202.4423^2}{559.6064^2} - \frac{547.2658^2}{463.2663^2}] + 1.032545\frac{547.2658^2}{2 \times 996}2.14799$$

$$= 105.6608 \text{ Pa}$$

$$(\Delta P_{13})_{SFM} = \frac{\rho_{II3}}{2}[(G_3^2/\rho_{E3}^2) - (G_1^2/\rho_{E1}^2)] + K_{13} \frac{G_1^2}{2\rho_l} \phi_{SFM}$$

$$= \frac{324.6952}{2}[\frac{344.8235^2}{478.9547^2} - \frac{547.2658^2}{463.2663^2}] + 1.139553\frac{547.2658^2}{2 \times 996}2.14799$$

$$= 225.7379 \text{ Pa}$$

$$(\Delta P_{12})_{RSM} = \frac{\rho_{II2}}{2}[(G_2^2/\rho_{II2}^2) - (G_1^2/\rho_{II1}^2)] + K_{12} \frac{G_1^2}{2\rho_l} (\phi_{RSM})_2.$$

56

$$= \frac{360.4426}{2}[\frac{2024423^2}{360.4426^2} - \frac{547.2658^2}{337.0609^2}] + 1.032545\frac{547.2658^2}{2\times996} 3.159939$$

$$= 72.31312 \text{ Pa}$$

$$(\Delta P_{13})_{RSM} = \frac{\rho_{II3}}{2} ((G_3^2/\rho_{II3}^2) - (G_1^2/\rho_{II1}^2)) + K_{13}\frac{G_1^2}{2\rho_t} (\phi_{RSM})_3$$

$$= \frac{3246952}{2}[(\frac{2024423^2}{3246952^2} - \frac{547.2658^2}{337.0609^2}] + 1.139553\frac{547.2658^2}{2\times996} 2.846547$$

$$= 242.8258 \text{ Pa}$$

Results are tabulated in table (B.10).

Determining the inlet flow regime of each test required estimating the superficial liquid and gas velocities. These superficial velocities can be calculated using equations (2.7, 2.8). Calculated values were used to determine the inlet flow regime using Mandhane map, 1974.

$$J_{G1} = G_1 x_1 / \rho_g$$

$$= \frac{547.2658\times0.002313}{1.177}$$

$$= 1.075448 \text{ m/s}$$

$$J_{\ell 1} = G_1 (1-x) / \rho_t$$

$$= \frac{547.2658\times(1-0.002313)}{996}$$

$$= 0.548193 \text{ m/s}$$

The flow regime obtained at this value is slug flow regime, and the same result is obtained for the remaining calculations.

The standard deviations between measured and predicted pressure difference values can be calculated from equations(4.7), sample calculation for measured
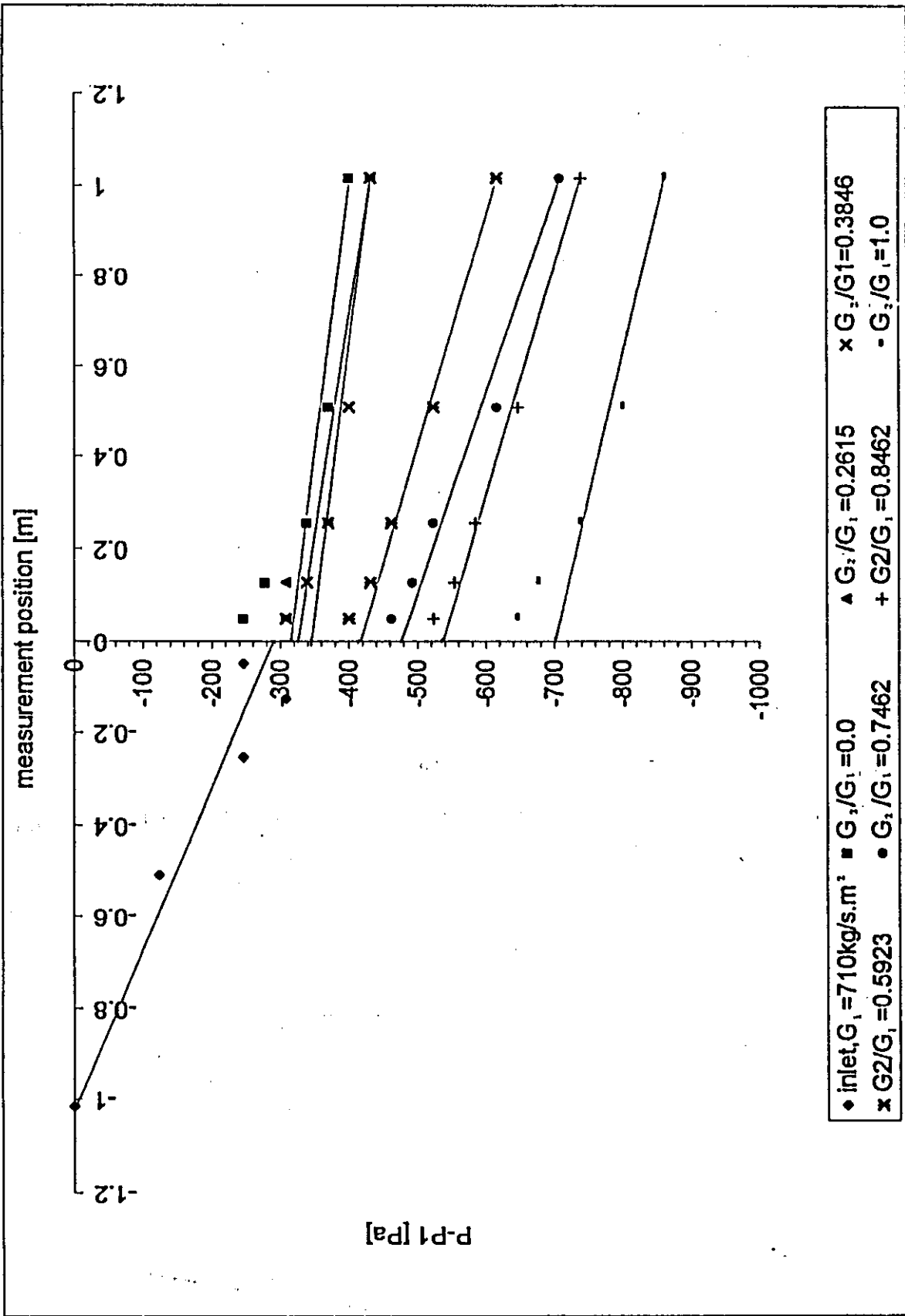
Figure (4.1) Schematic diagram of a typical single-phase flow pressure distribution in dividing T-junction
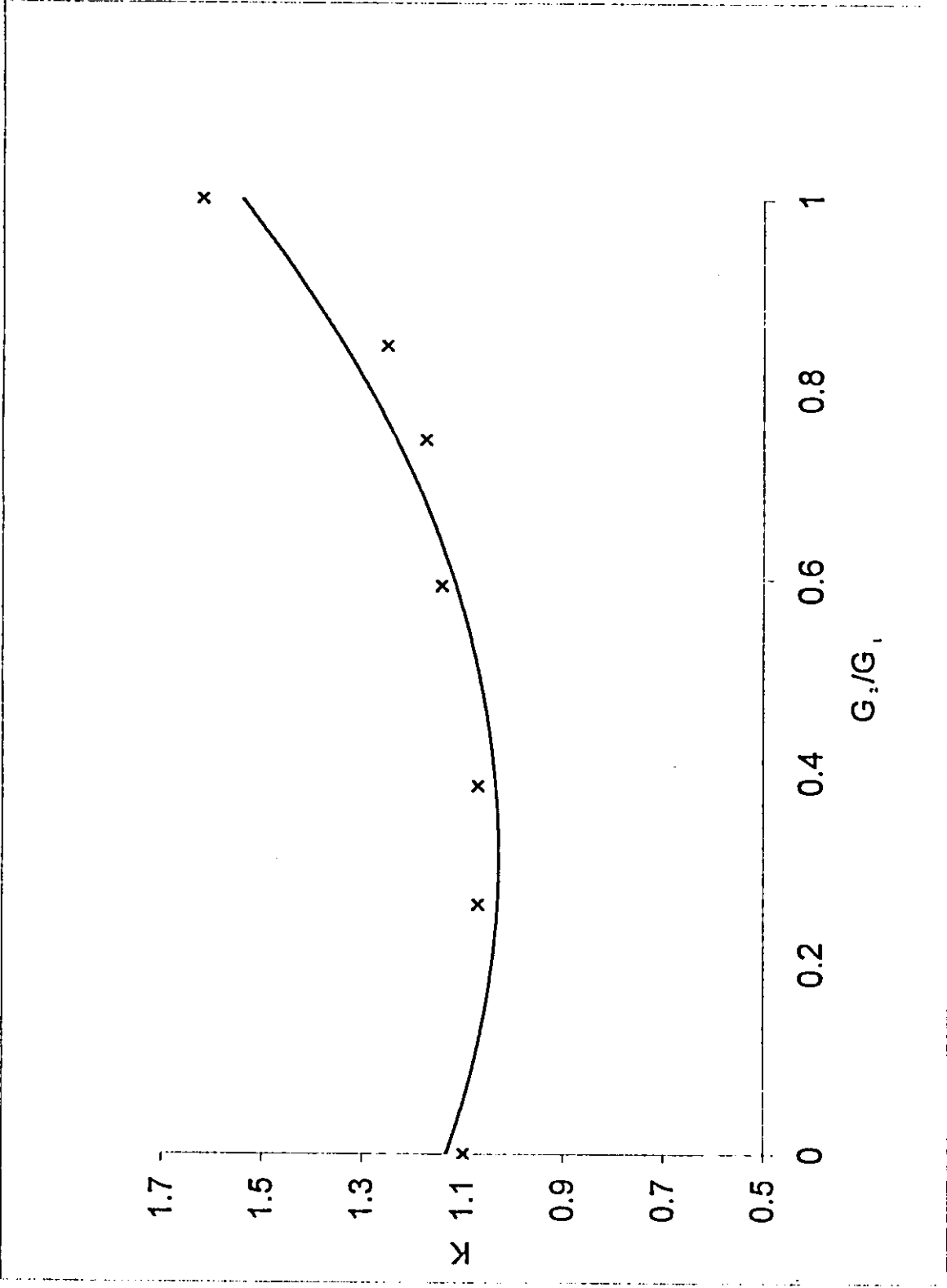
Figure (4.2) Present single-phase flow loss coefficient, k
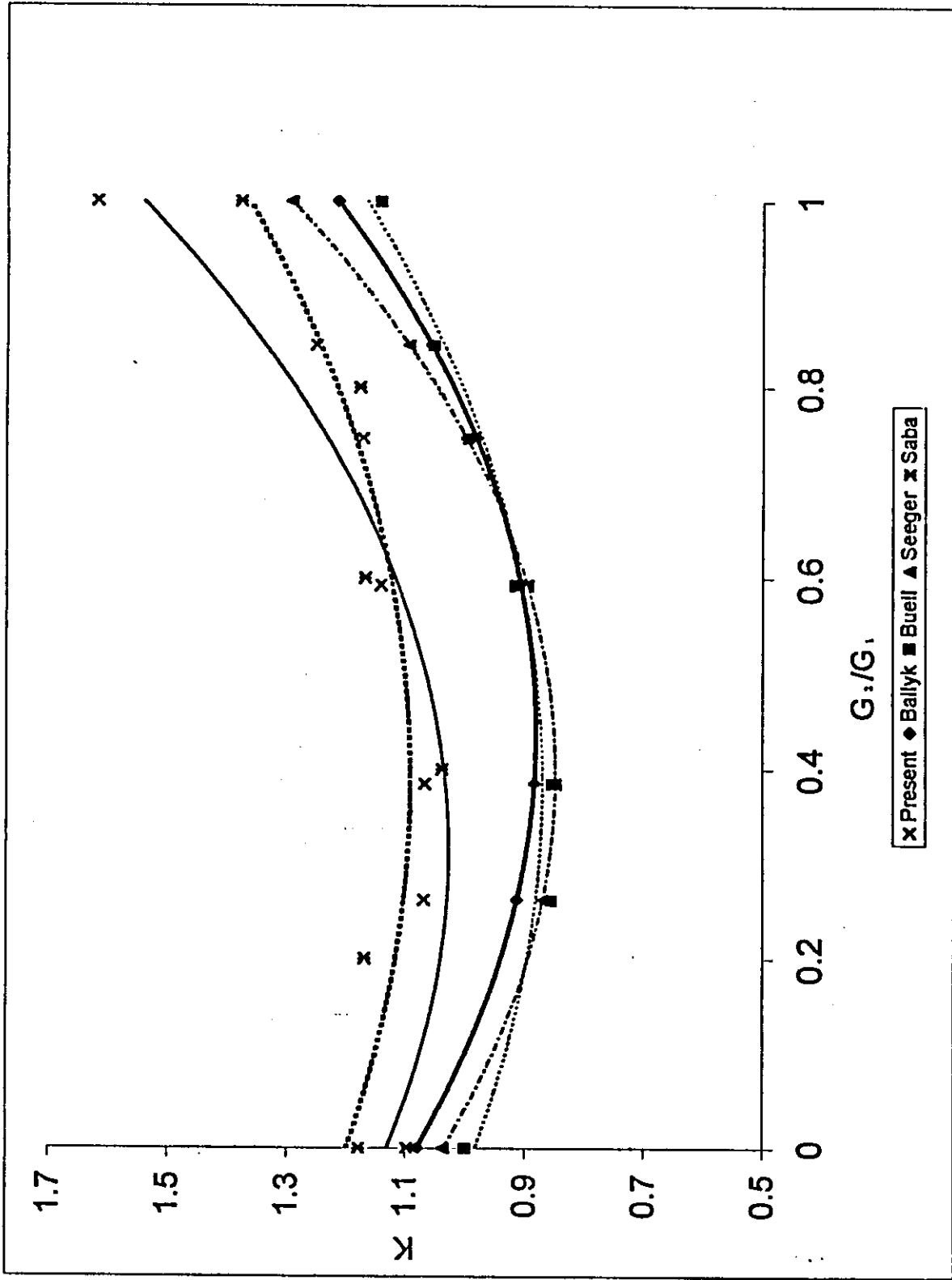
Figure (4.3) Single-phase flow loss coefficient, k

Legend: **✕** Present ◆ Ballyk ■ Buell ▲ Seeger **✕** Saba

Axis labels: K (vertical axis, values 0.5 to 1.7), G_3/G_1 (horizontal axis, values 0 to 1)

61
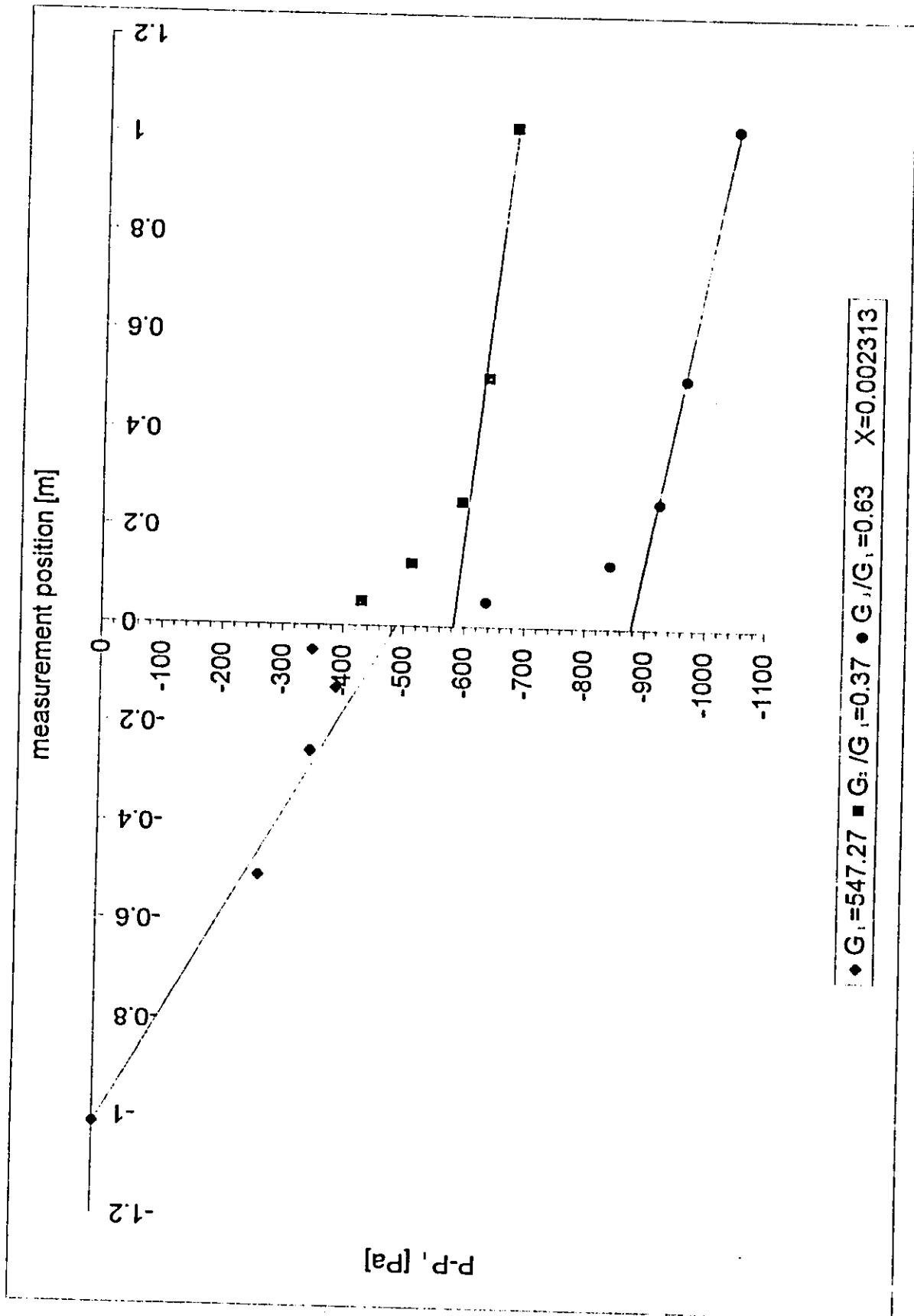
Figure (4.4) Schematic diagram of a typical two-phase flow pressure distribution in dividing T-junction

Legend: $G_1 = 547.27$ ■ $G_2/G_1 = 0.37$ ● $G_3/G_1 = 0.63$ X=0.002313
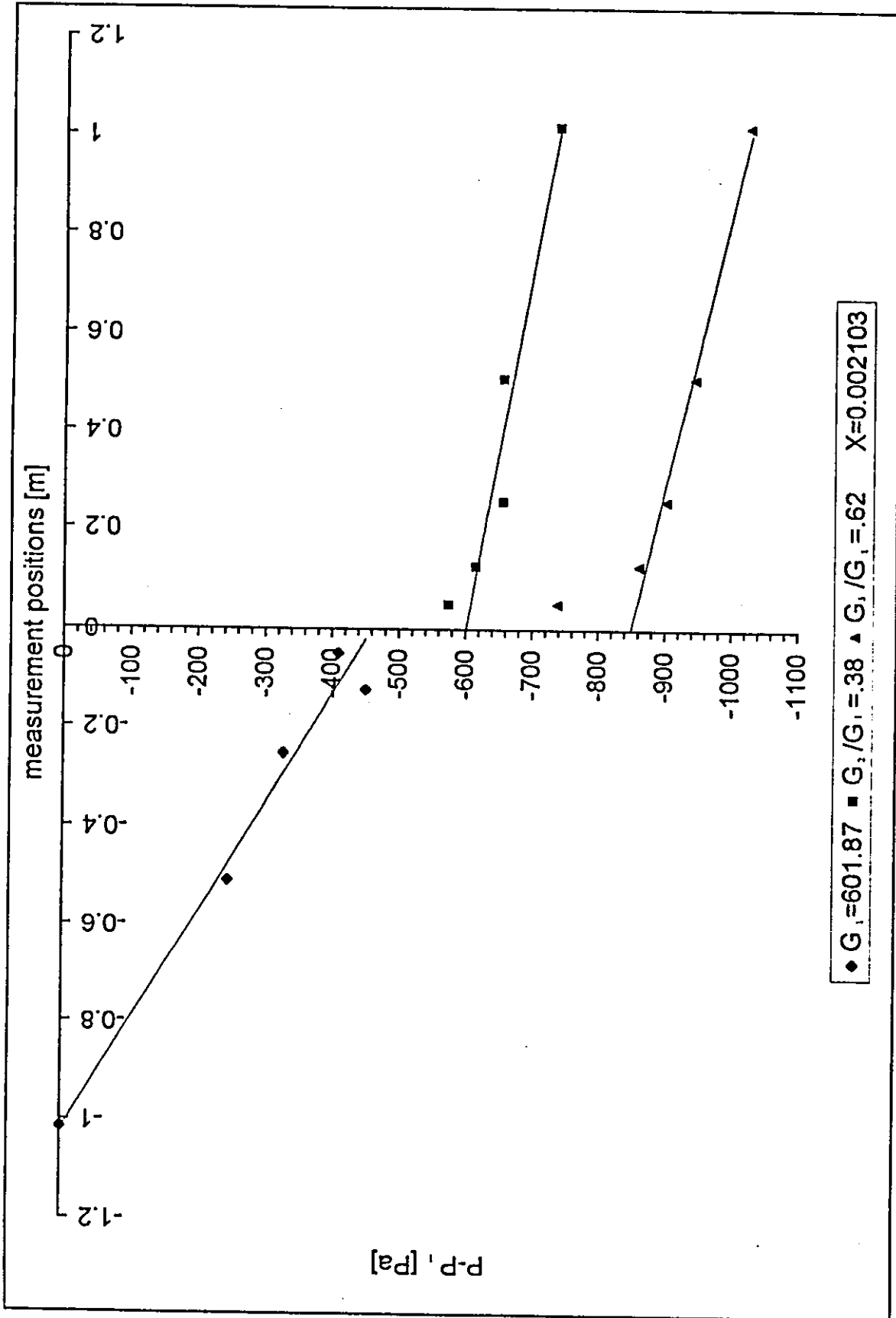
Figure (4.5) Schematic diagram of a typical two-phase flow pressure distribution in dividing T-junction
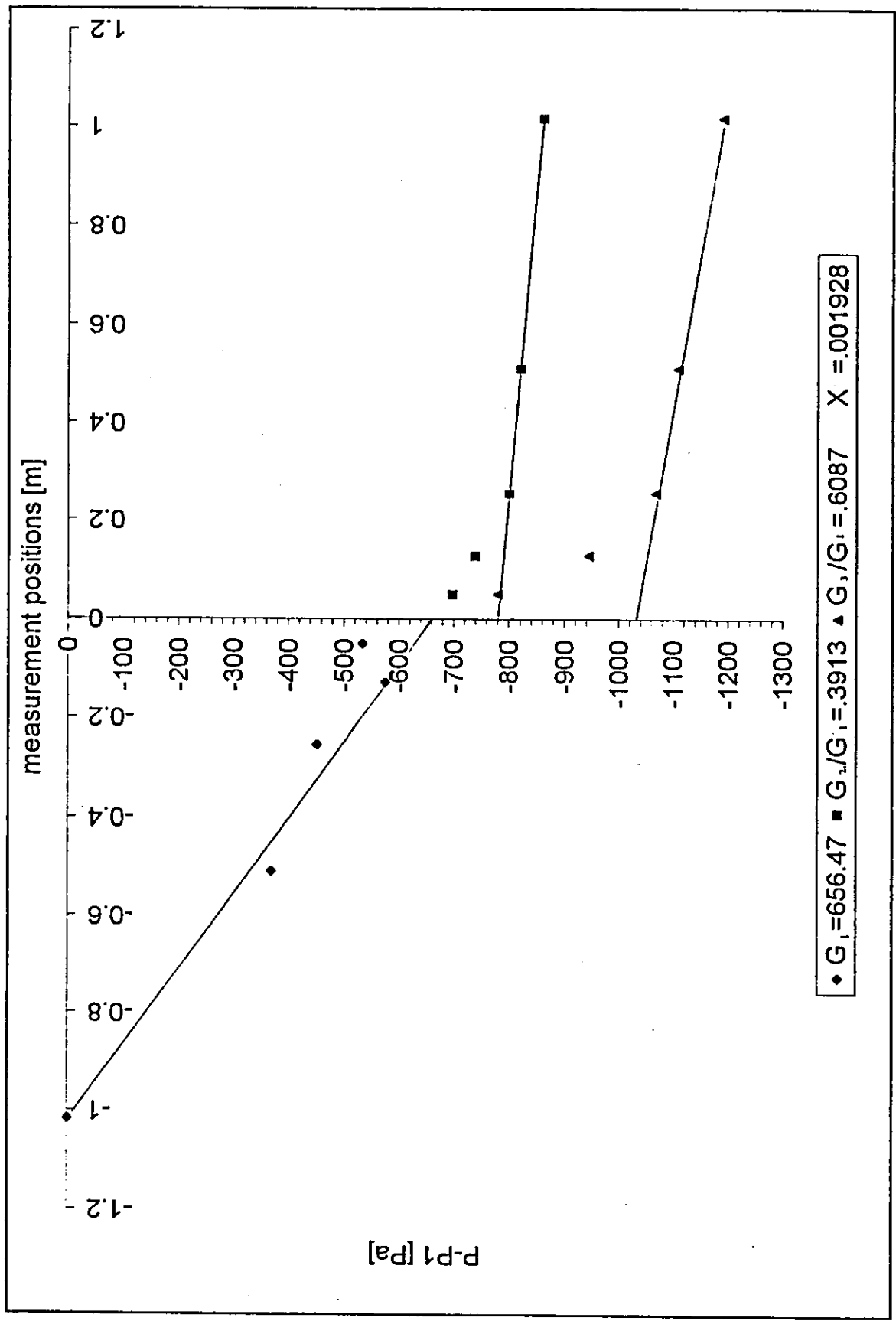
Figure (4.6) Schematic diagram of a typical two-phase flow pressure distribution in dividing T-junction
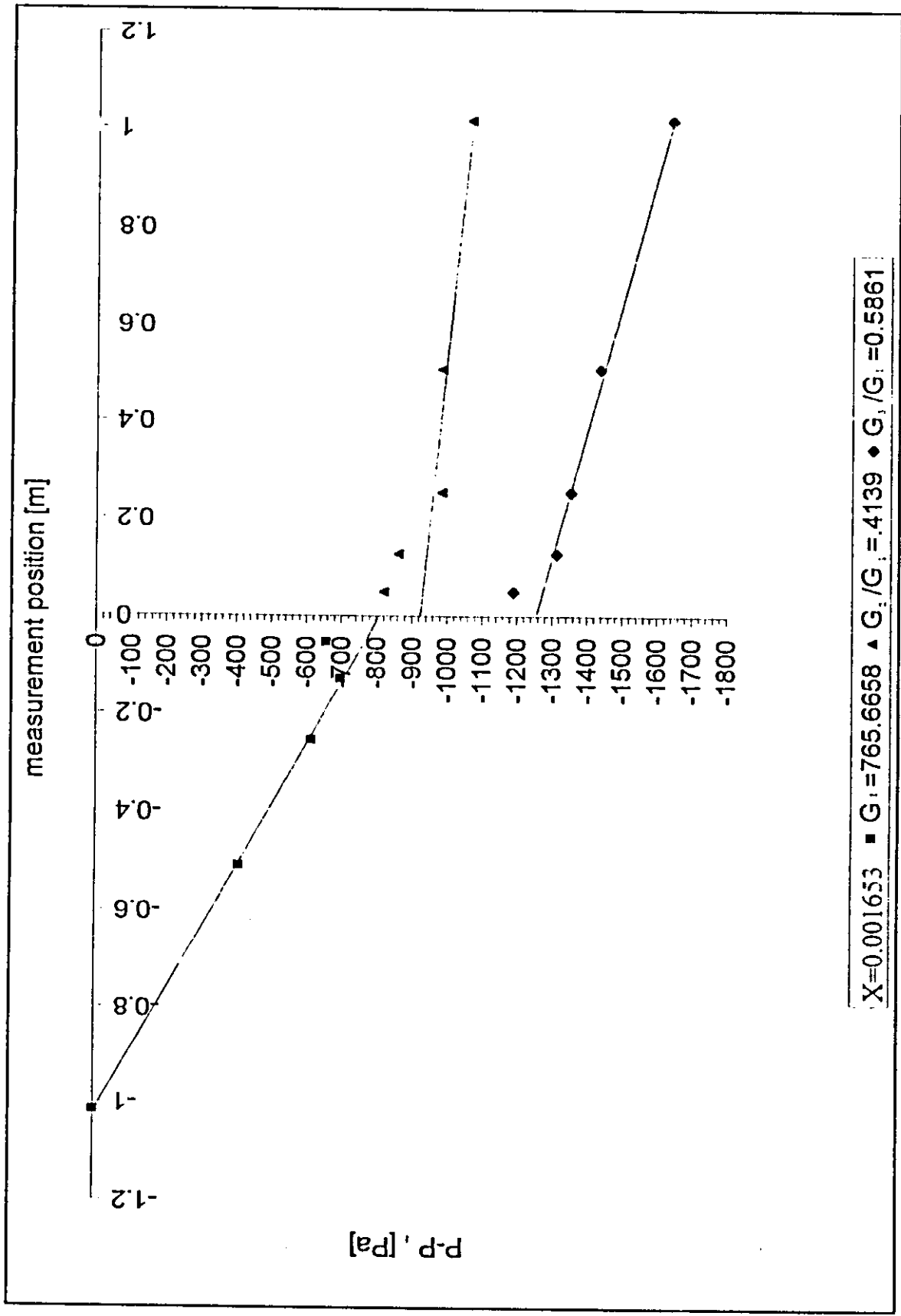
Figure (4.7) Schematic diagram of a typical two-phase flow pressure distribution in dividing T-junction

X=0.001653   ■ G₁=765.6658   ▲ G₃/G₁=.4139   ♦ G₂/G₁=0.5861
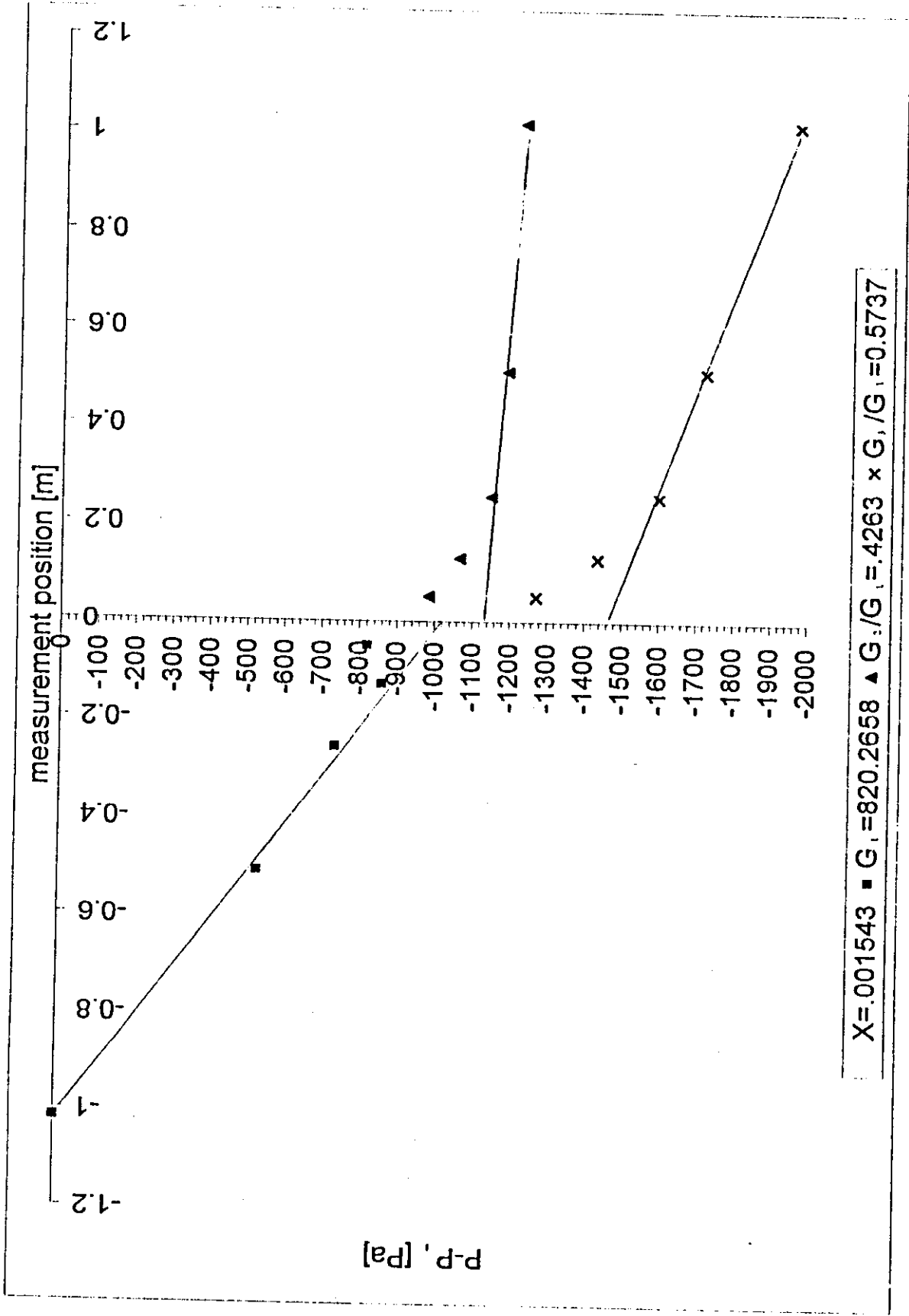
Figure (4.8) Schematic diagram of a typical two-phase flow pressure distribution in dividing T-junction

$X=.001543$ ■ $G_L =820.2658$ ▲ $G_3/G_1 =.4263$ × $G_1/G_1 =0.5737$

measurement position [m]

P-P , [Pa]
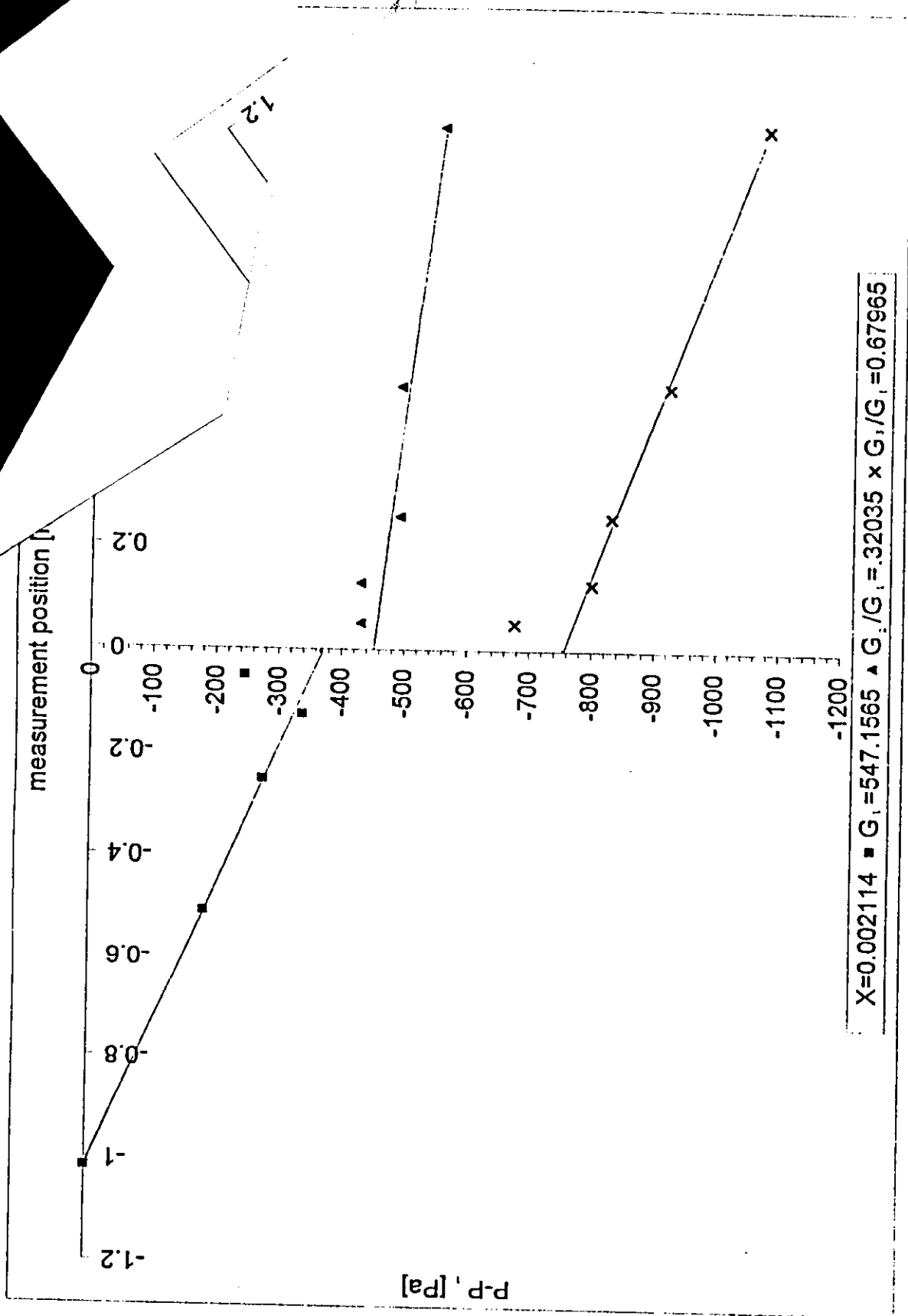
Figure (4.9) Schematic diagram of a typical two-phase flow pressure distribution in dividing T-junction

$$X=0.002114 \quad \blacksquare \quad G_1=547.1565 \quad \blacktriangle \quad G_3/G_1=.32035 \quad \times \quad G_2/G_1=0.67965$$
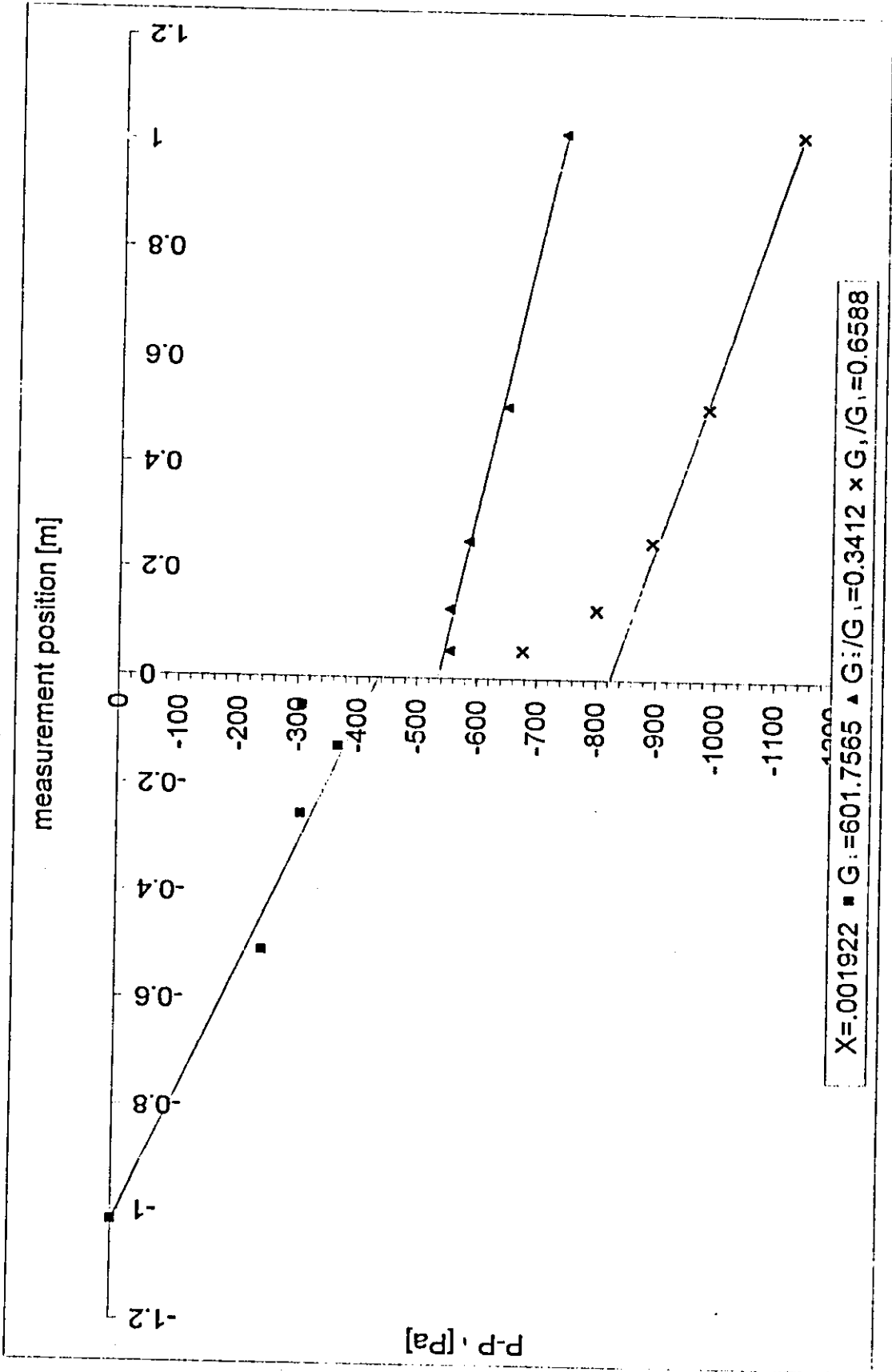
Figure (4.10) Schematic diagram of a typical two-phase flow pressure distribution in dividing T-junction

$X = .001922$ ■ $G_i = 601.7565$ ▲ $G_i/G_i = 0.3412$ × $G_i/G_i = 0.6588$
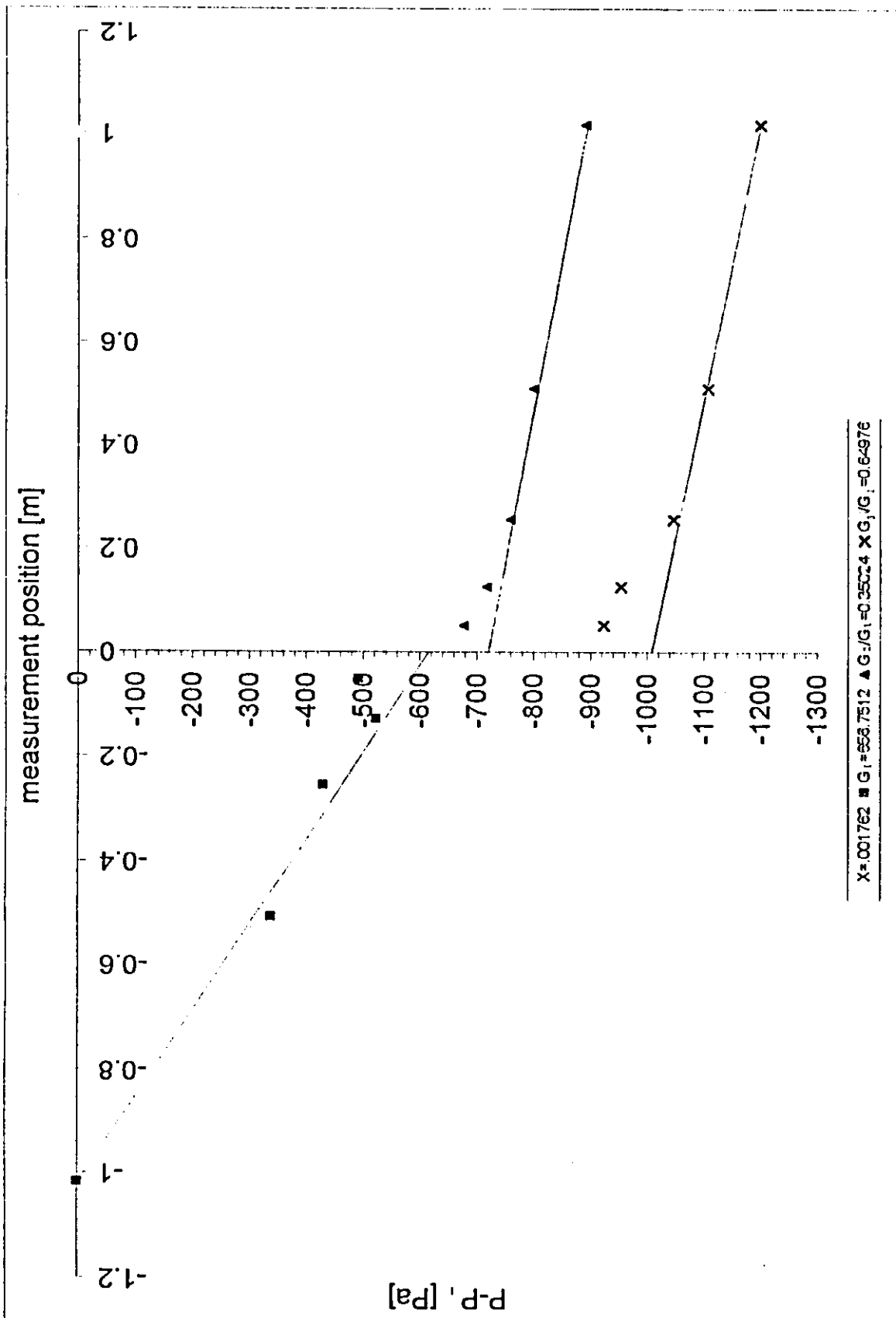
Figure (4.11) Schematic diagram of a typical two-phase flow pressure distribution in dividing T-junction
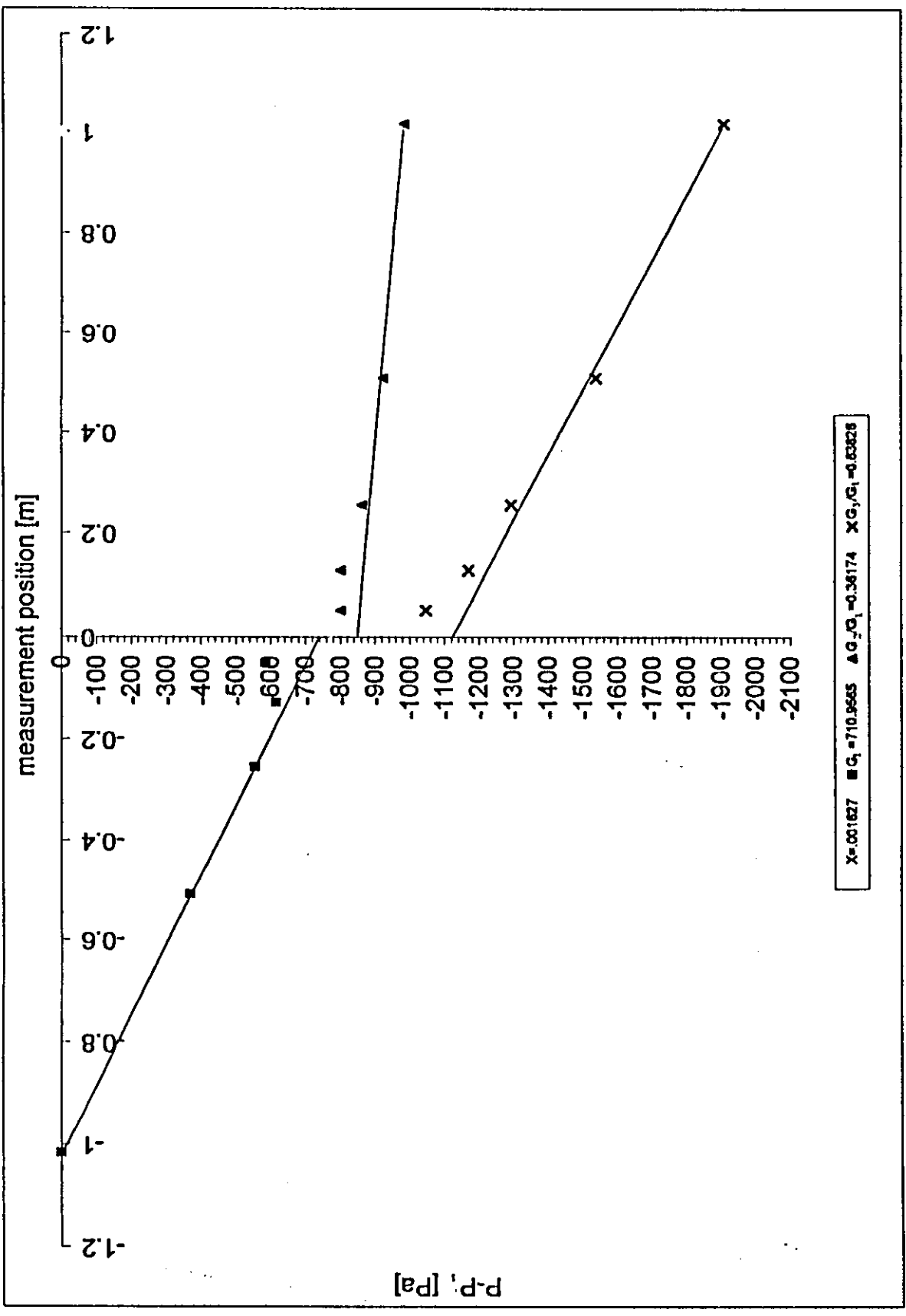
Figure (4.12) Schematic diagram of a typical two-phase flow pressure distribution in dividing T-junction

70
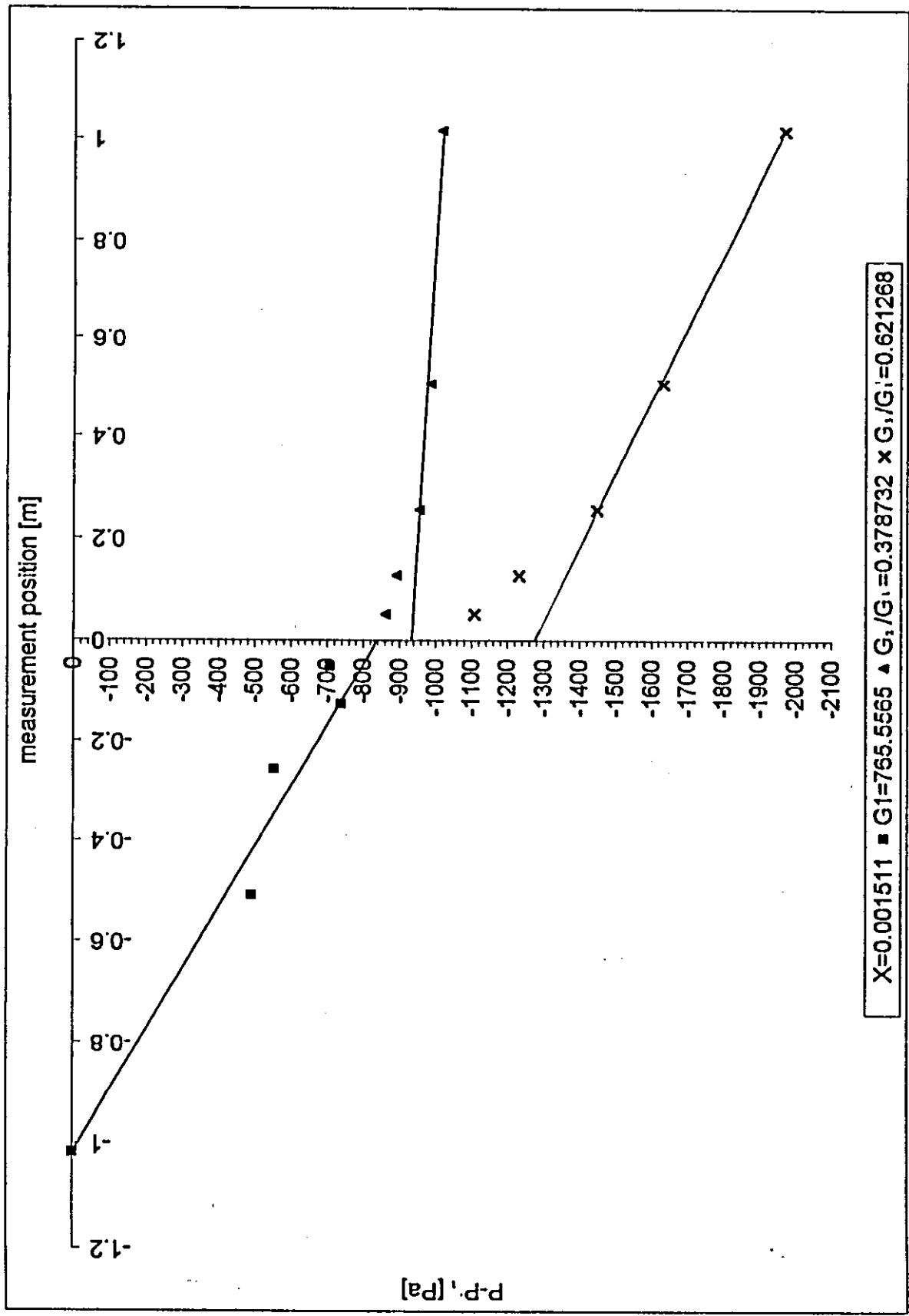
Figure (4.13) Schematic diagram of a typical two-phase flow pressure distribution in dividing T-junction

X=0.001511 ■ G₁=755.5565 ▲ G₃/G₁=0.378732 ✕ G₂/G₁=0.621268
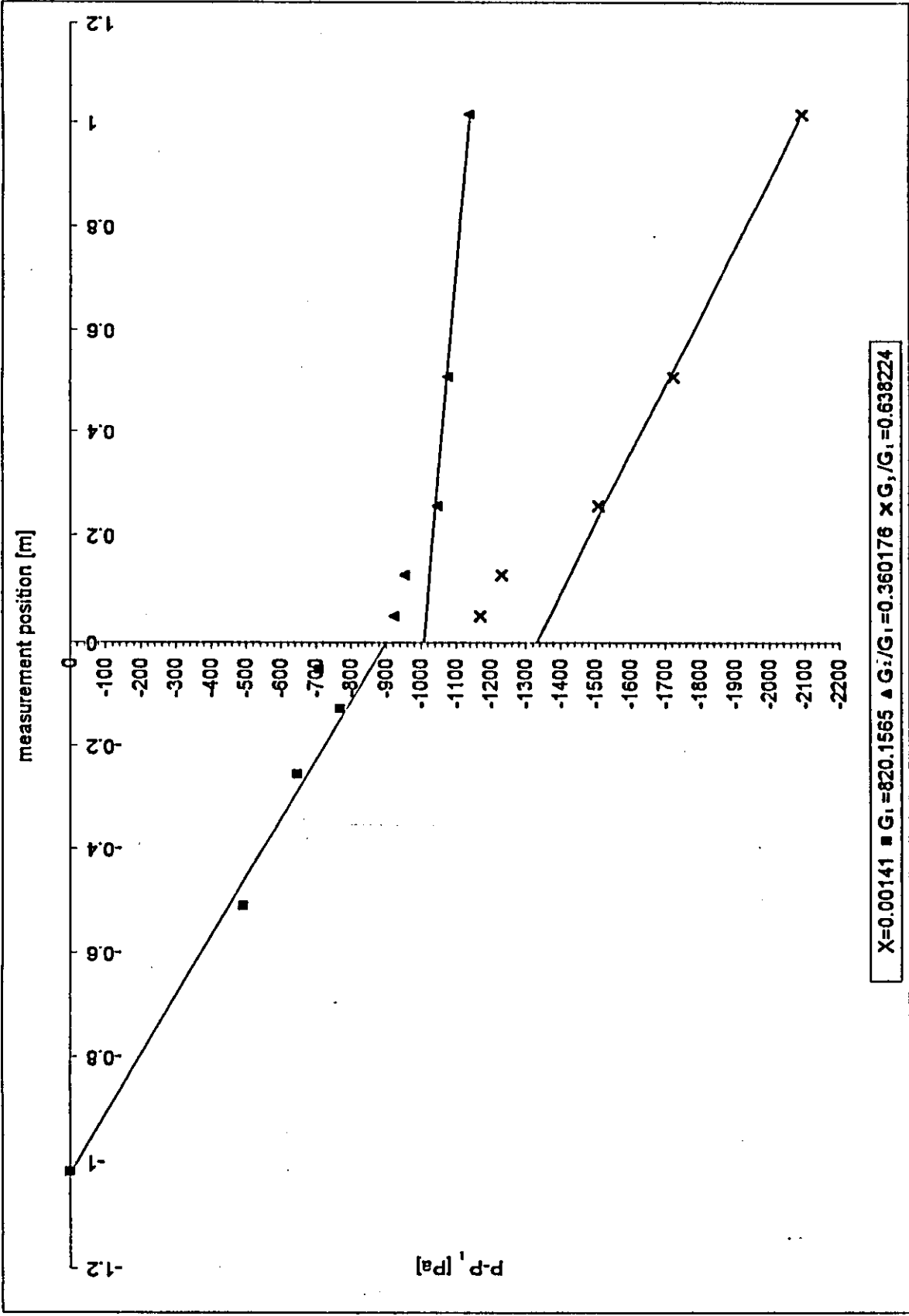
Figure (4.14) Schematic diagram of a typical two-phase flow pressure distribution in dividing T-junction

X=0.00141 ■ G₁=820.1565 ▲ G₂/G₁=0.360176 ✕ G₃/G₁=0.638224
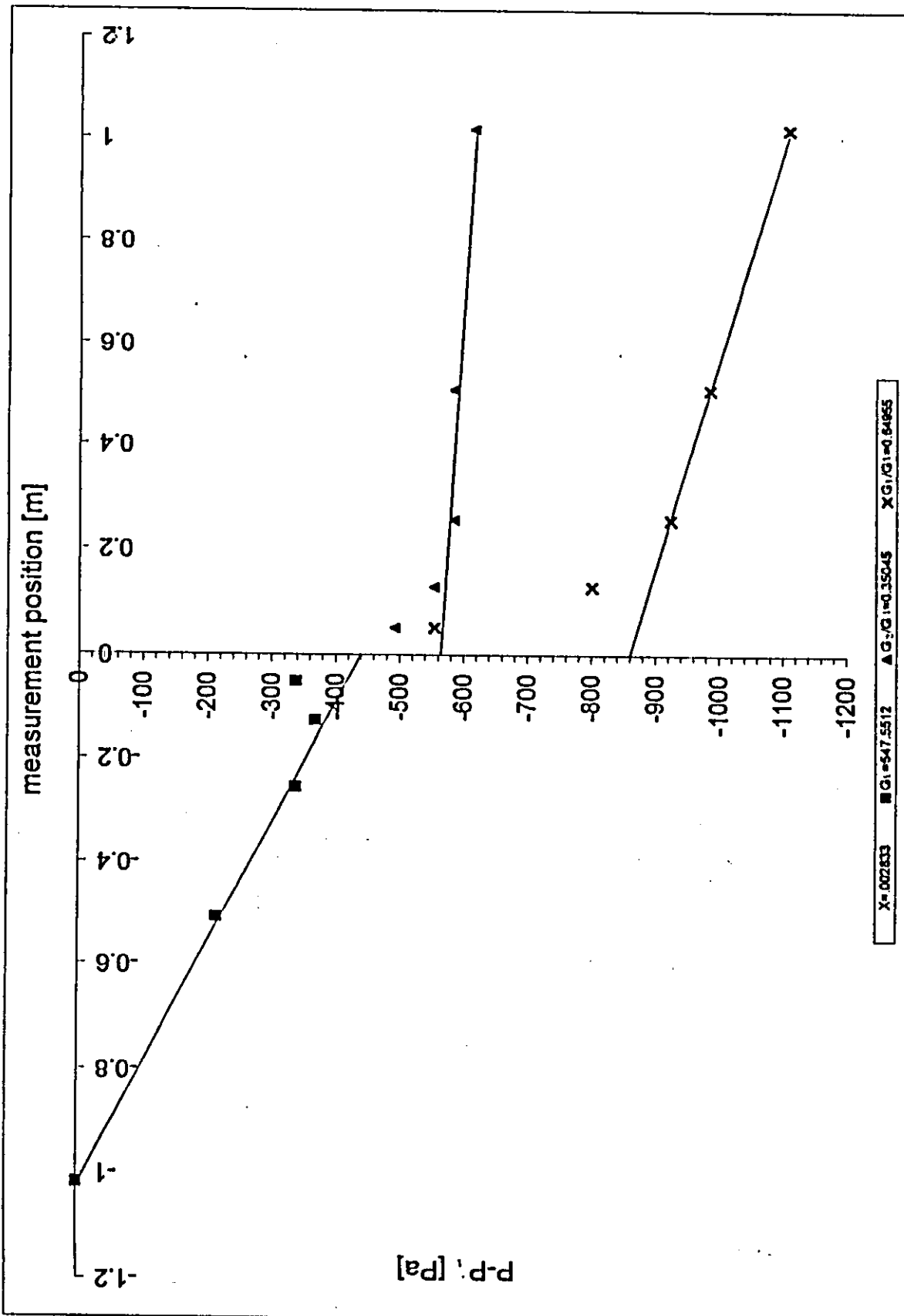
Figure (4.15) Schematic diagram of a typical two-phase flow pressure distribution in dividing T-junction

73
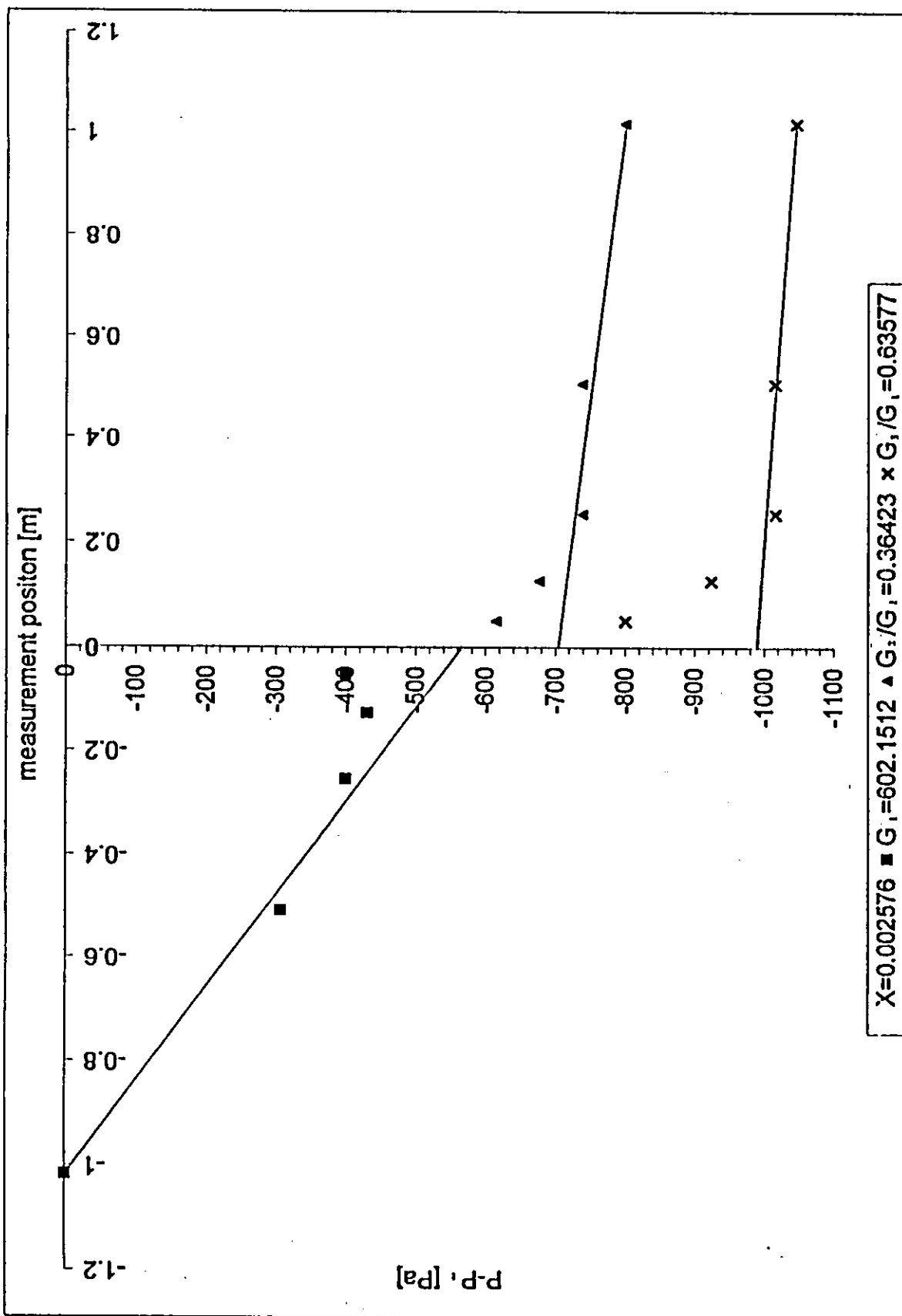
Figure (4.16) Schematic diagram of a typical two-phase flow pressure distribution in dividing T-junction

X=0.002576 ■ G₁=602.1512 ▲ G₂/G₁=0.36423 × G₃/G₁=0.63577
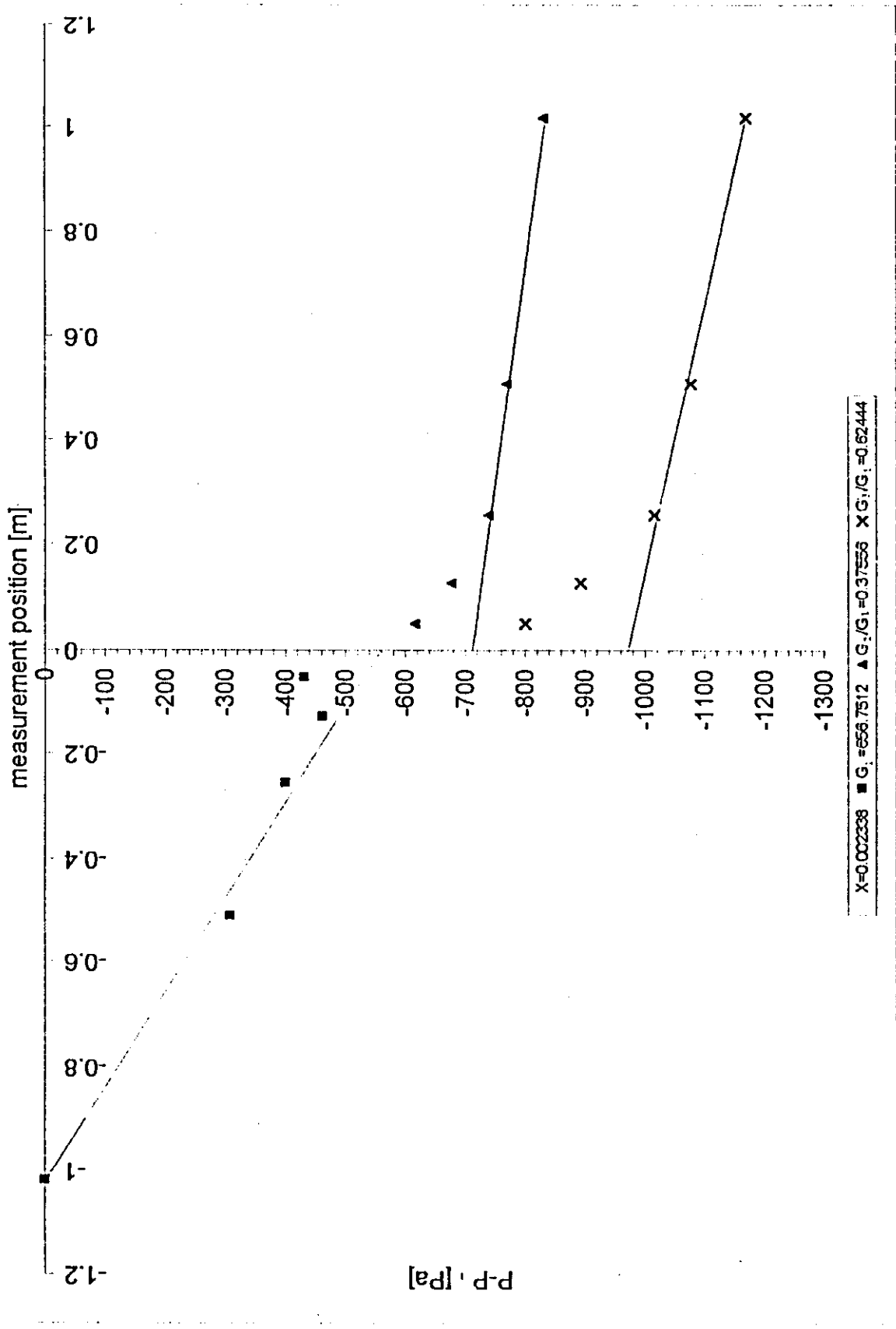
Figure (4.17) Schematic diagram of a typical two-phase flow pressure distribution in dividing T-junction
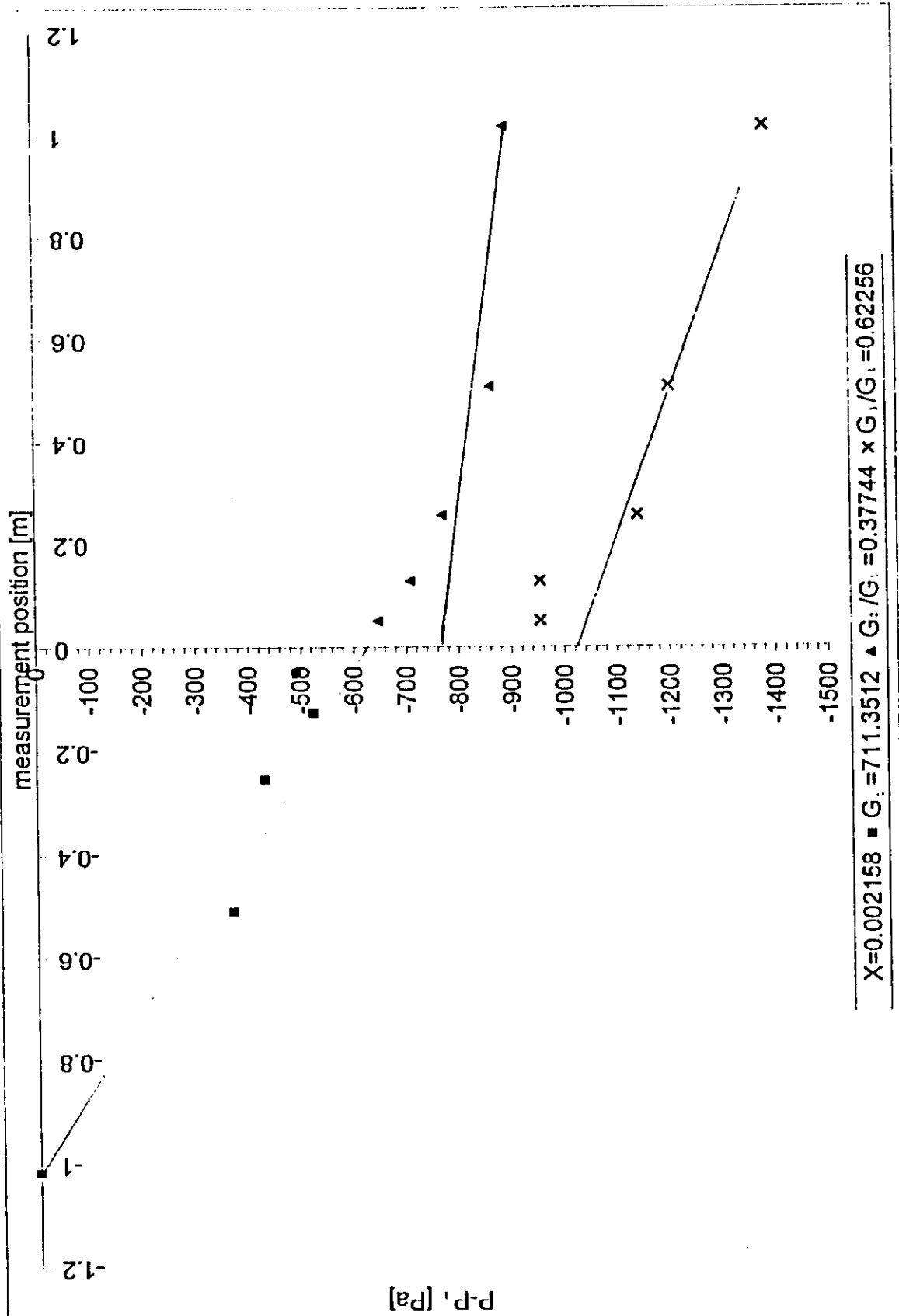
Figure (4.18) Schematic diagram of a typical two-phase flow pressure distribution in dividing T-junction

X=0.002158   ■ G₁ =711.3512   ▲ G₂/G₁ =0.37744   × G₃/G₁ =0.62256
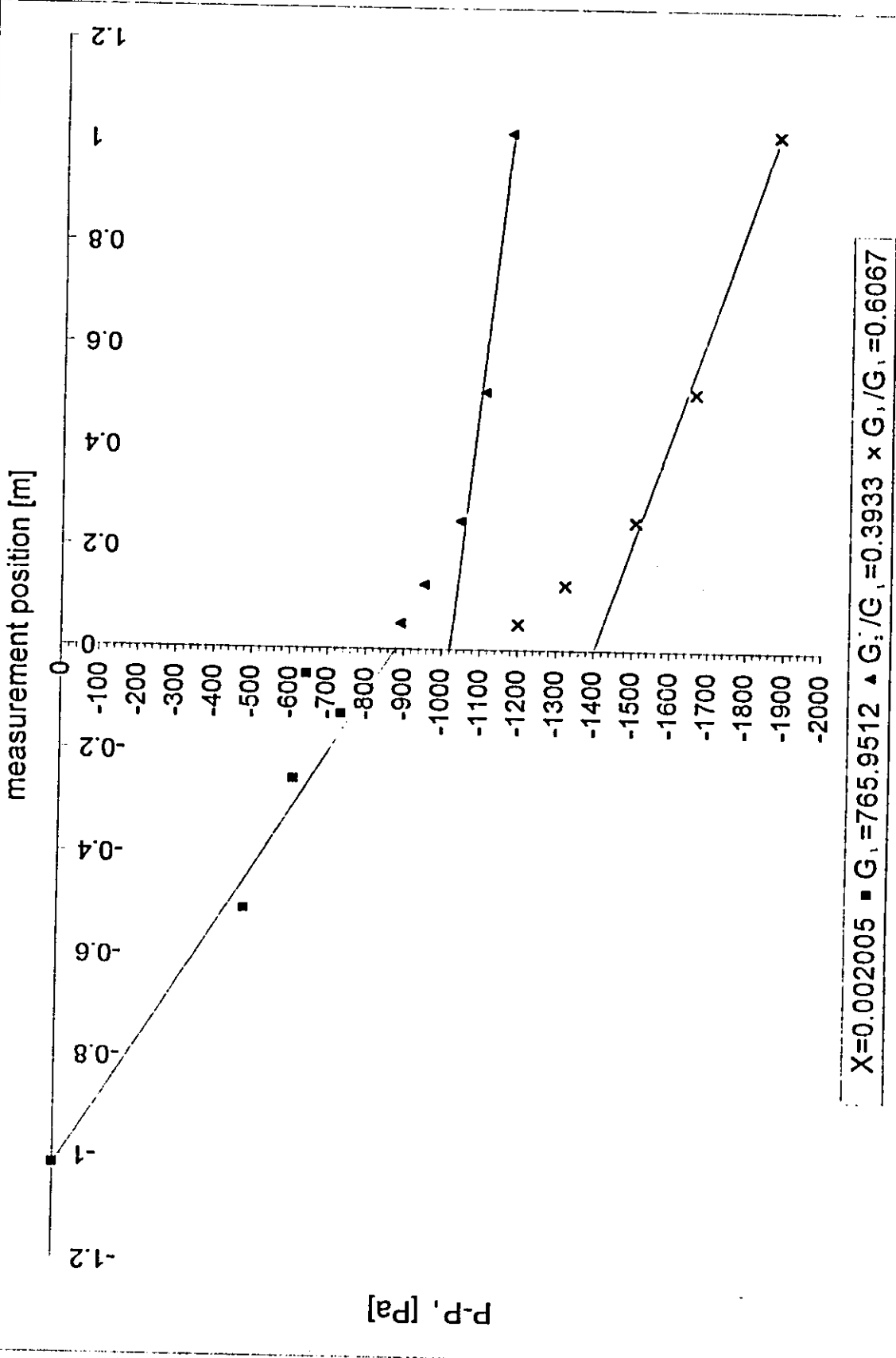
Figure (4.19) Schematic diagram of a typical two-phase flow pressure distribution in dividing T-junction

$X=0.002005$ ■ $G_1 = 765.9512$ ▲ $G_3/G_1 = 0.3933$ × $G_2/G_1 = 0.6067$

measurement position [m]

P-P₁ [Pa]
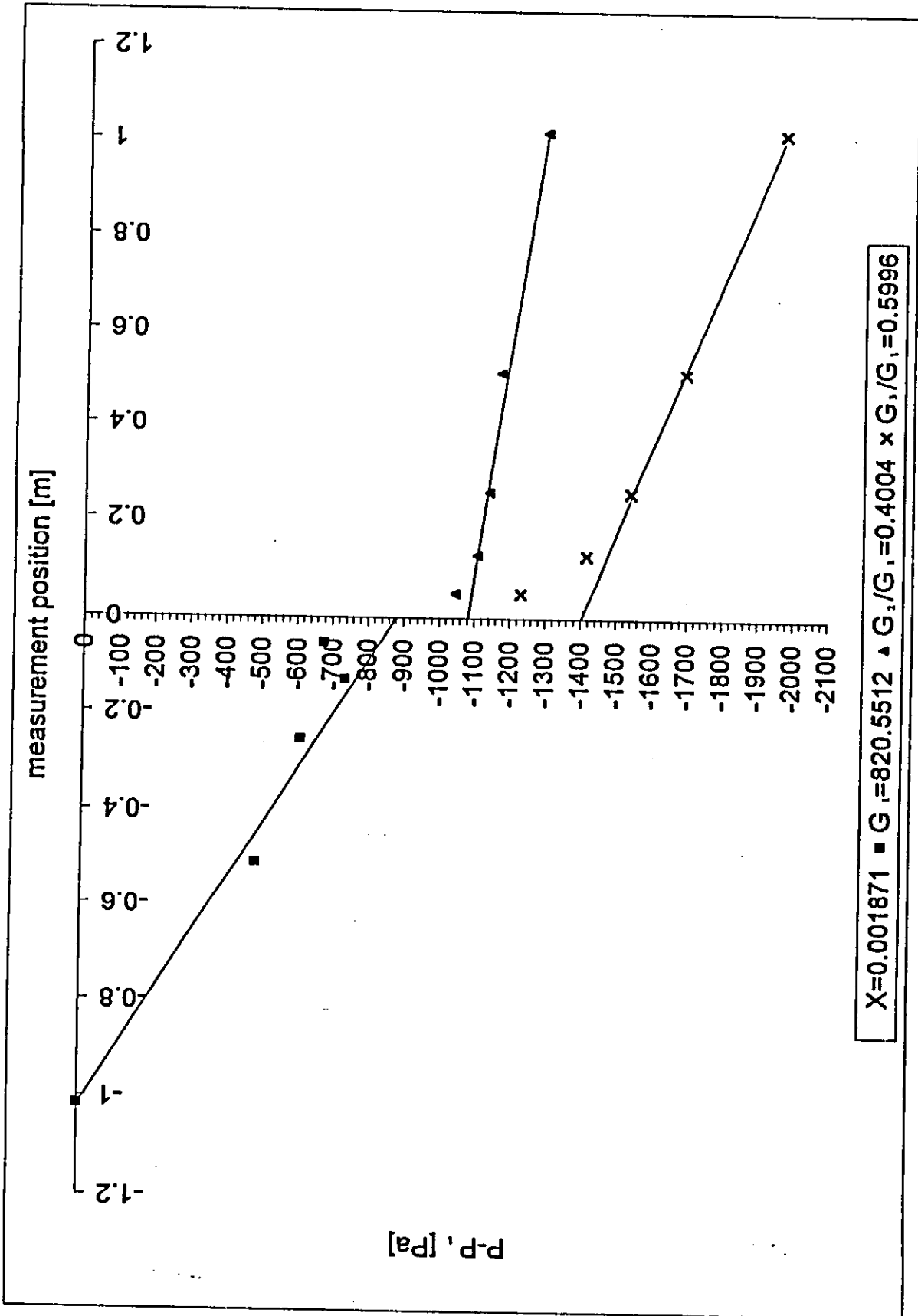
Figure (4.20) Schematic diagram of a typical two-phase flow pressure distribution in dividing T-junction

$X=0.001871$ $G_1=820.5512$ $G_3/G_1=0.4004 \times G_1/G_1=0.5996$
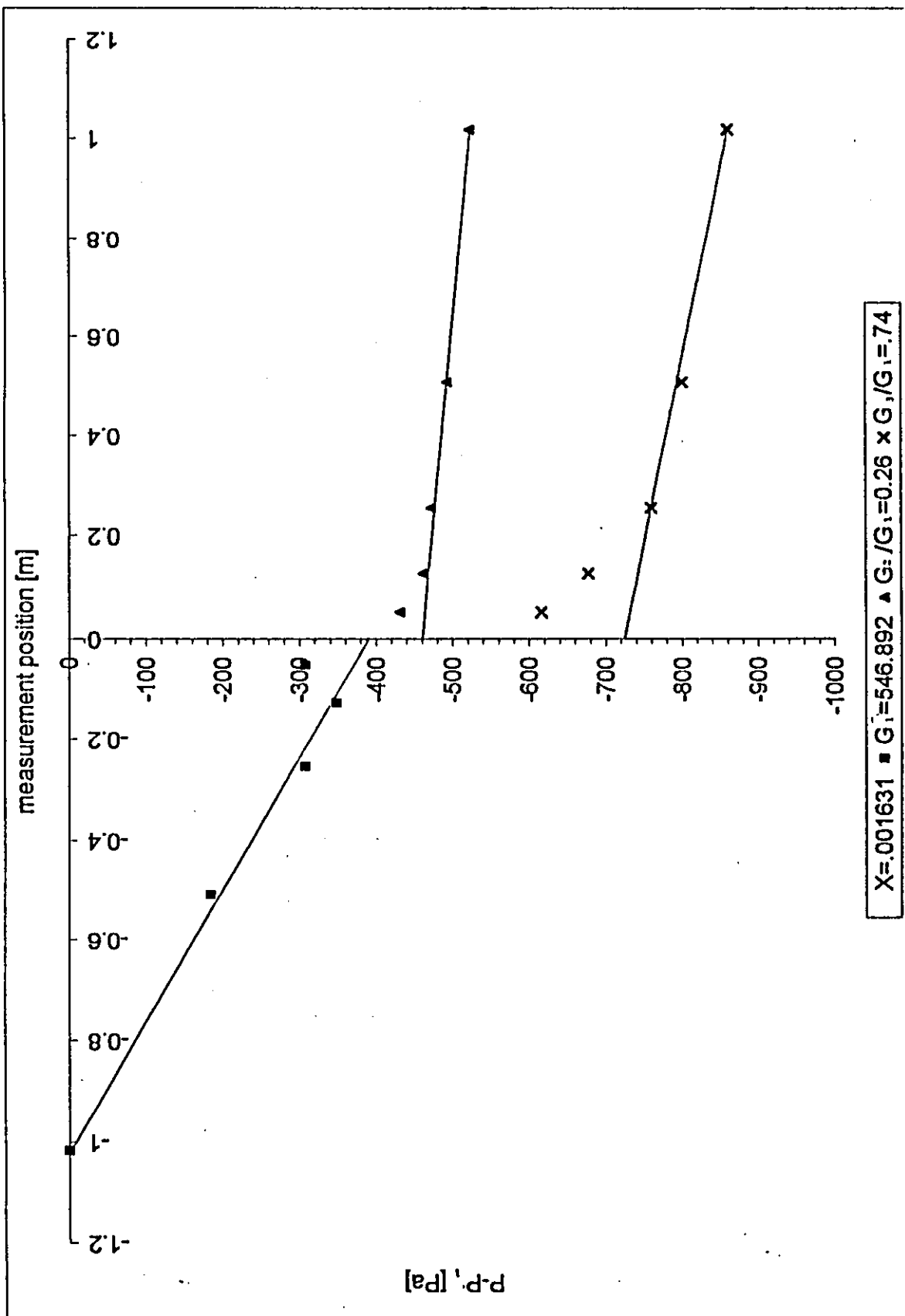
Figure (4.21) Schematic diagram of a typical two-phase flow pressure distribution in dividing T-junction

Graph legend: X=.001631 ■ G_1^-=546.892 ▲ G_2/G_1=0.26 × G_3/G_1=.74

x-axis: measurement position [m]

y-axis: P-P, [Pa]
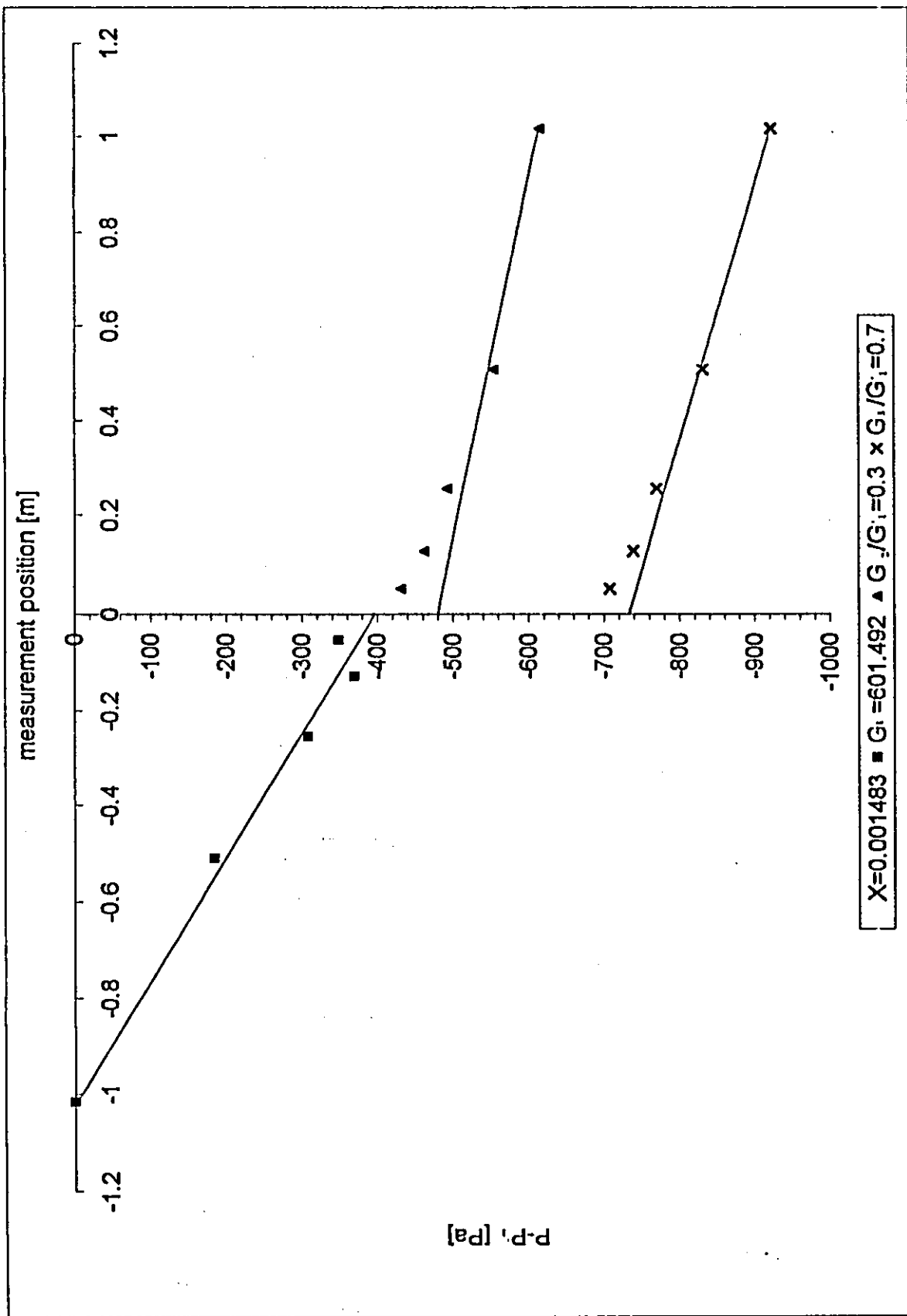
Figure (4.22) Schematic diagram of a typical two-phase flow pressure distribution in dividing T-junction
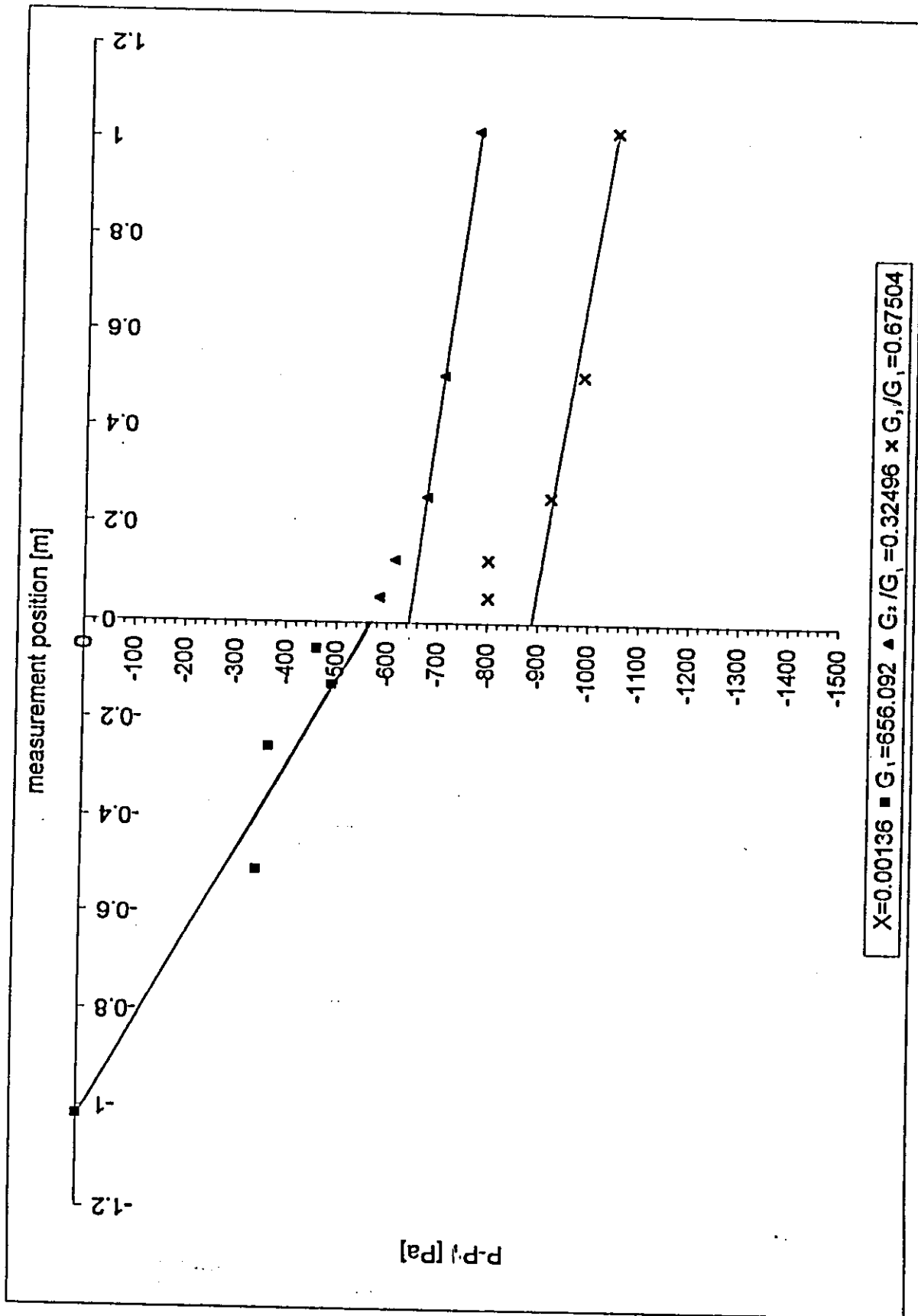
Figure (4.23) Schematic diagram of a typical two-phase flo pressure distribution in dividing T-junction

X=0.00136 ■ G₁=656.092 ▲ G₂/G₁ =0.32496 × G₃/G₁ =0.67504
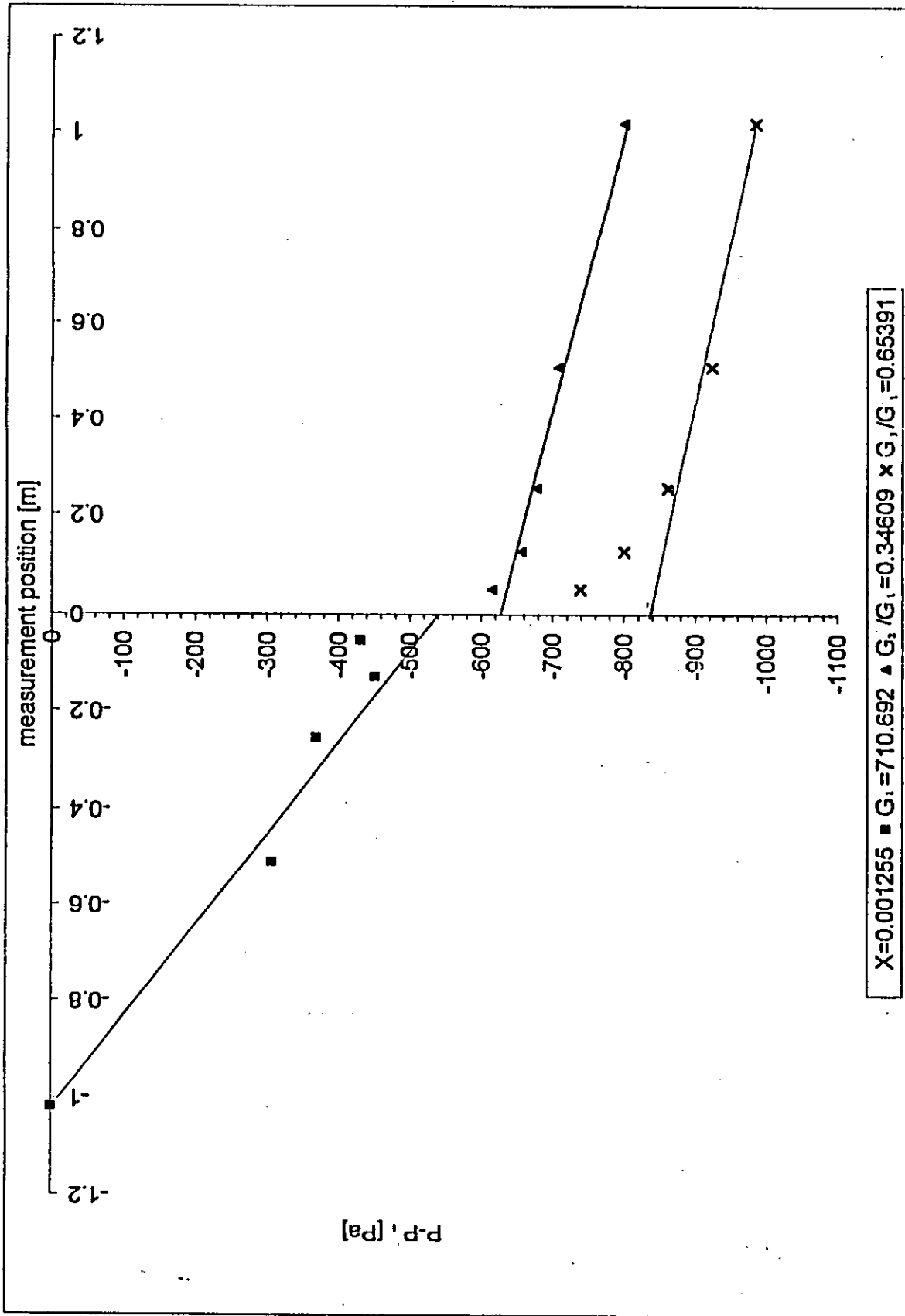
Figure (4.24) Schematic diagram of a typical two-phase flow pressure distribution in dividing T-junction

X=0.001255 ■ G_1=710.692 ▲ G_3/G_1=0.34609 × G_2/G_1=0.65391
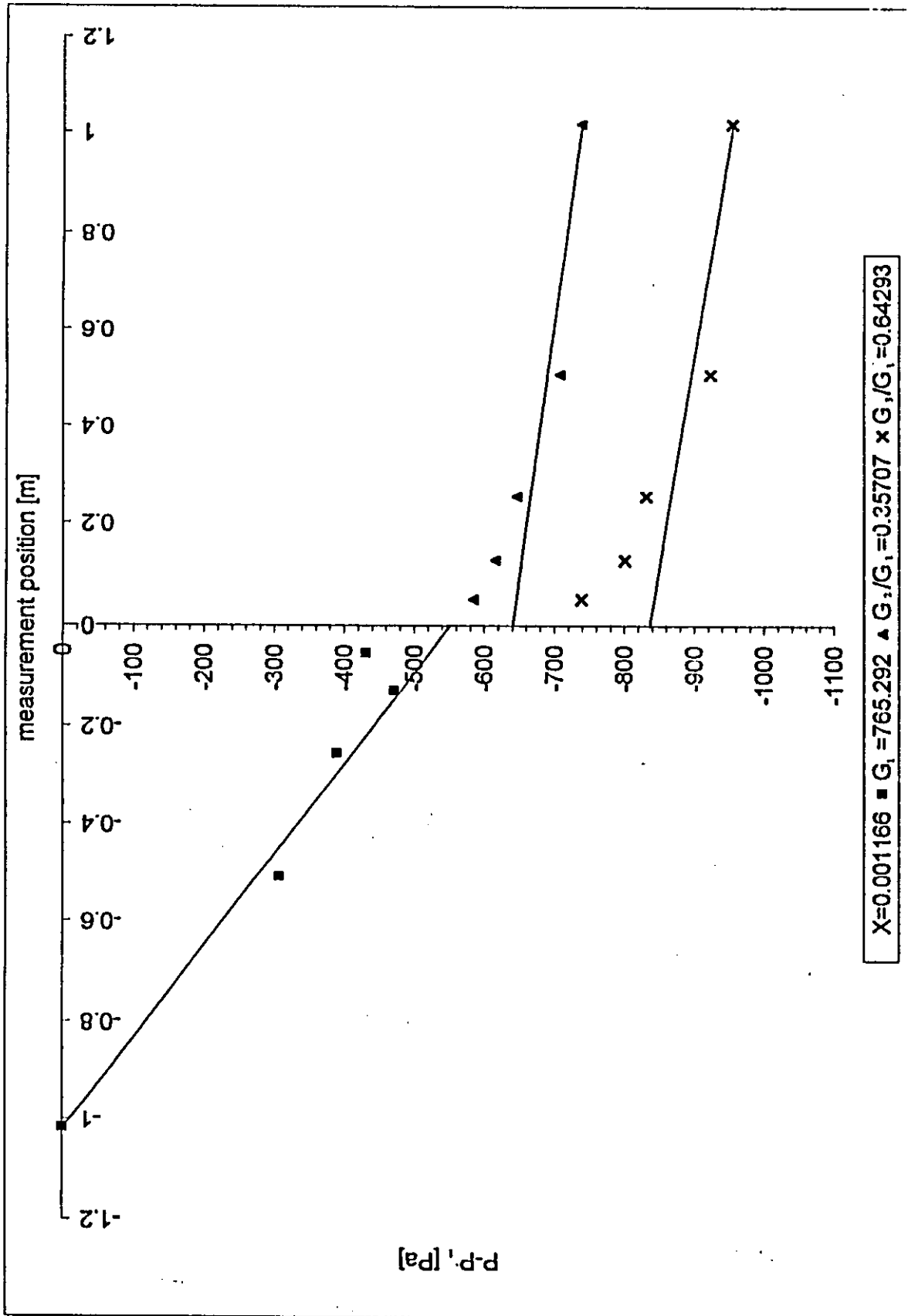
Figure (4.25) Schematic diagram of a typical two-phase flow pressure distribution in dividing T-junction

$X=0.001166$ ■ $G_1=765.292$ ▲ $G_2/G_1=0.35707$ × $G_3/G_1=0.64293$

measurement position [m]

P-P', [Pa]
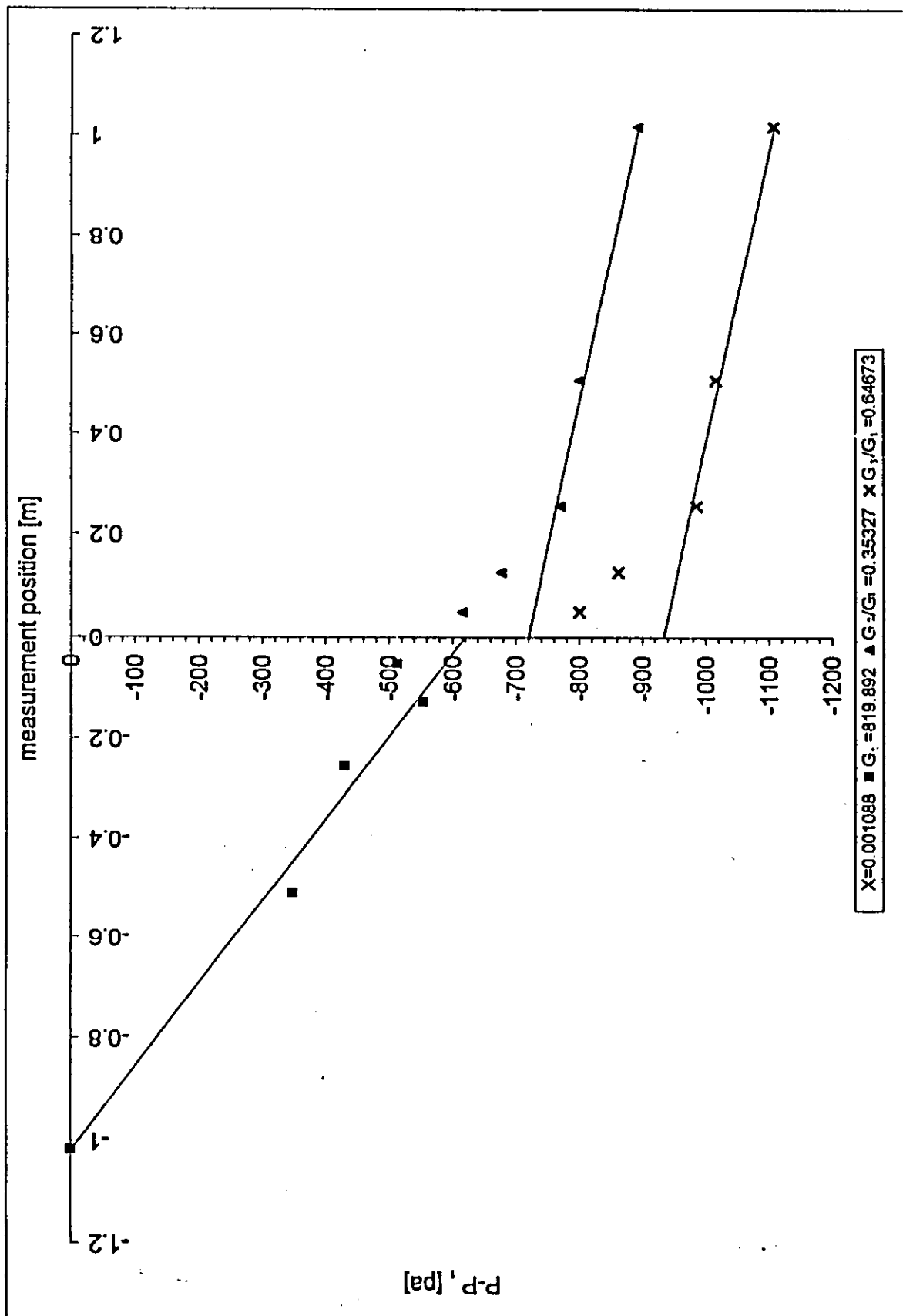
Figure (4.28) Schematic diagram of a typical two-phase flow pressure distribution in dividing T-junction
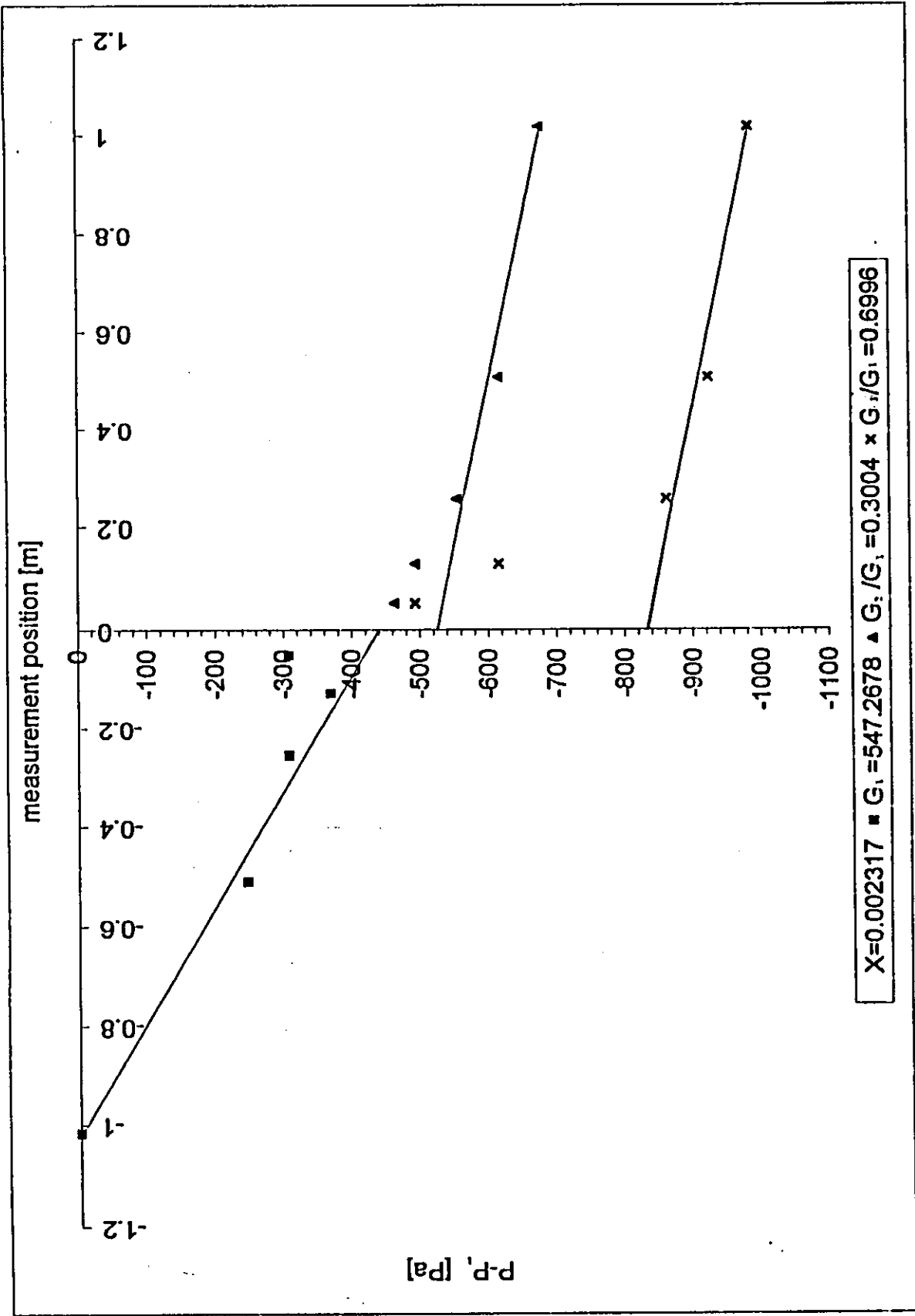
Figure (4.27) Schematic diagram of a typical two-phase flow pressure distribution in dividing T-junction

Legend in figure: X=0.002317 ■ G_1 =547.2678 ▲ G_2/G_1 =0.3004 × G_3/G_1 =0.6996

Axis labels: measurement position [m]; P-P$_1$ [Pa]

Figure (4.28) Schematic diagram of a typical two-phase flow pressure distribution in dividing T-junction

X=0.002106 ■ G₁ =601.8678 ▲ G₃/G₁ =0.35479 × G₂/G₁ =0.64521
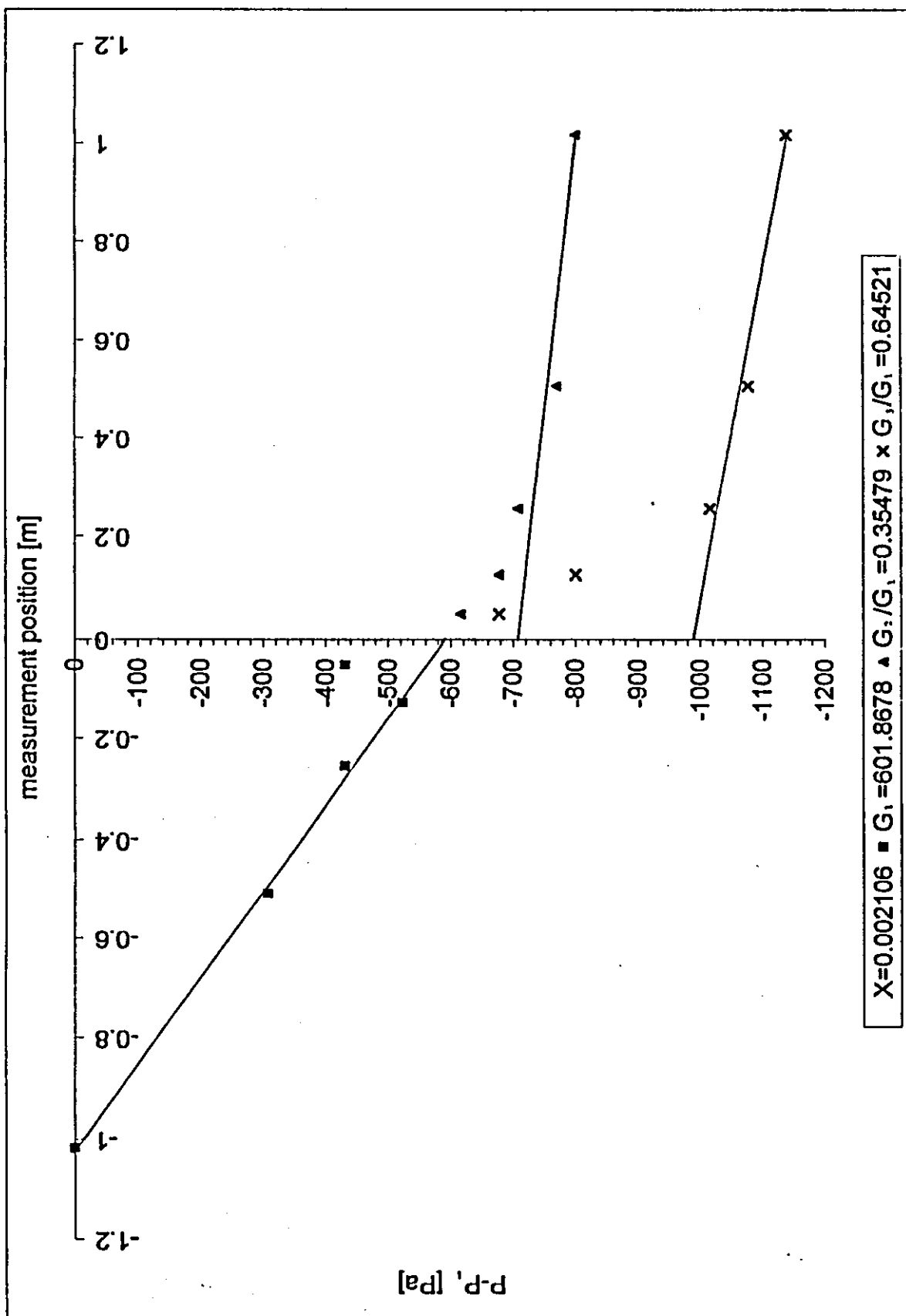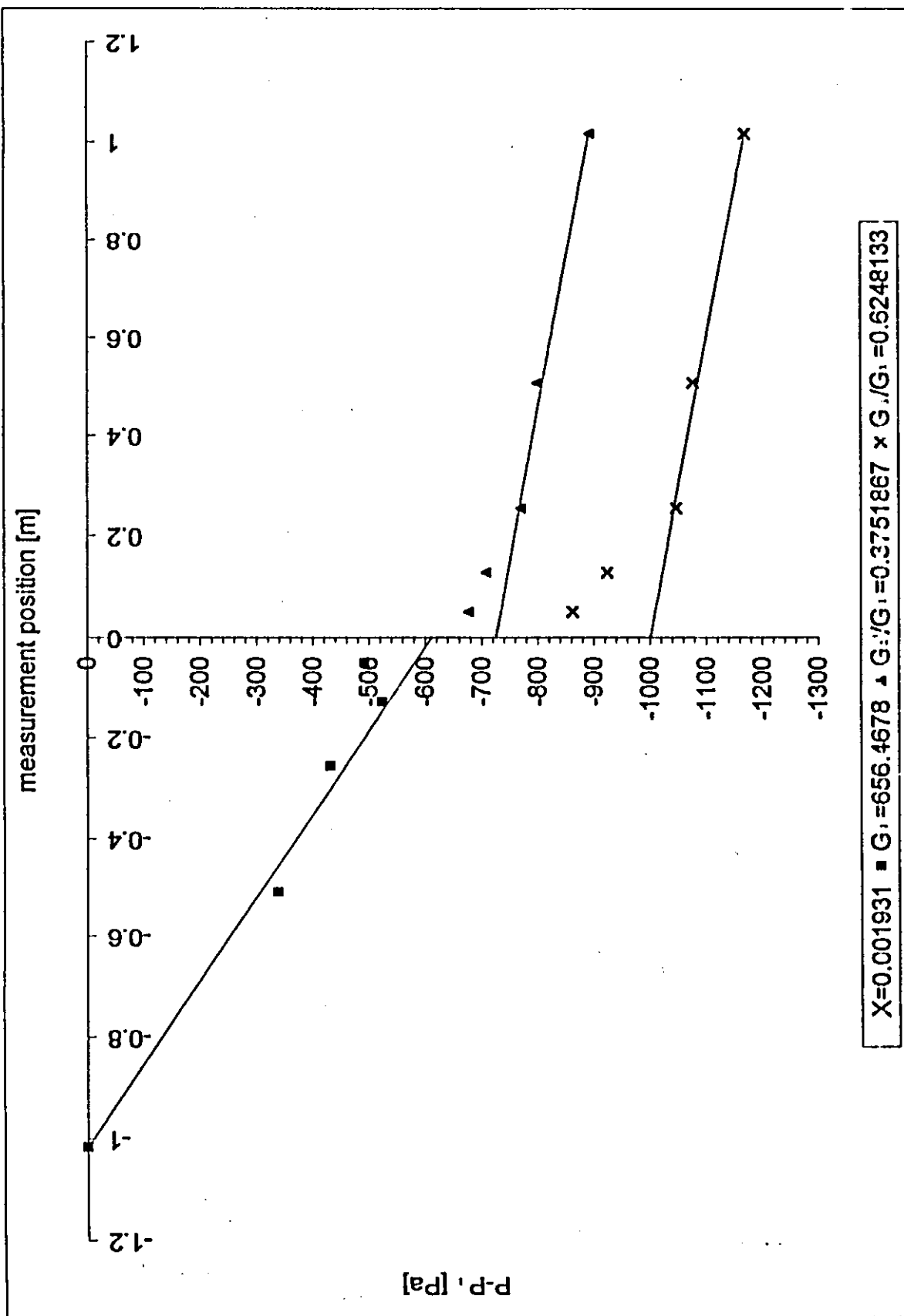
Figure (4.29) Schematic diagram of a typical two-phase flow pressure distribution in dividing T-junction

X=0.001931 ■ G₁=656.4678 ▲ G₂/G₁=0.3751867 × G₃/G₁=0.6248133
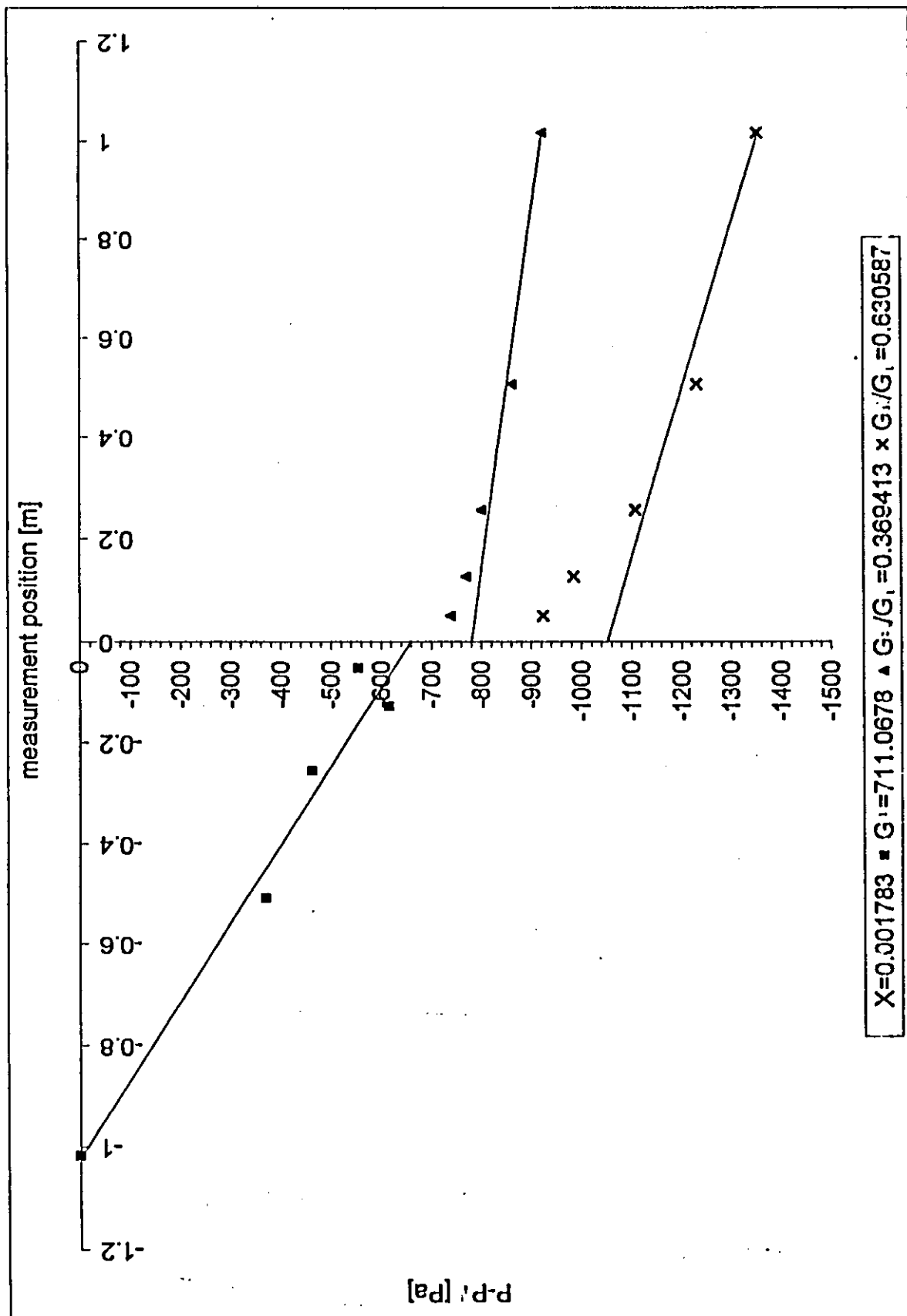
Figure (4.30) Schematic diagram of a typical two-phase flow pressure distribution in dividing T-junction

$X=0.001783 \quad \blacksquare \quad G_1=711.0678 \quad \blacktriangle \quad G_2/G_1=0.369413 \quad \times \quad G_3/G_1=0.630587$
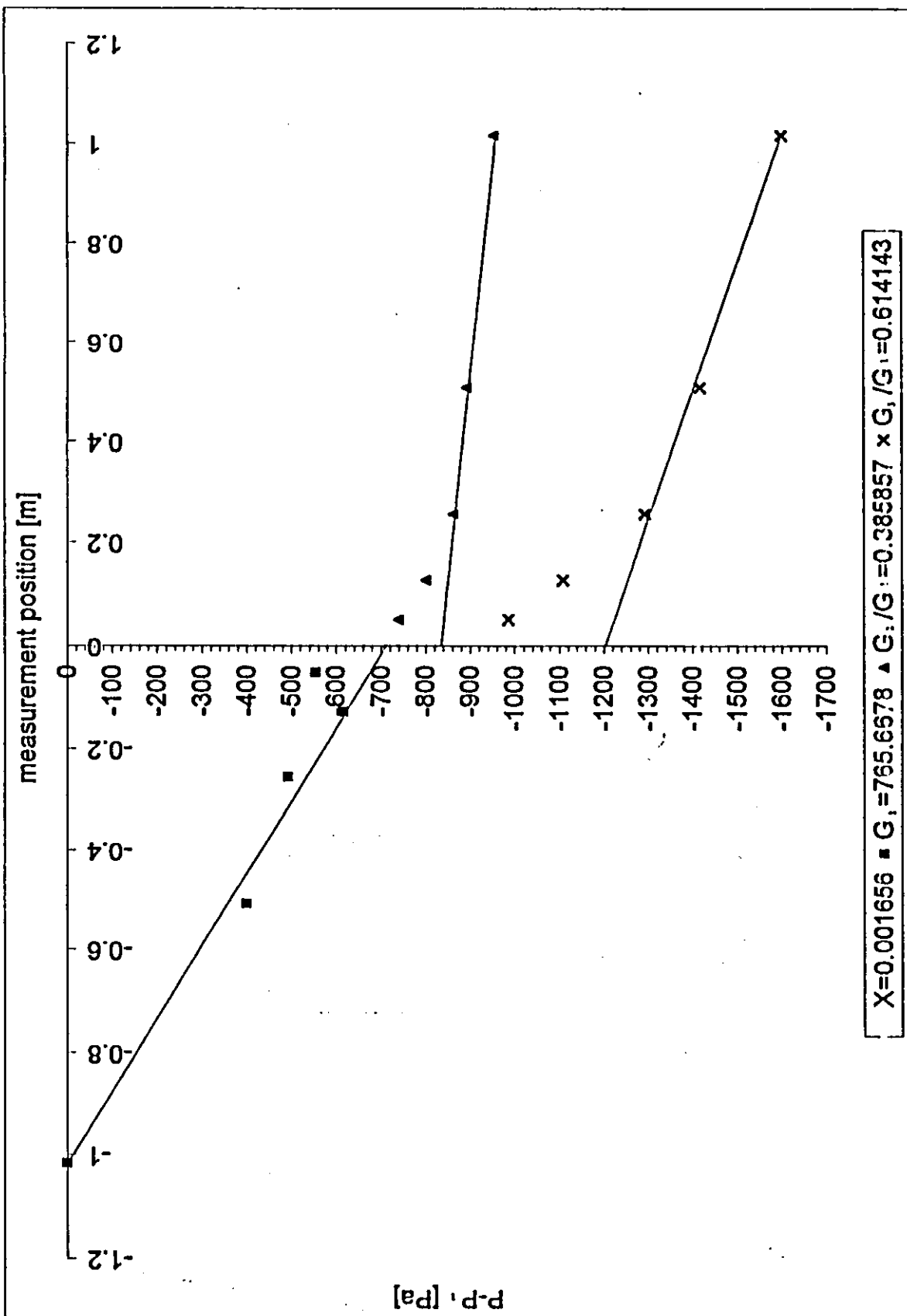
Figure (4.31) Schematic diagram of a typical two-phase flow pressure distribution in dividing T-junction

X=0.001656 ■ G₁ =765.6578 ▲ G₂/G₁ =0.385857 × G₃/G₁ =0.614143
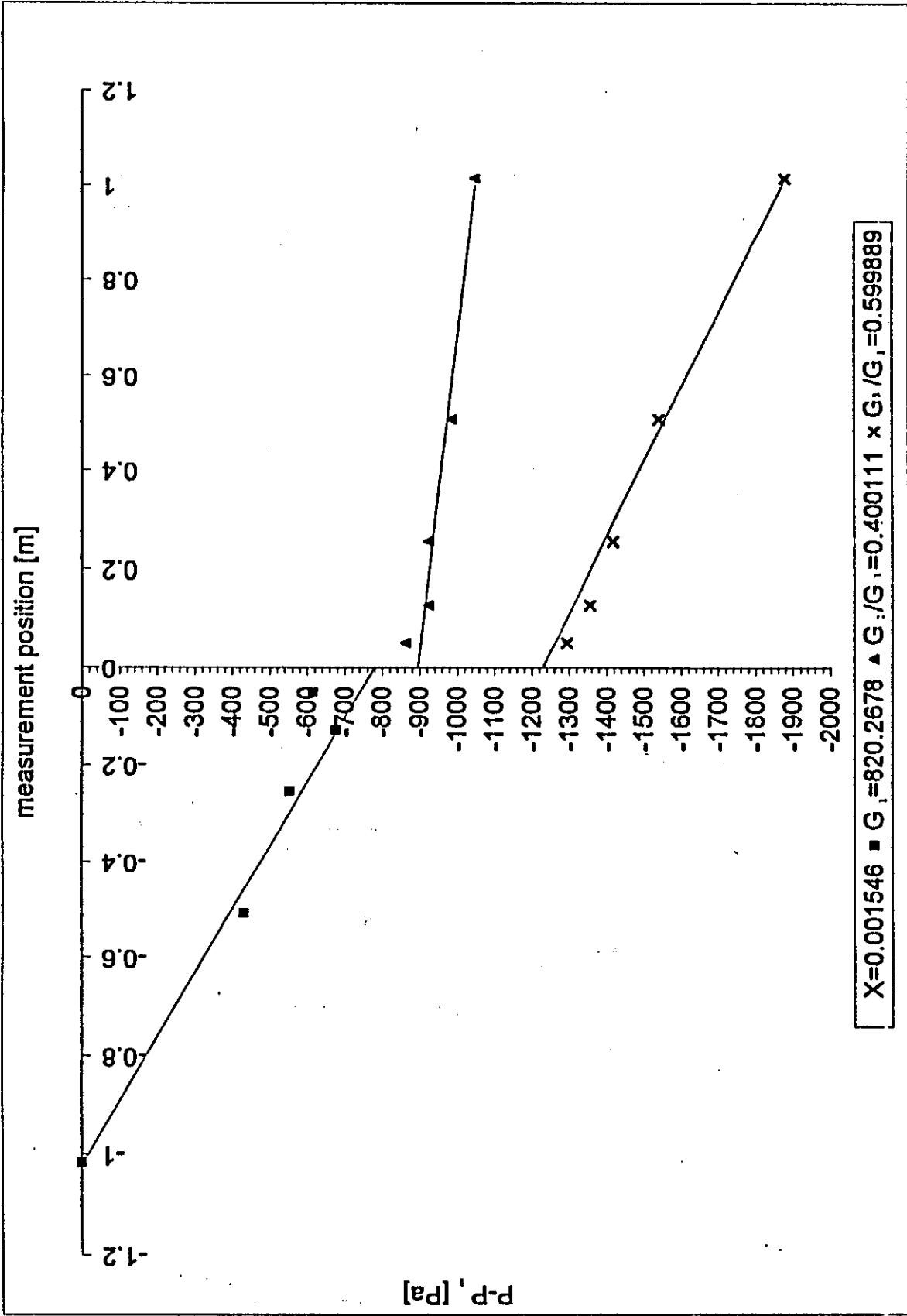
Figure (4.32) Schematic diagram of a typical two-phase flow pressure distribution in dividing T-junction

$X=0.001546$ $\blacksquare$ $G_1=820.2678$ $\blacktriangle$ $G_3/G_1=0.400111$ $\times$ $G_1/G_1=0.599889$

measurement position [m]

P-P , [Pa]
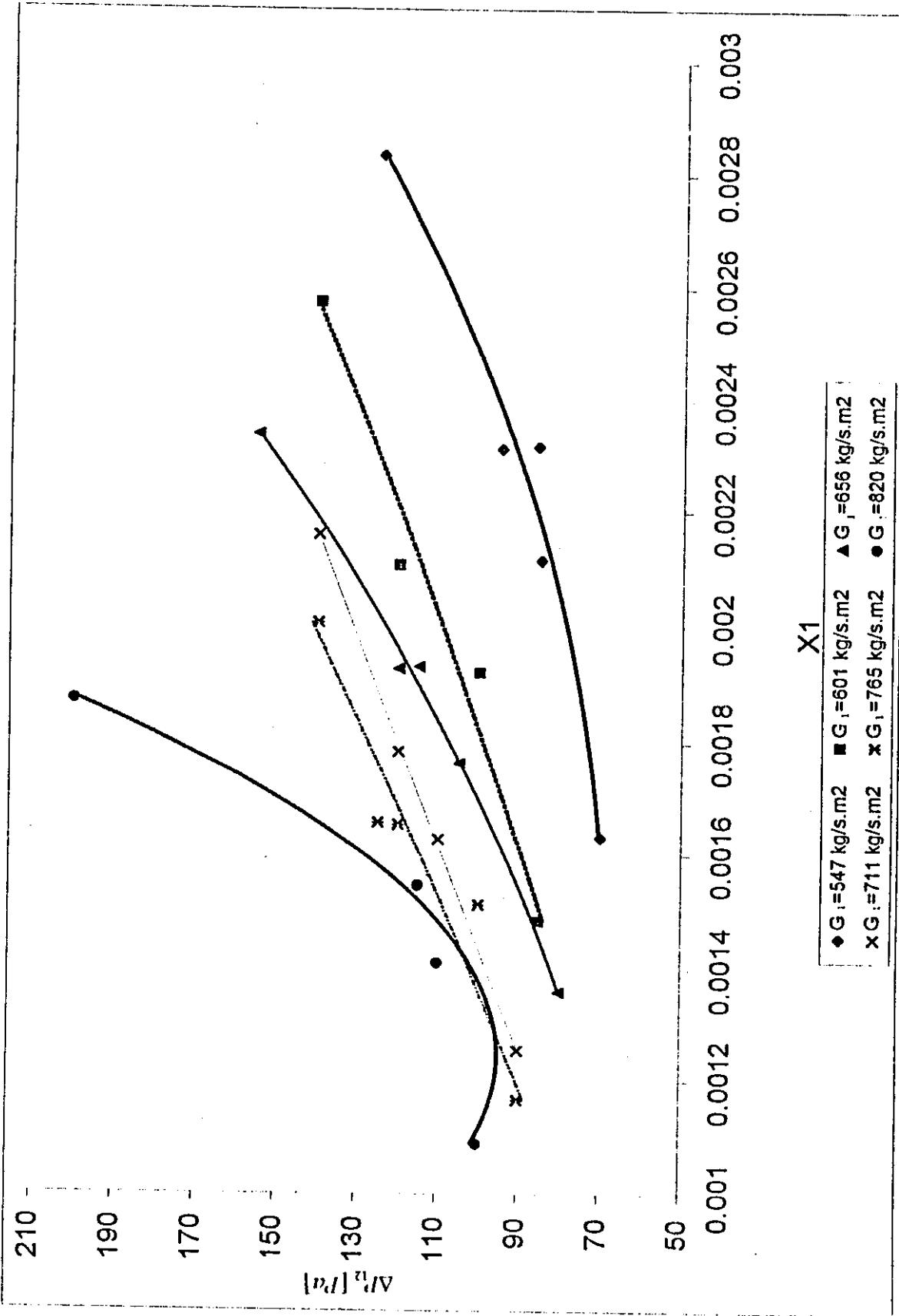
Figure (4.33) Two-phase flow pressure difference against inlet quality
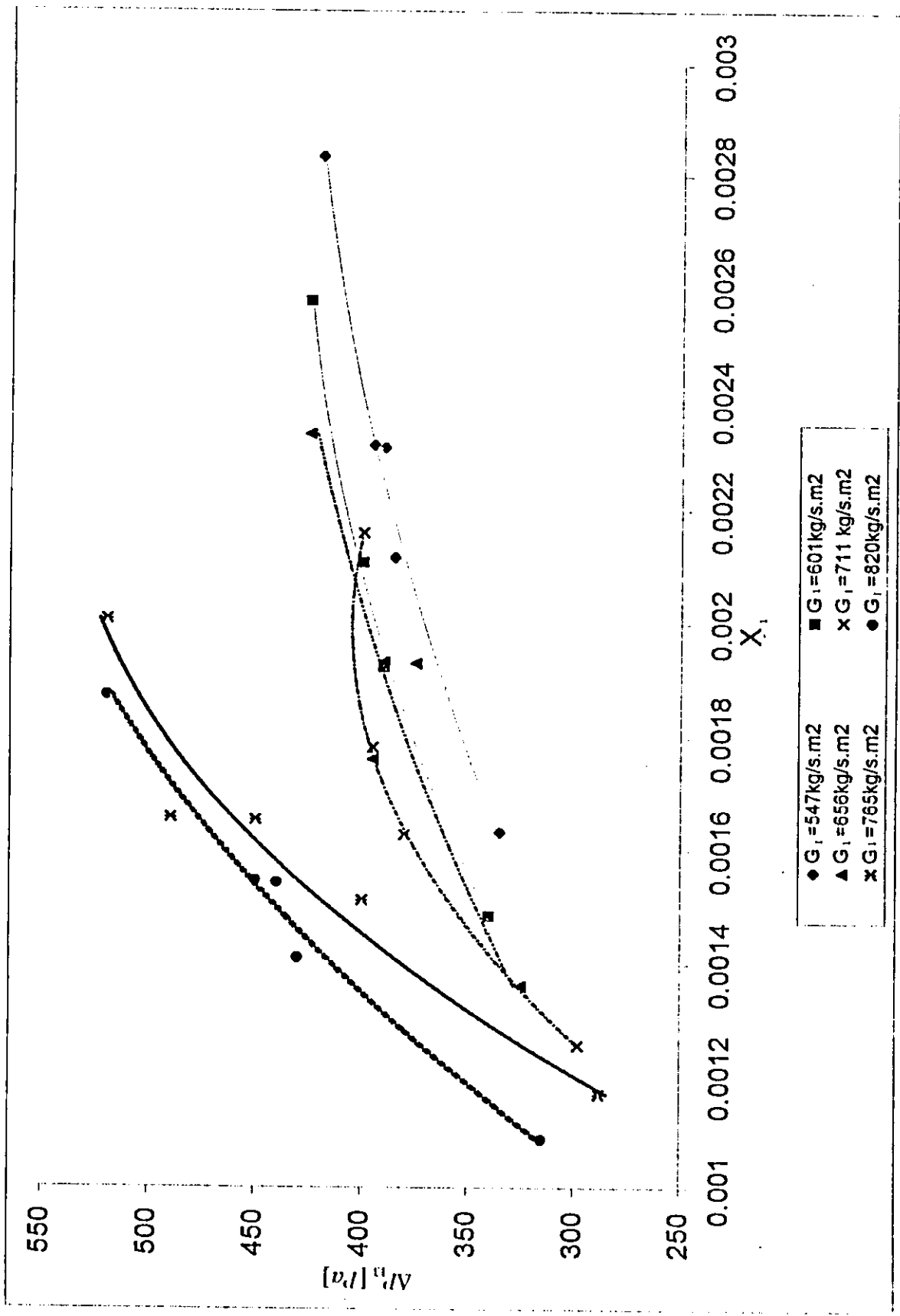
Figure (4.34) Two-phase flow pressure difference against inlet quality

Legend:
- ◆ G_i =547kg/s.m2
- ▲ G_i =656kg/s.m2
- ✕ G_i =765kg/s.m2
- ■ G_i =601kg/s.m2
- ✕ G_i =711 kg/s.m2
- ● G_i =820kg/s.m2

Y-axis: $\Delta P_{t,t}$ [Pa]

X-axis: X_i
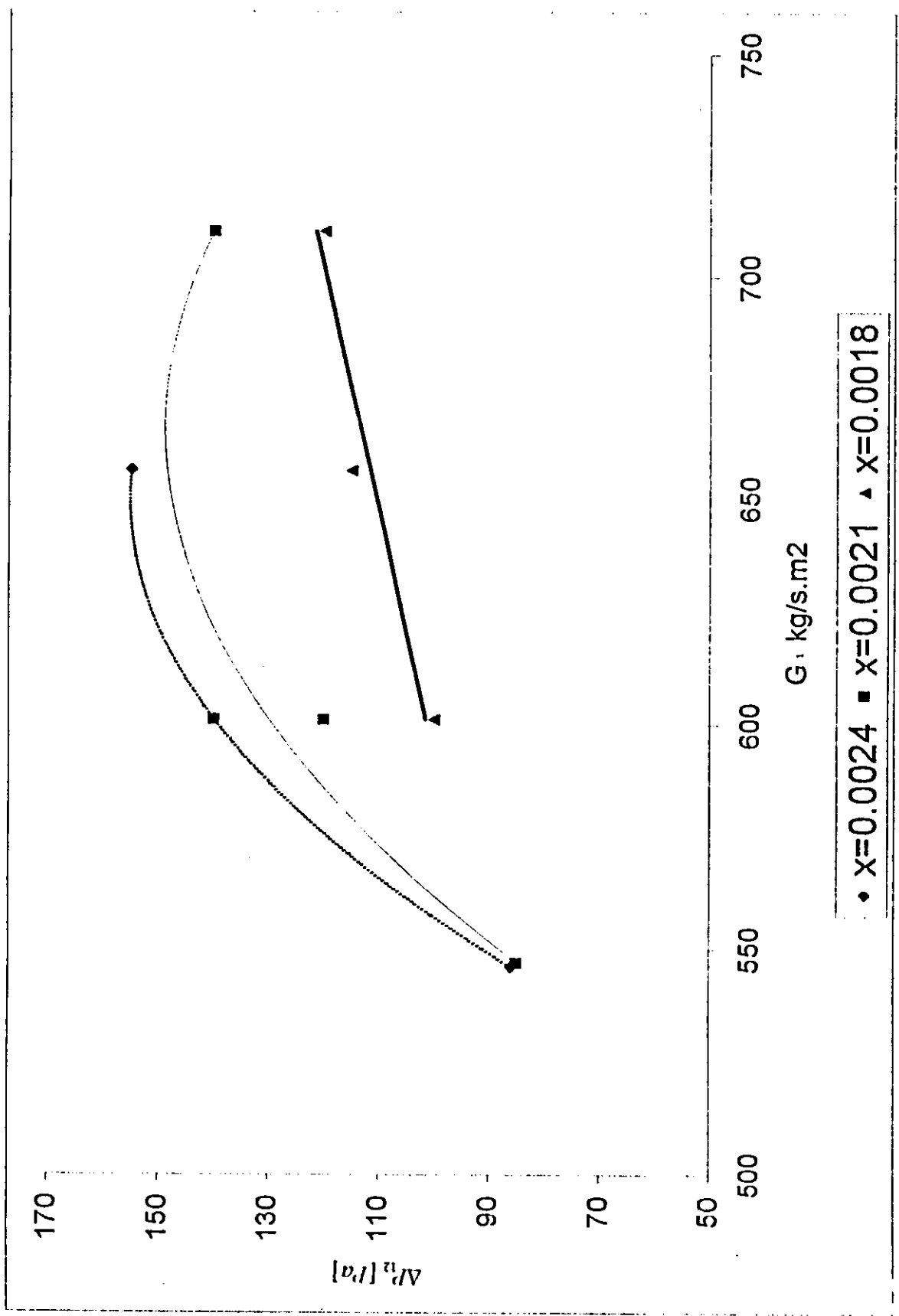
Figure (4.35) Inlet mass flux effect on the two-phase flow pressure drop

93
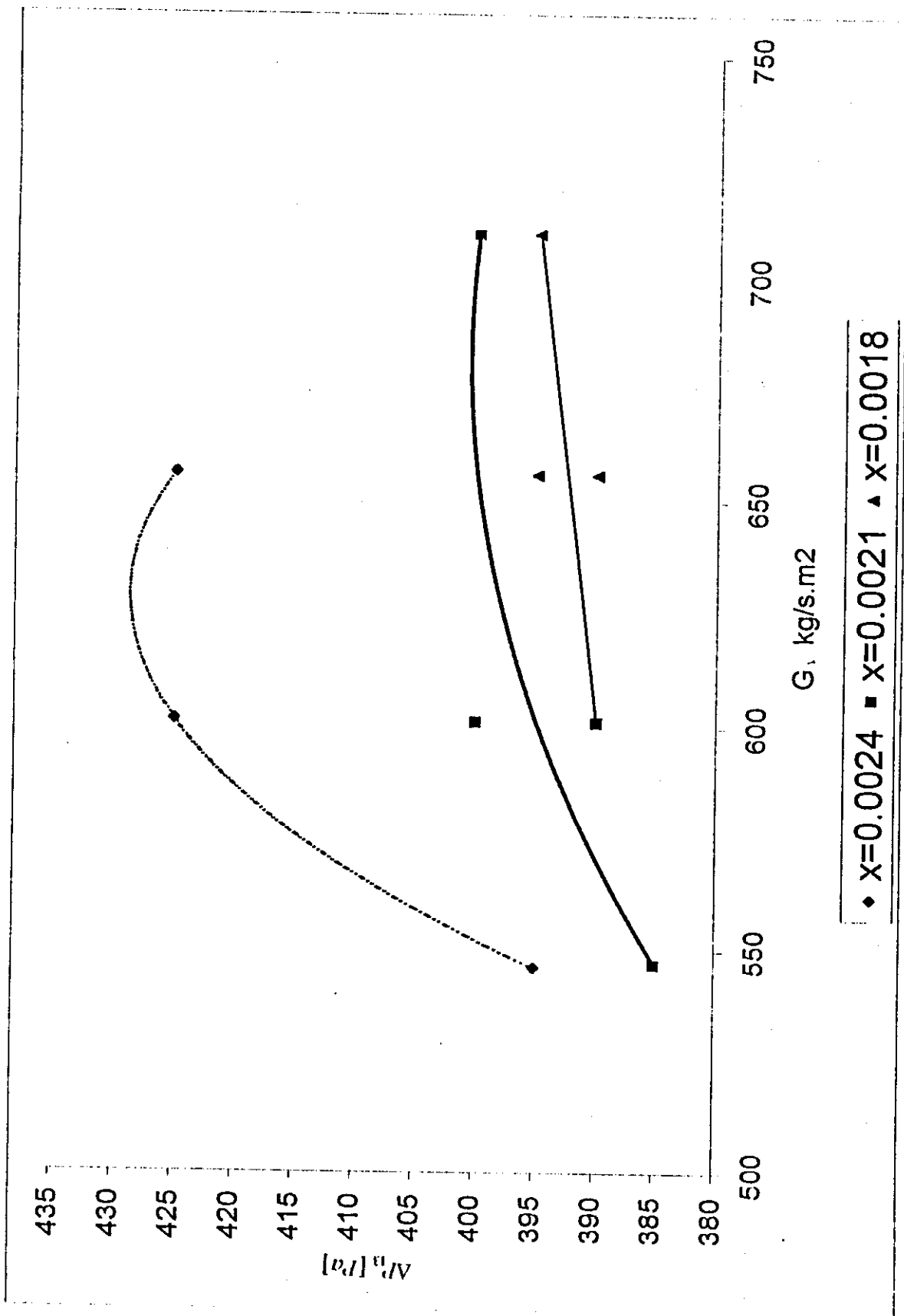
Figure (4.36) Inlet mass flux effect on the two-phase flow pressure drop
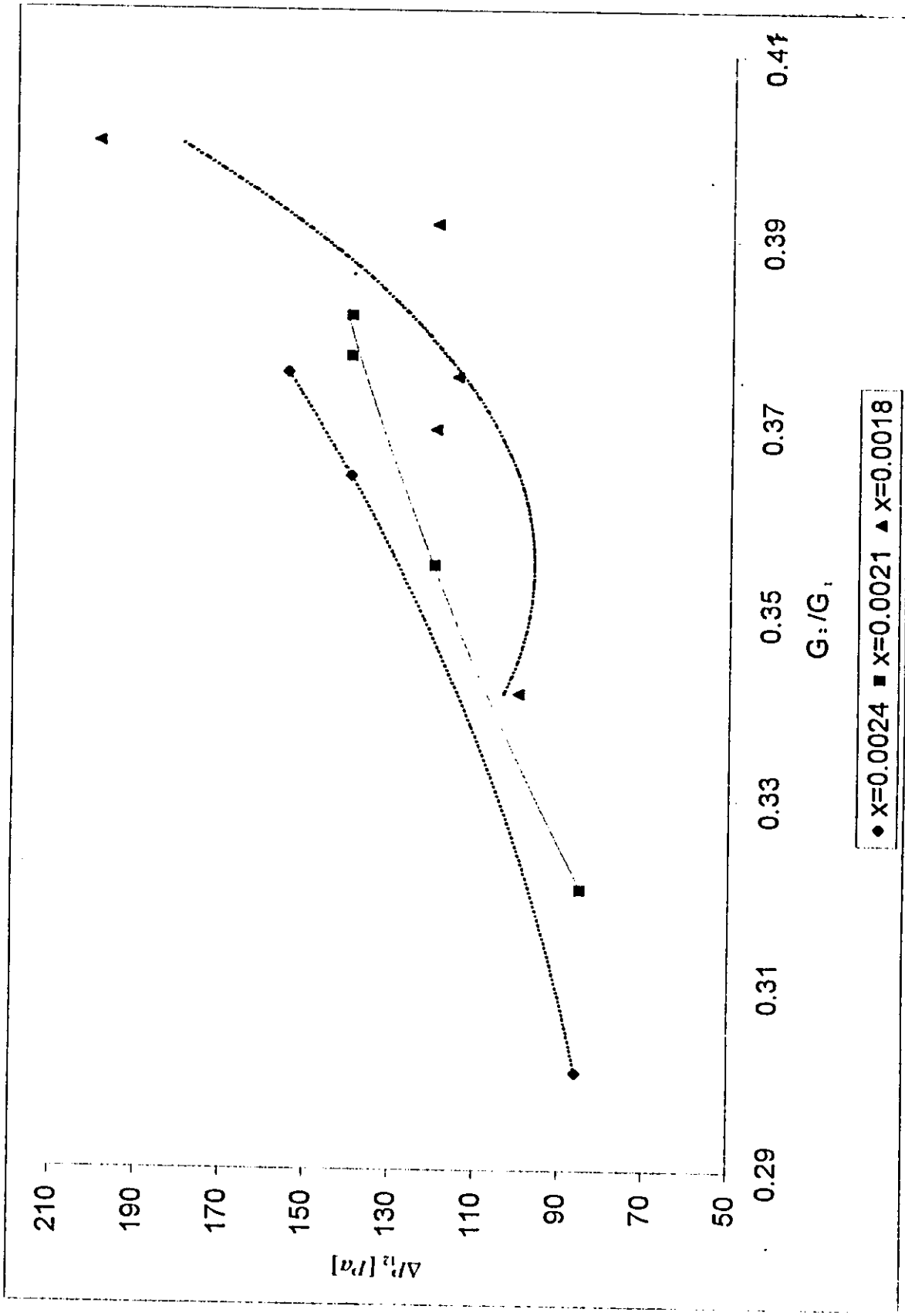
Figure (4.37) Effect of extraction rate on the two-phase flow pressure drop

95
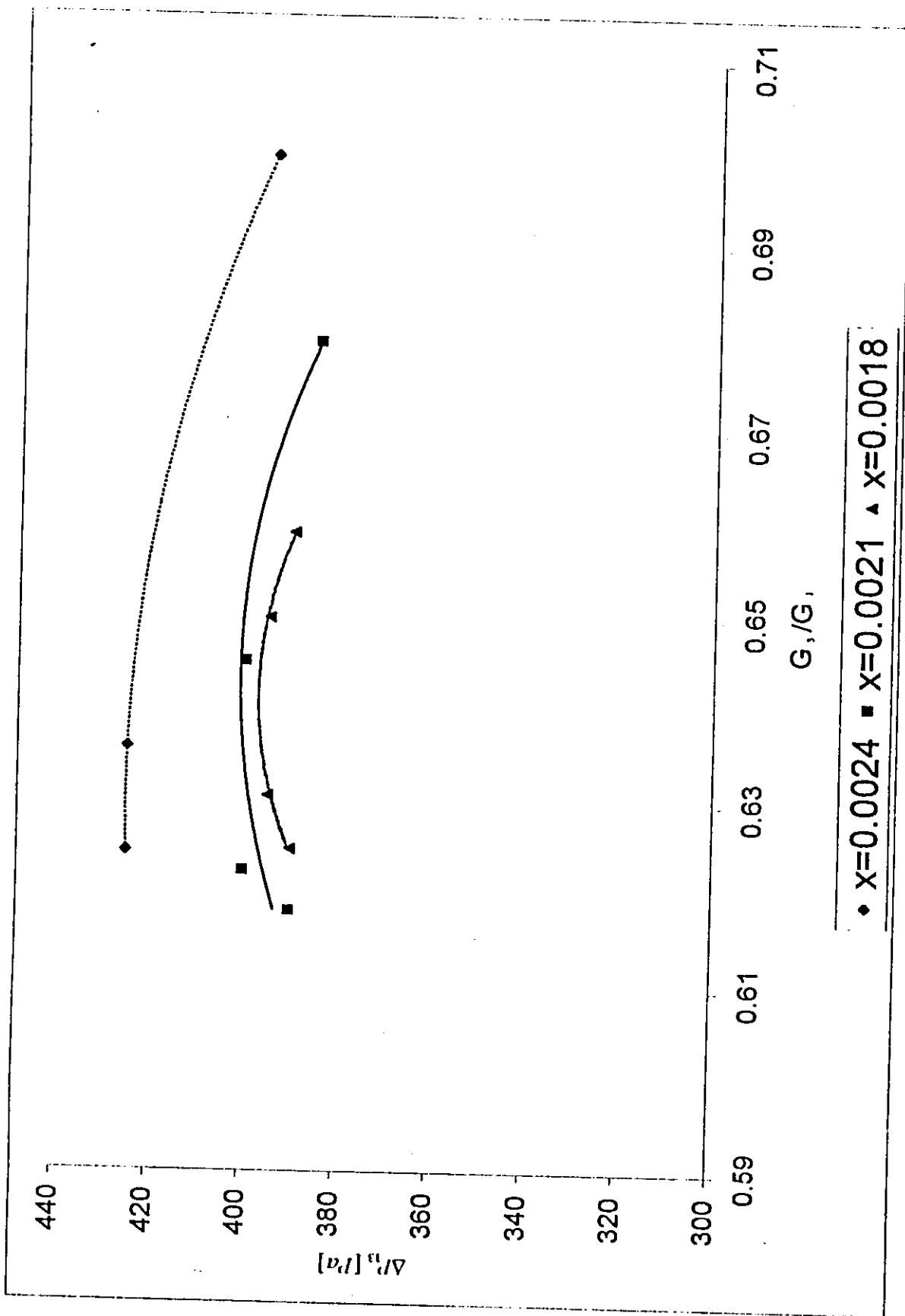
Figure (4.38) Effect of extraction rate on the two-phase flow pressure drop

♦ x=0.0024 ■ x=0.0021 ▲ x=0.0018
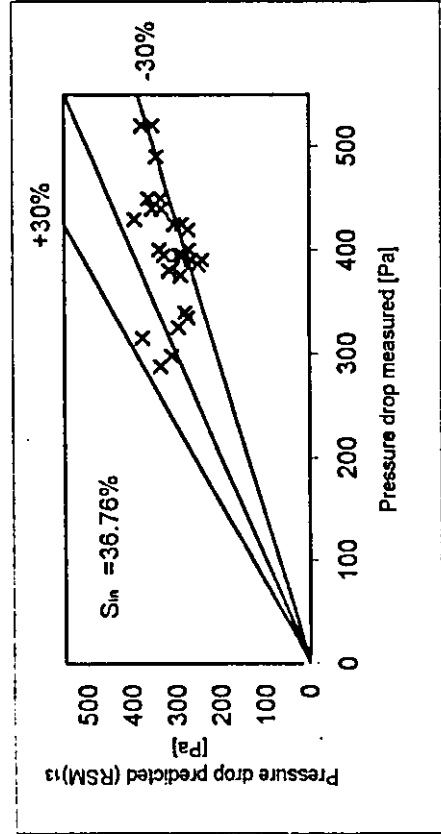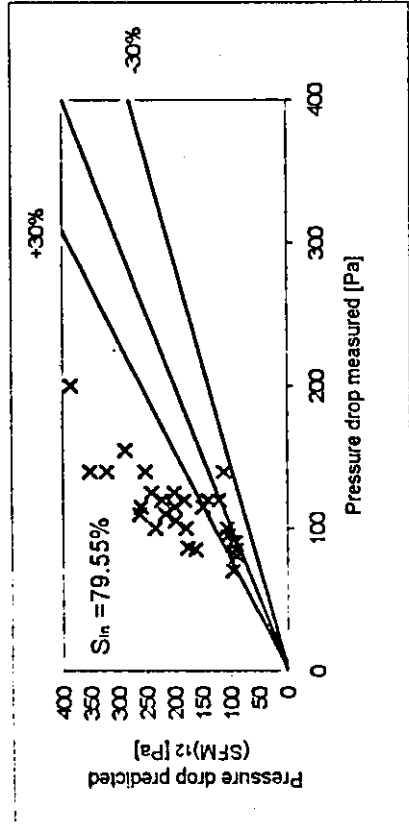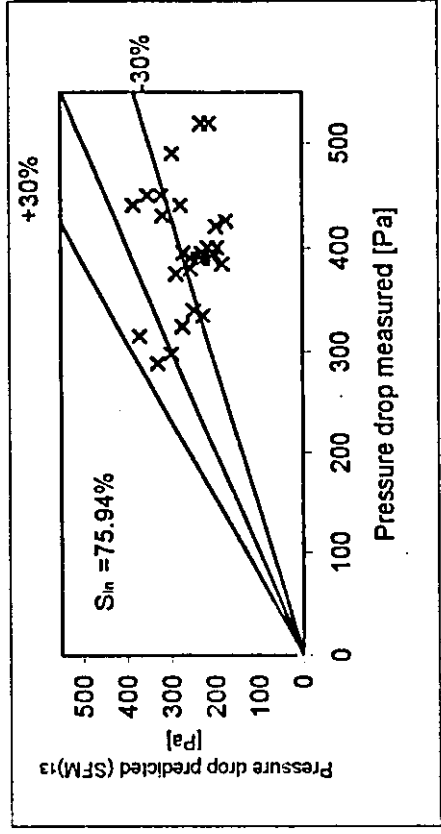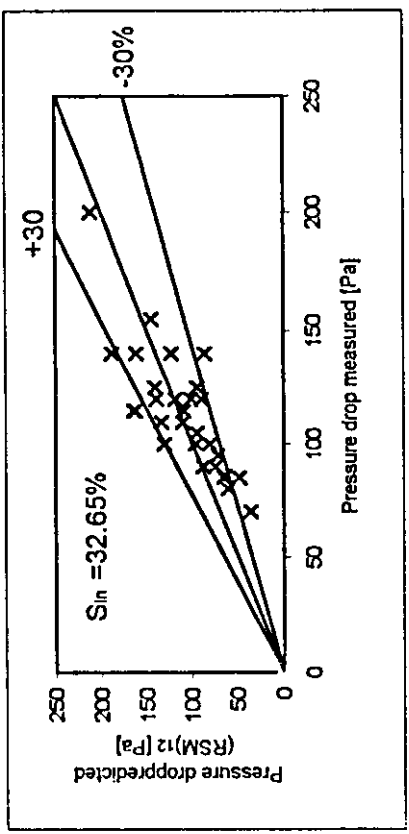
Figure (4.39) Reproductive accuracy of the pressure drop values with (SFM) and (RSM)

97

4.3 Discussion of the results

4.3.1 Single phase flow :

The average pressures P_1, P_2 at the T-junction inlet and branch-2 at different extraction rates $0.0 \leq G_2/G_1 \leq 1$ and constant inlet mass flux $G_1=710$ kg/s.m^2 are shown in figure (4.1). These average values were obtained by extrapolating the fully developed pressure gradients at the inlet and branch up to the centerline of the tee, since a constant pressure gradient due to wall friction will be assumed on each leg, where the pressure drop along a straight pipe can be calculated from the following equation:

$$\Delta P = \frac{fl\rho v^2}{2D}$$

where; f, D, $_V$, g and ρ (the friction factor, pipe diameter, average velocity, acceleration due to gravity and fluid density) are taken to be constants for the same material, constant inlet mass flux, constant temprature. and equal pipe diameter, then the pressure drop will proportional directly to the pipe length.

Referring to figure (4.2), it is clear that the pressure drop (ΔP) will be increased with increasing G_2/G_1 which is consistence with Bernoulli principle. Here the loss coefficient (K) is assumed to be the same for the two branches due to many reasons such as equal branch diameters, equal branch lengths and similar orientation (horizontal).

The variation of the single phase flow loss coefficient (K) against G_2/G_1 is shown in figure (4.3). It is clear that the trend of the present data agrees well with similar reported results. However, the values of K become much larger

98

for $G_2/G_1 > 0.6$, this difference can be related to the difference in the nominal diameter (50, 37.6 mm) used in Saba, Buell and Seeger experiments while 25.4mm inner diameter were used in the present study, the difference in the material type since PVC were used, but Saba and Seeger used carbon steel. Buell used commercial Type k-copper and Ballyk used stainless steel. On other hand, there is a difference in the flow direction through the T-junction, where in the present study the flow is divided into two branches while in their study the flow divides into run and branch.

4.3.2 Two-Phase flow :

Two-phase flow pressure difference depends on many parameters such as: the inlet flow regime, inlet quality and extraction rates.

Generally, the pressure drop values associated with two-phase flow are significantly higher than those for single-phase flow. This is cleared from comparing the results obtained for single-phase flow experiments at inlet mass flux $G_1=709.8$ kg/s.m^2, shown in figure (4.1) and those for two-phase flow experiments at $G_1= 710$ kg/s.m^2 shown in figures (4.12, 4.18, 4.24, 4.30), at the same extraction rate, where the two-phase flow pressure difference is about twice of that for single-phase flow. This result is consistent with that reported by Powers, 1992, who states that the actual pressure drop in horizontal construction dewatering pipe containing both water and air can be from 150 to 200 percent of the drop due to water flowing in the pipe alone. The difference between the two flow types referred to the introduction of a second phase which causes a sharp rise in pressure drop due to the following: 1) the cross-sectional area available for the flow of one phase is reduced by the introduction of the second; 2) the flow boundary is no longer a relatively smooth pipe, but is rough, irregular, mobile interface between two-phases; 3)

the introduction of a second phase can cause a very unsteady flow accompanied by an intense turbulence.

Figures (4.4-4.32) obtained at different inlet flow rates, extraction rates and inlet qualities but at the same system pressure ($P_s = 1$ bar) were used to estimate for the average pressures P_1, P_2 and P_3 at the inlet and branches by extrapolating the fully developed pressure gradients to the centerline of the T-junction, as explained previously in the single phase flow discussion.

One can see from figures (4.4-4.32) that the pressure drop along the inlet test leg is increased with increasing the inlet mass flux, taking in consideration the effect of inlet quality, which is consistent with fundamentals of single-phase flow. The pressure differences $\Delta P_{12}, \Delta P_{13}$ were taken from these figures and plotted against the inlet mass flux(G_1) figures (4.35, 4.36)), the inlet quality x_1 figures (4.33, 4.34) and the extraction rates (G_2/G_1)& (G_3/G_1), figures (4.37, 4.38).

The variations of $\Delta P_{12}, \Delta P_{13}$ with the inlet quality x_1, at constant inlet mass flux are shown in figures (4.33, 4.34), from which the pressure difference is noticed to be increased with increasing the inlet mass flux (G_1). The difference in the trend shape between figure (4.33) and figure (4.34) were related to the influence of the branch qualities on the pressure drop along the branch legs.

The effect of the inlet mass flux (G_1) on the branch pressure differences $\Delta P_{12}, \Delta P_{13}$ at constant inlet qualities is shown in figures (4.35, 4.36). From these figures, the pressure differences $\Delta P_{12}, \Delta P_{13}$ increases for a given x_1 with increasing G_1, and also increases at a given G_1 with increasing x_1.

From the above discussion it is clear that the inlet mass flux (G_1)and the inlet quality x_1 are not enough to describe the two-phase flow pressure differences at a given flow pattern. The extraction rate (G_2/G_1) or (G_3/G_1) are the other significant parameter. Figures (4.37, 4.38) shows that $\Delta P_{12}, \Delta P_{13}$ increase with increasing x_1 at a given extraction rate, while Figure (4.37) shows that ΔP_{12} increases with increasing (G_2/G_1) which is an expected result. An opposite trend for that can be noticed in figure (4.38). But, actually, they are the same, at which for high values of (G_3/G_1), the trends fall down due to low inlet mass flux (G_1) which consequently reduces the pressure difference value.

From obtained results it is clear that the pressure difference values at branch-3 (ΔP_{13}) is larger than that at branch-2 (ΔP_{12}). These differences can be related to the high extraction rate at branch-3 with respect to branch-2. Low extraction rates at branch two related to the existence of the air-water separator, which cause a back pressure and then preference of the flow to branch-3.

The statistical mean predictive accuracy of the measured pressure difference values with the separated flow model and Riemann & Seeger model are plotted in the parity plot as shown in figure (4.39), from obtained results of the logarithmic standard deviation and the scatter of the results, Reimann & Seeger model shows better predictions of the present data than that of the separated flow model.

CHAPTER 5

CONCLUSIONS AND RECOMMENDATIONS

5.1 Conclusions

In this work, a two-phase flow test loop was designed, constructed. Experimental investigations for slug flow regime with variable inlet mass fluxes, extraction rates and qualities were carried out. The following conclusions can be stated:

1. The experimental set up designed in this work was sufficient to study the slug flow characteristics and two-phase flow in general.

2. The obtained results for the pressure differences associated with two-phase flow in a horizontal orientation was found to be twice that of single-phase flow.

3. Experimental results showed that the pressure difference is a function of inlet mass flux (G_1), the inlet quality (x_1), and the extraction rates (G_2/G_1 and G_3/G_1).

4. There is a strong interdependence between the separation phenomena and the pressure distribution.

5. Results obtained were better fitted with Reimann and Seeger model than that of separated flow model. using Reimann and Seeger model.

4.3 Recommend

test loop that constructed through this study is ...sed for further studies as:

The two-...

recom...low pattern on the pressure difference phenomenon.

distribution phenomena on the T-junction with horizontal and branches orientations.

...tudying the effect of diameter ratio (D_{branch}/D_{inlet}) on the phase distribution and pressure difference phenomena.

4. Studying the phase distribution and pressure difference phenomena at different branches orientation(horizontal, vertical upward and down ward), different types of fittings (elbows, bends, values, ...), different types of fluids as a working fluid, using another material types such as stainless steel, copper, ...

5. Studying the phase distribution and pressure drop phenomena using two inlets and one outlet.

6. REFERENCES

Azzopardi, B.J. & Baker, S.R. 1981. "Two-phase flow in a "T"-junction: the effect of flow pattern in vertical upflow", *AERE-R* 10174.

Azzopardi, B.J. & Whalley, B.P. 1982. "The effect of flow patterns on two-phase flow in a T-junction", *International Journal of Multiphase flow* paper, 8: 491-507

Ballyk J.D., Shokry M. and Chan A.M.C. 1988. "Steam water annular flow in a horizontal dividing T-Junction", *International Journal of Multiphase flow* paper, 14 (3): 265-285.

Buell J.R., Soliman H.M. and Sims G.E. 1994. "two-phase pressure drop and phase distribution at a horizontal tee junction", *International Journal of Multiphase flow* paper, 20 (5): 819-836.

Chisholm, D. 1967. "Pressure losses in bends and tees during steam-water flow", *NEL Report* 318, National Engineering Lab., Glasgow, Scotland.

Fouda, A.E., Rhodes, E. 1974. "Two-phase annular flow stream division in a simple tee", *Transactions of the institute of chemical engineers*, 52: 354-360

Henry, J.A.R. 1981. "Dividing annular flow in a horizontal tee", *International Journal of Multiphase flow*, 7: 343-355.

Honan, T.J. & Lahey, R.T. 1981. "The measurement of phase separation in wyes and tees. Nuclear Engineering and design, 64: 93-102

Hwang, et al. 1988. "Phase separation in dividing two-phase flows", *International Journal of Multiphase flow* paper, 14: 439-458.

Kataoka, I., Ishii, M., 1983. "Entrainment and deposition rates of droplets in annular tow-phase flow". In: Proc. *ASME/JSME Therm. Engng Joint Conf.*, Honolulu, Hawaii, 1: 69-80.

Mandhane, J.M. et al. 1974. " A flow pattern map for gas-liquid flow in horizontal pipes", *International Journal of Multiphase flow* paper, 537-553.

McCreery, G.E. 1984. "A correlation for phase separation in a Tee". *Multiphase flow and heat transfer III*. Part B: Applications (Edited by Veziroglu, T.N. and Bergles, A.E.).

Mills, A. F., 1995. " *Heat and mass transfer*", Richard D. Irwin, Inc.

Peramaki, m. p. 2001. " The significance of two-phase flow regimes in designing Multi-Phase extraction systems", *Journal of Porous Media*, 4,ISSN 1091-028X.

Reimann J. and Seeger W. 1986. "Two-phase flow in a tee junction with a horizontal inlet–part2: pressure differences", *International Journal of Multiphase flow* paper, 12 (4): 587-608.

Rouhani, S.Z. 1969. "Modified correlations for void fraction and two-phase pressure drop", *AB Atomenergie*, AE-RtV-841.

Rubel et al. 1988. "Phase distribution during steam-water flow in a horizontal T-junction", *International Journal of Multiphase flow* paper, 12 (4): 587-608.

Saba, N. & Lahey, R.T. 1982., "Phase separation phenomena in branching conduits", *NUREG/CR*-2590, Department of Nuclear Engineering, Rensselear Polytechnic institute, tute, Troy, NY.

Saba, N. & Lahey, R., Jr. (1984), "The analysis of phase separation phenomena in branching conduits", *International Journal of Multiphase flow* paper, 10: 1-20.

Schmidt J. and Friedel L. 1997. "Two-phase pressure drop across sudden contractions in duct areas", *International Journal of Multiphase flow* paper,23 (2): 283-299.

R. 1994. "Predictive methods for two-phase flow

Schmidt H. and tee junctions with combining conduits", *International*

pressur *ltiphase flow* paper,14 (4): 425-438.

Johann J. and Muller U. 1986. "Two-phase flow in a tee

with a horizontal inlet –part 1: phase separation", *International*

Seege *l of Multiphase flow* paper, 12 (4): 575-585.

.., Ballyk, J. D. & Chan, A. M. C. 1987. "On the characteristics of

/-phase flow in network branches". *Canadian Electrical Association*

CEA) Report 325G430.

s, G.b. 1969. *"One dimensional Two-phase flow"*, McGraw-Hill, Inc.

alters L. C. et al.1997. "Two-phase flow pressure drop and phase

distribution at reduced tee junctions", *International Journal of*

Multiphase flow paper, 24: 775-792.

Zwtzmann, K. B. 1982. "Phasenseparation und Druckabfall in zweiphasig

durchströmten vertikalen Rohrabzweigungen". Ph.D. Thesis,

University of Hannover, FRG.

Zuber, N. & Findlay, J. A. 1965. "Average volumetric concentration in two-

phase flow systems". *J. Heat Transfer* 87: 453-458

Table A.1 Measured data for single-phase flow test at $T_1=25.2\ ^\circ C$

Inlet water volume flow rate ($\dot{V}=1300\ \ell/hr$)

Distance at inlet (mm)	H_1 (mmHg)	Distance at branch2 (mm)	$\dot{V}_2=0.0$ ℓ/hr H_2 (mm Hg)	$\dot{V}_2=340$ ℓ/hr H_2 (mm Hg)	$\dot{V}_2=500$ ℓ/hr H_2 (mm Hg)	$\dot{V}_2=770$ ℓ/hr H_2 (mm Hg)	$\dot{V}_2=970$ ℓ/hr H_2 (mm Hg)	$\dot{V}_2=1100$ ℓ/hr H_2 (mm Hg)	$\dot{V}_2=1300$ ℓ/hr H_2 (mm Hg)
-1.016	1.5	0.0508	3.5	3	4	5.5	6.5	6.5	7
-0.508	2.75	0.127	4	3.25	4.25	5.75	7	7	7.25
-0.254	3.5	0.254	4.25	3.5	4.5	6	7.5	7.5	7.5
-0.127	3.75	0.508	4.5	3.75	4.75	6.75	7.75	7.75	8
-0.0508	3.5	1.016	5	4	5	7.25	8.5	8.5	9

Table A.2.1 Measured data for average pressure heads of two-phase flow test at $P_s = 1$ bar

Distance (m)	$\dot{V}_{1w} = 1000\ell/hr$ $\dot{V}_{2w} = 370\ell/hr$ $T_1 = 26.6\,^{\circ}C$ Manometer head (mm Hg)	$\dot{V}_{1w} = 1100\ell/hr$ $\dot{V}_{2w} = 420\ell/hr$ $T_1 = 28.1\,^{\circ}C$ Manometer head (mm Hg)	$\dot{V}_{1w} = 1200\ell/hr$ $\dot{V}_{2w} = 470\ell/hr$ $T_1 = 28.3\,^{\circ}C$ Manometer head (mm Hg)	$\dot{V}_{1w} = 1400\ell/hr$ $\dot{V}_{2w} = 580\ell/hr$ $T_1 = 28.5\,^{\circ}C$ Manometer head (mm Hg)	$\dot{V}_{1w} = 1500\ell/hr$ $\dot{V}_{2w} = 640\ell/hr$ $T_1 = 28.8\,^{\circ}C$ Manometer head (mm Hg)
-1.016	3.83	4	4	4.33	4
-0.508	6	6	7	7.67	8.33
-0.254	6.67	6.67	7.67	9.33	10
-0.127	7	7.67	8.67	10	11
-0.0508	6.67	7.33	8.33	9.67	10.67
0.0508	7.33	8.67	9.67	11	12
0.127	8	9	10	11.33	12.67
0.254	8.67	9.33	10.5	12.33	13.33
0.508	9	9.33	10.67	12.33	13.67
1.016	9.33	10	11	13	14
0.0508	9	10	10.33	14	14.33
0.127	10.67	11	11.67	15	15.67
0.254	11.33	11.33	12.67	15.33	17
0.508	11.67	11.67	13	16	18
1.016	12.33	12.33	13.67	17.67	20

110

Table A.2.2 Measured data for average pressure heads of two-phase flow test at $P_s = 1$ bar

Distance (m)	$\dot{V}_{1w}=1000\ell/hr$ $\dot{V}_{2w}=320\ell/hr$ $T_1=24.7°C$ Manometer head (mm Hg)	$\dot{V}_{1w}=1100\ell/hr$ $\dot{V}_{2w}=375\ell/hr$ $T_1=24.7°C$ Manometer head (mm Hg)	$\dot{V}_{1w}=1200\ell/hr$ $\dot{V}_{2w}=420\ell/hr$ $T_1=24.7°C$ Manometer head (mm Hg)	$\dot{V}_{1w}=1300\ell/hr$ $\dot{V}_{2w}=470\ell/hr$ $T_1=24.8°C$ Manometer head (mm Hg)	$\dot{V}_{1w}=1400\ell/hr$ $\dot{V}_{2w}=530\ell/hr$ $T_1=24.8°C$ Manometer head (mm Hg)	$\dot{V}_{1w}=1500\ell/hr$ $\dot{V}_{2w}=540\ell/hr$ $T_1=24.8°C$ Manometer head (mm Hg)
-1.016	3.5	3.5	3.5	3.5	4	4
-0.508	5	5.5	6.25	6.5	8	8
-0.254	5.75	6	7	8	8.5	9.25
-0.127	6.25	6.5	7.75	8.5	10	10.25
-0.0508	5.5	6	7.5	8.25	9.75	9.75
0.0508	7	8	9	10	11	11.5
0.127	7	8	9.33	10	11.25	11.75
0.254	7.5	8.25	9.67	10.5	11.75	12.5
0.508	7.5	8.75	10	11	12	12.75
1.016	8	9.5	10.75	11.5	12.25	13.25
0.0508	9	9	11	12	13	13.5
0.127	10	10	11.25	13	14	14
0.254	10.25	10.75	12	14	15.75	16.25
0.508	11	11.5	12.5	16	17.25	18
1.016	12.25	12.75	13.25	19	20	21

111

Table A.2.3 Measured data for average pressure heads of two-phase flow test at $P_s = 1$ bar

Distance (m)	$\dot{V}_{1w}=1000\ell/hr$ $\dot{V}_{2w}=350\ell/hr$ $T_1=26.3°C$ Manometer head (mm Hg)	$\dot{V}_{1w}=1100\ell/hr$ $\dot{V}_{2w}=400\ell/hr$ $T_1=26.8°C$ Manometer head (mm Hg)	$\dot{V}_{1w}=1200\ell/hr$ $\dot{V}_{2w}=450\ell/hr$ $T_1=27°C$ Manometer head (mm Hg)	$\dot{V}_1=1300\ell/hr$ $\dot{V}_{2w}=490\ell/hr$ $T_1=27.2°C$ Manometer head (mm Hg)	$\dot{V}_{1w}=1400\ell/hr$ $\dot{V}_{2w}=550\ell/hr$ $T_1=27.6°C$ Manometer head (mm Hg)	$\dot{V}_{1w}=1500\ell/hr$ $\dot{V}_{2w}=600\ell/hr$ $T_1=27.7°C$ Manometer head (mm Hg)
-1.016	4	4	4	4.25	3.75	4
-0.508	5.75	6.5	6.5	7.25	7.75	8
-0.254	6.75	7.25	7.25	7.75	8.75	9
-0.127	7	7.5	7.75	8.5	9.75	10
-0.0508	6.75	7.25	7.5	8.25	9	9.5
0.0508	8	9	9	9.5	11	12.5
0.127	8.5	9.5	9.5	10	11.5	13
0.254	8.75	10	10	10.5	12.25	13.25
0.508	8.75	10	10.25	11.25	12.75	13.5
1.016	9	10.5	10.75	11.5	13.25	14.5
0.0508	8.5	10.5	10.5	12	13.5	14
0.127	10.5	11.5	11.25	12	14.5	15.5
0.254	11.5	12.25	12.25	10.5	16	16.5
0.508	12	12.25	12.75	14	17.25	17.75
1.016	13	12.5	13.5	15.5	19	20

112

Table A.2.4 Measured data for average pressure heads of two-phase flow test at $P_s = 1$ bar

Distance (m)	$\dot{V}_{1w}=1000\ell/hr$ $\dot{V}_{2w}=260\ell/hr$ $T_1=25°C$ Manometer head (mm Hg)	$\dot{V}_{1w}=1100\ell/hr$ $\dot{V}_{2w}=330\ell/hr$ $T_1=25.1°C$ Manometer head (mm Hg)	$\dot{V}_{1w}=1200\ell/hr$ $\dot{V}_{2w}=390\ell/hr$ $T_1=25.1°C$ Manometer head (mm Hg)	$\dot{V}_1=1300\ell/hr$ $\dot{V}_{2w}=450\ell/hr$ $T_1=25.1°C$ Manometer head (mm Hg)	$\dot{V}_{1w}=1400\ell/hr$ $\dot{V}_{2w}=500\ell/hr$ $T_1=25.2°C$ Manometer head (mm Hg)	$\dot{V}_{1w}=1500\ell/hr$ $\dot{V}_{2w}=530\ell/hr$ $T_1=25.2°C$ Manometer head (mm Hg)
-1.016	3.5	3.5	3.5	4	4.5	4.5
-0.508	5	5	6.33	6.5	7	7.33
-0.254	6	6	6.5	7	7.67	8
-0.127	6.33	6.5	7.5	7.67	8.33	9
-0.0508	6	6.33	7.25	7.5	8	8.67
0.0508	7	7	8.25	9	9.25	9.5
0.127	7.25	7.25	8.5	9.33	9.5	10
0.254	7.33	7.5	9	9.5	9.75	10.75
0.508	7.5	8	9.25	9.75	10.25	11
1.016	7.75	8.5	9.75	10.5	10.5	11.75
0.0503	8.5	9.25	10	10	10.5	11
0.127	9	9.5	10	10.5	11	11.5
0.254	9.67	9.75	11	11	11.25	12.5
0.508	10	10.25	11.5	11.5	12	12.75
1.016	10.5	11	12	12	12.25	13.5

Table A.2.5 Measured data for average pressure heads of two-phase flow test at P₃ = 1 bar

Distance (m)	$\dot{V}_{1w}=1000\ell/hr$ $\dot{V}_{2w}=300\ell/hr$ $T_1=24.3°C$ Manometer head (mm Hg)	$\dot{V}_{1w}=1100\ell/hr$ $\dot{V}_{2w}=390\ell/hr$ $T_1=24.4°C$ Manometer head (mm Hg)	$\dot{V}_{1w}=1200\ell/hr$ $\dot{V}_{2w}=450\ell/hr$ $T_1=24.4°C$ Manometer head (mm Hg)	$\dot{V}_1=1300\ell/hr$ $\dot{V}_{2w}=480\ell/hr$ $T_1=24.5°C$ Manometer head (mm Hg)	$\dot{V}_{1w}=1400\ell/hr$ $\dot{V}_{2w}=540\ell/hr$ $T_1=24.5°C$ Manometer head (mm Hg)	$\dot{V}_{1w}=1500\ell/hr$ $\dot{V}_{2w}=600\ell/hr$ $T_1=24.5°C$ Manometer head (mm Hg)
-1.016	3.5	3.5	4	4	4.5	4.5
-0.508	5.5	6	6.75	7	7.75	8
-0.254	6	7	7.5	7.75	8.5	9
-0.127	6.5	7.75	8.25	9	9.5	10
-0.0508	6	7	8	8.5	9	9.5
0.0508	7.25	8.5	9.5	10	10.5	11.5
0.127	7.5	9	9.75	10.25	11	12
0.254	8	9.25	10.25	10.5	11.5	12
0.508	8.5	9.75	10.5	11	11.75	12.5
1.016	9	10	11.25	11.5	12.25	13
0.0508	7.5	9	11	11.5	12.5	15
0.127	8.5	10	11.5	12	13.5	15.5
0.254	10.5	11.75	12.5	13	15	16
0.508	11	12.25	12.75	14	16	17
1.016	11.5	12.75	13.5	15	17.5	19.75

114

Table A.3 Measured data for air mass flow rate through an orifice and pitot tube

Orifice differential head ΔP (mm wg)	P_3 (bar abs.)	T_3 (°C)	Pitot tube manometer dynamic head h_d(mm)	Pipe diameter (mm)	Manometer liquid density Kg/m^3
3	1	42	1	8	787
2.5	1	42	4.5	6	970
4.5	1	42	11	6	787
		42	15		
		48	16		
		48	16		
		48	16		
		48	16		
1.5	1	44	1	8	970
3	1	41	2	8	787

115

Table B.1 Results obtained for single-phase flow system pressure difference, $T_1=25\ ^\circ C$
Inlet mass flux $(G_1) = 709.8$ kg/s

Distance at inlet (mm)	$(\Delta P_{st})_1$ Pa	Distance at branch2 (mm)	$G_2=0.0$ Kg/s.m² $(\Delta P_{st})_2$ Pa	$G_2=185.64$ Kg/s.m² $(\Delta P_{st})_2$ Pa	$G_2=273$ Kg/s.m² $(\Delta P_{st})_2$ Pa	$G_2=420.42$ Kg/s.m² $(\Delta P_{st})_2$ Pa	$G_2=529.6$ Kg/s.m² $(\Delta P_{st})_2$ Pa	$G_2=600.6$ Kg/s.m² $(\Delta P_{st})_2$ Pa	$G_2=709.8$ Kg/s.m² $(\Delta P_{st})_2$ Pa
-1.016	184.6674	0.0508	430.8905	369.3347	492.4463	677.1137	800.2252	800.2252	861.781
-0.508	338.5568	0.127	492.4463	400.1126	523.2242	707.8916	861.781	861.781	892.5589
-0.254	430.8905	0.254	523.2242	430.8905	554.0021	738.6695	923.3368	923.3368	923.3368
-0.127	461.6684	0.508	554.0021	461.6684	584.78	831.0031	954.1147	954.1147	984.8926
-0.0508	430.8905	1.016	615.5579	492.4463	615.5579	892.5589	1046.448	1046.448	1108.004

117

Table B.2 Results obtained for single-phase flow pressure difference with tap#1, T_1=25 °C
Inlet mass flux (G_1) = 709.8 kg/s

Distance at inlet (mm)	$(\Delta P_{lt})_1$ Pa	Distance at branch2 (mm)	G_2=0.0 Kg/s.m^2 $(\Delta P_{lt})_2$ Pa	G_2=185.64 Kg/s.m^2 $(\Delta P_{lt})_2$ Pa	G_2=273 Kg/s.m^2 $(\Delta P_{lt})_2$ Pa	G_2=420.42 Kg/s.m^2 $(\Delta P_{lt})_2$ Pa	G_2=529.6 Kg/s.m^2 $(\Delta P_{lt})_2$ Pa	G_2=600.6 Kg/s.m^2 $(\Delta P_{lt})_2$ Pa	G_2=709.8 Kg/s.m^2 $(\Delta P_{lt})_2$ Pa
-1.016	0.0	0.0508	-246.221	-184.665	-307.776	-492.444	-615.555	-615.555	-677.111
-0.508	-153.887	0.127	-307.776	-215.443	-338.554	-523.222	-677.111	-677.111	-707.889
-0.254	-246.221	0.254	-338.554	-246.221	-369.332	-553.999	-738.667	-738.667	-738.667
-0.127	-273.998	0.508	-369.332	-276.998	-400.11	-646.333	-769.445	-769.445	-800.223
-0.0508	-246.221	1.016	-430.888	-307.776	-430.888	-707.889	-861.778	-861.778	-923.334

118

Table B.3 Results obtained for single-phase loss coefficient (k)

G_2/G_1	P_{12} (Pa)	K (Present)	K (Ballyk)	K (Buell)	K (Seeger)	G_2/G_1	K (Saba)
0.0	25	1.09885	1.081	1.0	1.0369	0.0	1.18
0.2615	35	1.070008	0.91379	0.856414	0.870172	0.2	1.17
0.3846	55	1.069553	0.884789	0.854145	0.849081	0.4	1.04
0.5923	125	1.143431	0.907998	0.915936	0.896789	0.6	1.17
0.7462	185	1.174676	0.983628	0.995531	0.999604	0.8	1.18
0.8462	245	1.252676	1.05943	1.054272	1.09719	1.0	1.38
1.0	410	1.62114	1.217	1.144	1.2946		

Table B.4.1 Results obtained for air and water mass flow rates and inlet and outlet qualities

$\dot{m}_{a1}$ Kg/s	$\dot{m}_{a2}$ Kg/s	$\dot{m}_{a3}$ Kg/s	$\dot{m}_{w1}$ Kg/s	$\dot{m}_{w2}$ Kg/s	$\dot{m}_{w3}$ Kg/s	X_1	X_2	X_3
0.000641	0.000214	0.000427	0.276666	0.102366	0.1743	0.002313	0.00208617	0.002446
			0.304333	0.1162	0.188133	0.002103	0.00183827	0.002267
			0.331999	0.130033	0.201966	0.001928	0.00164303	0.002112
			0.387332	0.160466	0.226866	0.001653	0.00133184	0.00188
			0.414999	0.177066	0.237933	0.001543	0.00120713	0.001793

Table B.4.2 Results obtained for air and water mass flow rates and inlet and outlet qualities

$\dot{m}_{a1}$ Kg/s	$\dot{m}_{a2}$ Kg/s	$\dot{m}_{a3}$ Kg/s	$\dot{m}_{w1}$ Kg/s	$\dot{m}_{w2}$ Kg/s	$\dot{m}_{w3}$ Kg/s	X_1	X_2	X_3
0.000586	0.000284	0.000302	0.276666	0.088533	0.188133	0.002114	0.00319758	0.001603
			0.304333	0.10375	0.200583	0.001922	0.00279883	0.001503
			0.331999	0.1162	0.215799	0.001762	0.0024381	0.001397
			0.359666	0.130033	0.229633	0.001627	0.0021793	0.001313
			0.387332	0.146633	0.240699	0.001511	0.00193306	0.001253
			0.414999	0.1494	0.265599	0.00141	0.00189734	0.001136

120

Table B.4.3 Results obtained for air and water mass flow rates and inlet and outlet qualities

$\dot{m}_{a1}$ Kg/s	$\dot{m}_{a2}$ Kg/s	$\dot{m}_{a3}$ Kg/s	$\dot{m}_{w1}$ Kg/s	$\dot{m}_{w2}$ Kg/s	$\dot{m}_{w3}$ Kg/s	X_1	X_2	X_3
0.000786	0.0004	0.000386	0.276666	0.096833	0.179833	0.002833	0.00411383	0.002142
0.000786	0.000467	0.000319	0.304333	0.110666	0.193666	0.002576	0.00420216	0.001644
0.000778	0.000482	0.000296	0.331999	0.1245	0.2075	0.002338	0.00385657	0.001424
0.000778	0.000482	0.000296	0.359666	0.135566	0.224099	0.002158	0.00354286	0.001319
0.000778	0.000482	0.000296	0.387332	0.152166	0.235166	0.002005	0.00315759	0.001257
0.000778	0.000482	0.000296	0.414999	0.166	0.248999	0.001871	0.00289522	0.001187

Table B.4.4 Results obtained for air and water mass flow rates and inlet and outlet qualities

$\dot{m}_{a1}$ Kg/s	$\dot{m}_{a2}$ Kg/s	$\dot{m}_{a3}$ Kg/s	$\dot{m}_{w1}$ Kg/s	$\dot{m}_{w2}$ Kg/s	$\dot{m}_{w3}$ Kg/s	X_1	X_2	X_3
0.000452	0.000134	0.000318	0.276666	0.071933	0.204733	0.001631	0.00185938	0.001551
			0.304333	0.0913	0.213033	0.001483	0.00146554	0.001491
			0.331999	0.1079	0.224099	0.00136	0.00124035	0.001417
			0.359666	0.1245	0.235166	0.001255	0.00107515	0.00135
			0.387332	0.138333	0.248999	0.001166	0.00096774	0.001275
			0.414999	0.146633	0.268366	0.001088	0.00091301	0.001184

121

Table B.4.5 Results obtained for air and water mass flow rates and inlet and outlet qualities

$\dot{m}_{a1}$ Kg/s	$\dot{m}_{a2}$ Kg/s	$\dot{m}_{a3}$ Kg/s	$\dot{m}_{w1}$ Kg/s	$\dot{m}_{w2}$ Kg/s	$\dot{m}_{w3}$ Kg/s	X_1	X_2	X_3
0.000642	0.000303	0.000339	0.276666	0.083	0.193666	0.002317	0.00363733	0.001749
			0.304333	0.1079	0.196433	0.002106	0.0028003	0.001725
			0.331999	0.1245	0.2075	0.001931	0.00242783	0.001633
			0.359666	0.1328	0.226866	0.001783	0.00227644	0.001494
			0.387332	0.1494	0.237933	0.001656	0.00202401	0.001424
			0.414999	0.166	0.248999	0.001546	0.00182198	0.001361

Table B.5.1 Results obtained for air and water mass fluxes, total mass fluxes and superficial gas and liquid velocities

G_{1a} Kg/s.m^2	G_{2a} Kg/s.m^2	G_{3a} Kg/s.m^2	G_{1w} Kg/s.m^2	G_{2w} Kg/s.m^{2v}	G_{3w} Kg/s.m^2	G_1 Kg/s.m^2	G_2 Kg/s.m^2	G_3 Kg/s.m^2	J_{G1} m/s	J_{fl} m/s
1.265819	0.422334	0.843485	546	202.02	343.98	547.2658	202.4423	344.8235	1.075448	0.548193
			600.6	229.32	371.28	601.8658	229.7423	372.1235		0.603012
			655.2	256.62	398.58	656.4658	257.0423	399.4235		0.657831
			746.4	316.68	447.72	765.6658	317.1023	448.5635		0.76747
			819	349.44	469.56	820.2658	349.8623	470.4035		0.822289

Table B.5.2 Results obtained for air and water mass fluxes, total mass fluxes and superficial gas and liquid velocities

G_{1a} Kg/s.m^2	G_{2a} Kg/s.m^2	G_{3a} Kg/s.m^2	G_{1w} Kg/s.m^2	G_{2w} Kg/s.m^{2v}	G_{3w} Kg/s.m^2	G_1 Kg/s.m^2	G_2 Kg/s.m^2	G_3 Kg/s.m^2	J_{G1} m/s	J_{fl} m/s
1.156486	0.560481	0.596005	546	174.72	371.28	547.1565	175.2805	371.876	0.982558	0.548193
			600.6	204.75	395.85	601.7565	205.3105	396.446		0.603012
			655.2	229.32	425.88	656.3565	229.8805	426.476		0.657831
			709.8	256.62	453.18	710.9565	257.1805	453.776		0.712651
			764.4	289.38	475.02	765.5565	289.9405	475.616		0.76747
			819	294.84	524.16	820.1565	295.4005	524.756		0.822289

123

Table B.5.3 Results obtained for air and water mass fluxes, total mass fluxes and superficial gas and liquid velocities

G_{1a} Kg/s.m²	G_{2a} Kg/s.m²	G_{3a} Kg/s.m²	G_{1w} Kg/s.m²	G_{2w} Kg/s.m²ᵛ	G_{3w} Kg/s.m²	G_1 Kg/s.m²	G_2 Kg/s.m²	G_3 Kg/s.m²	J_{G1} m/s	J_{l1} m/s
1.551191	0.78941	0.761781	546	191.1	354.9	547.5512	191.8894	355.6618	1.317901	0.548193
1.551191	0.921636	0.629554	600.6	218.4	382.2	602.1512	219.3216	382.8296	1.317901	0.603012
1.535402	0.951239	0.584163	655.2	245.7	409.5	656.7354	246.6512	410.0842	1.304488	0.657831
1.535402	0.951239	0.584163	709.8	267.54	442.26	711.3354	268.4912	442.8442	1.304488	0.712651
1.535402	0.951239	0.584163	764.4	300.3	464.1	765.9354	301.2512	464.6842	1.304488	0.76747
1.535402	0.951239	0.584163	819	327.6	491.4	820.5354	328.5512	491.9842	1.304488	0.822289

Table B.5.4 Results obtained for air and water mass fluxes, total mass fluxes and superficial gas and liquid velocities

G_{1a} Kg/s.m²	G_{2a} Kg/s.m²	G_{3a} Kg/s.m²	G_{1w} Kg/s.m²	G_{2w} Kg/s.m²ᵛ	G_{3w} Kg/s.m²	G_1 Kg/s.m²	G_2 Kg/s.m²	G_3 Kg/s.m²	J_{G1} m/s	J_{l1} m/s
0.892033	0.264452	0.627581	546	141.96	404.04	546.892	142.2245	404.6676	0.757877	0.548193
			600.6	180.18	420.42	601.492	180.4445	421.0476		0.603012
			655.2	212.94	442.26	656.092	213.2045	442.8876		0.657831
			709.8	245.7	464.1	710.692	245.9645	464.7276		0.712651
			764.4	273	491.4	765.292	273.2645	492.0276		0.76747
			819	289.38	529.62	819.892	289.6445	530.2476		0.822289

124

Table B.5.5 Results obtained for air and water mass fluxes, total mass fluxes and superficial gas and liquid velocities

G_{1a} Kg/s.m²	G_{2a} Kg/s.m²	G_{3a} Kg/s.m²	G_{1w} Kg/s.m²	G_{2w} Kg/s.m²ᵛ	G_{3w} Kg/s.m²	G_1 Kg/s.m²	G_2 Kg/s.m²	G_3 Kg/s.m²	J_{G1} m/s	J_{a} m/s
1.267792	0.597978	0.669814	546	163.8	382.2	547.2678	164.398	382.8698	1.077125	0.548193
			600.6	212.94	387.66	601.8678	213.538	388.3298		0.603012
			655.2	245.7	409.5	656.4678	246.298	410.1698		0.657831
			709.8	262.08	447.72	711.0678	262.678	448.3898		0.712651
			764.4	294.84	469.56	765.6678	295.438	470.2298		0.76747
			819	327.6	491.4	820.2678	328.198	492.0698		0.822289

125

Table B.6.2 Results obtained for pressure differences values at different measurement positions

Distance (m)	G2/G1=0.320348 G3/G1=0.679652 X1=0.002114		G2/G1=0.341185 G3/G1=0.658815 X1=0.001922		G2/G1=0.350237 G3/G1=0.649763 X1=0.001762		G2/G1=0.361739 G3/G1=0.638261 X1=0.001627		G2/G1=0.378732 G3/G1=0.621268 X1=0.001511		G2/G1=0.360176 G3/G1=0.639824 X1=0.00141	
	ΔP_{st} (Pa)	ΔP_{lt} (Pa)	ΔP_{st} (Pa)	ΔP_{lt} (Pa)	ΔP_{st} (Pa)	ΔP_{lt} (Pa)	ΔP_{st} (Pa)	ΔP_{lt} (Pa)	ΔP_{st} (Pa)	ΔP_{lt} (Pa)	ΔP (Pa)	ΔP_{lt} (Pa)
-1.016	430.892	0.0	430.892	0.0	430.892	0.0	430.892	0.0	430.448	0.0	492.448	0.0
-0.508	615.56	-184.668	677.116	-246.224	769.45	-338.558	800.228	-369.336	984.896	-492.448	984.896	-492.448
-0.254	707.894	-277.002	738.672	-307.78	861.784	-430.892	984.896	-554.004	1046.45	-554.004	1138.79	-646.338
-0.127	769.45	-338.558	800.228	-369.336	954.118	-523.226	1046.45	-615.56	1231.12	-738.672	1261.9	-769.45
-0.0508	677.116	-246.224	738.672	-307.78	923.34	-492.448	1015.67	-584.782	1200.34	-707.894	1200.34	-707.894
0.0508	861.784	-430.892	984.896	-554.004	1108.01	-677.116	1231.12	-800.228	1354.23	-861.784	1415.79	-923.34
0.127	861.784	-430.892	984.896	-554.004	1148.64	-717.743	1231.12	-800.228	1385.01	-892.562	1446.57	-954.118
0.0254	923.34	-492.448	1015.67	-584.782	1190.49	-759.601	1292.68	-861.784	1446.57	-954.118	1538.9	-1046.45
0.508	923.34	-492.448	1077.23	-646.338	1231.12	-800.228	1354.23	-923.34	1477.34	-984.896	1569.68	-1077.23
1.016	984.896	-554.004	1169.56	-738.672	1323.45	-892.56	1415.79	-984.896	1508.12	-1015.67	1631.23	-1138.79
0.0508	1108.00	-677.116	1108.01	-677.116	1354.23	-923.34	1477.34	-1046.45	1600.46	-1108.01	1662.01	-1169.59
0.127	1231.12	-800.228	1231.12	-800.228	1385.01	-954.118	1600.46	-1169.56	1723.57	-1231.12	1723.57	-1231.12
0.0254	1261.9	-831.006	1323.45	-892.562	1477.34	-1046.45	1723.79	-1292.68	1939.01	-1446.57	2000.57	-1508.12
0.508	1354.23	-923.34	1415.79	-984.896	1538.9	-1108.01	1969.79	-1538.9	2123.68	-1631.23	2216.02	-1723.57
1.016	1508.12	-1077.23	1569.68	-1138.79	1631.23	-1200.34	2339.13	-1908.24	2462.24	-1969.79	2585.35	-2092.9

127

Table B.6.4 Results obtained for pressure differences values at different measurement positions

Distance (m)	$G_2/G_1=0.260059$ $G_3/G_1=0.7399405$ $X_1=0.001631$		$G_2/G_1=0.0.299995$ $G_3/G_1=0.70000525$ $X_1=0.001483$		$G_2/G_1=0.324961$ $G_3/G_1=0.6750388$ $X_1=0.00136$		$G_2/G_1=0.346091$ $G_3/G_1=0.6539085$ $X_1=0.001255$		$G_2/G_1=0.357072$ $G_3/G_1=0.6429278$ 7 $X_1=0.001166$		$G_2/G_1=0.353271$ $G_3/G_1=0.6467285$ 4 $X_1=0.001088$	
	ΔP_{st} (Pa)	ΔP_{lt} (Pa)	ΔP_{st} (Pa)	ΔP_{lt} (Pa)	ΔP_{st} (Pa)	ΔP_{lt} (Pa)	ΔP_{st} (Pa)	ΔP_{lt} (Pa)	ΔP_{st} (Pa)	ΔP_{lt} (Pa)	ΔP_{st} (Pa)	ΔP_{lt} (Pa)
-1.016	430.892	0.0	430.892	0.0	430.892	0.0	492.448	0.0	554.004	0.0	554.004	0.0
-0.508	615.558	-184.666	615.558	-184.666	779.299	-348.41	800.228	-307.78	861.784	-307.78	902.411	-348.407
-0.254	738.67	-307.778	738.67	-307.778	800.228	-369.336	861.784	-369.336	944.269	-390.265	984.896	-430.892
-0.127	779.296	-348.405	800.225	-369.335	923.34	-492.448	944.269	-451.821	1025.52	-471.519	1108.01	-554.004
-0.0508	738.67	-307.778	779.296	-348.406	892.562	-461.67	923.34	-430.892	984.896	-430.892	1067.38	-513.377
0.0508	861.78	-430.888	861.78	-430.891	1015.67	-584.782	1108.01	-615.56	1138.8	-584.782	1169.56	-615.56
0.127	892.559	-461.667	892.559	-461.668	1046.45	-615.56	1148.64	-656.187	1169.56	-615.56	1231.12	-677.116
0.0254	902.408	-471.517	923.337	-492.446	1108.01	-677.116	1169.56	-677.116	1200.34	-646.338	1323.45	-769.45
0.508	923.337	-492.446	984.893	-554.002	1138.34	-707.894	1200.34	-707.894	1261.9	-707.894	1354.23	-800.228
1.016	954.115	-523.224	1046.45	-615.558	1200.34	-769.45	1292.68	-800.228	1292.68	-738.672	1446.57	-892.562
0.0508	1046.45	-615.558	1138.78	-707.892	1231.12	-800.228	1231.12	-738.672	1292.68	-738.672	1354.23	-800.228
0.127	1108.00	-677.114	1169.56	-738.669	1231.12	-800.228	1292.68	-800.228	1354.23	-800.228	1415.79	-861.784
0.0254	1190.49	-759.598	1200.34	-769.447	1354.23	-923.34	1354.23	-861.784	1385.01	-831.006	1538.9	-984.896
0.508	1231.12	-800.225	1261.89	-831.003	1415.79	-984.896	1415.79	-923.34	1477.34	-923.34	1569.68	-1015.67
1.016	1292.67	-861.781	1354.23	-923.337	1477.34	-1046.45	1477.34	-984.896	1508.12	-954.118	1662.01	-1108.01

129

Table B.6.5 Results obtained for pressure differences values at different measurement positions

Distance (m)	G2/G1=0.300398 G3/G1=0.6996023 X1=0.002317		G2/G1=0.354792 G3/G1=0.64520783 X1=0.002106		G2/G1=0.375187 G3/G1=0.6248133 X1=0.001931		G2/G1=0.369413 G3/G1=0.6305866 X1=0.001783		G2/G1=0.385857 G3/G1=0.6141434 X1=0.001656		G2/G1=0.400111 G3/G1=0.5998892 3 X1=0.001546	
	ΔP_{st} (Pa)	ΔP_{lt} (Pa)	ΔP_{st} (Pa)	ΔP_{lt} (Pa)	ΔP_{st} (Pa)	ΔP_{lt} (Pa)	ΔP_{st} (Pa)	ΔP_{lt} (Pa)	ΔP_{st} (Pa)	ΔP_{lt} (Pa)	ΔP_{st} (Pa)	ΔP_{lt} (Pa)
-1.016	430.892	0.0	430.892	0.0	492.448	0.0	492.448	0.0	554.004	0.0	554.004	0.0
-0.508	677.114	-246.223	738.67	-307.779	831.006	-338.558	861.784	-369.336	954.118	-400.114	984.896	-430.892
-0.254	738.67	-307.779	861.78	-430.891	923.34	-430.892	954.118	-461.67	1046.45	-492.448	1108.01	-554.004
-0.127	800.225	-369.335	954.115	-523.224	1015.57	-523.226	1108.01	-615.56	1169.56	-615.56	1231.12	-677.116
-0.0508	738.67	-307.779	861.78	-430.891	984.896	-492.448	1046.45	-554.004	1108.01	-554.004	1169.56	-615.56
0.0508	892.559	-461.668	1046.45	-615.558	1169.56	-677.116	1231.12	-738.672	1292.68	-738.672	1415.79	-861.784
0.127	923.337	-492.446	1108.00	-677.114	1200.34	-707.894	1261.9	-769.45	1354.23	-800.228	1477.34	-923.34
0.0254	984.893	-554.002	1138.78	-707.892	1261.9	-769.45	1292.68	-800.228	1415.79	-861.784	1477.34	-923.34
0.508	1046.45	-615.558	1200.34	-769.447	1292.68	-800.228	1354.23	-861.784	1446.57	-892.562	1538.9	-984.896
1.016	1108.00	-677.114	1231.12	-800.225	1385.01	-892.562	1415.79	-923.34	1508.12	-954.118	1600.46	-1046.45
0.0508	923.337	-492.446	1108.00	-677.114	1354.23	-861.784	1415.79	-923.34	1538.9	-984.896	1846.68	-1292.68
0.127	1046.45	-615.558	1231.12	-800.225	1415.79	-923.34	1477.34	-984.896	1662.01	-1108.01	1908.24	-1354.23
0.0254	1292.67	-861.781	1446.56	-1015.67	1538.9	-1046.45	1600.46	-1108.01	1846.68	-1292.68	1969.79	-1415.79
0.508	1354.23	-923.337	1508.12	-1077.23	1569.69	-1077.23	1723.57	-1231.12	1969.79	-1415.79	2092.90	-1538.9
1.016	1415.78	-984.893	1569.67	-1138.78	1662.01	-1169.56	1846.68	-1354.23	2154.46	-1600.46	2431.46	-1877.46

130

Table B.7 Results obtained for pressure difference values at different inlet mass fluxes, inlet qualities and extraction rates

G_1 (kg/s.m²)	G_2/G_1	G_3/G_1	X_1	Measured values				
				P_1 (bar)	P_2 (bar)	P_3 (bar)	ΔP_{12} (bar)	ΔP_{13} (bar)
547.2658	0.369916	0.630084	0.002313	488	583	878	95	390
601.8658	0.381717	0.618283	0.002103	460	600	850	140	390
656.4658	0.391555	0.608445	0.001928	660	780	1035	120	375
765.6658	0.414152	0.585848	0.001653	805	925	1255	120	450
820.2658	0.426523	0.573477	0.001543	1020	1135	1460	115	440
547.1565	0.320348	0.679652	0.002114	370	455	755	85	420
601.7565	0.341185	0.658815	0.001922	435	535	825	100	425
656.3565	0.350237	0.649763	0.001762	615	720	1010	105	425
710.9565	0.361739	0.638261	0.001627	740	850	1120	110	400
765.5565	0.378732	0.621268	0.001511	835	935	1275	100	520
820.1565	0.360176	0.639824	0.00141	900	1010	1330	110	520
547.5512	0.35045	0.64955	0.002833	440	565	860	125	385
602.1512	0.36423	0.63577	0.002576	565	705	990	140	390
656.7354	0.375572	0.624428	0.002338	560	715	985	155	395
711.3354	0.377447	0.622553	0.002158	625	765	1025	140	380
765.9354	0.393312	0.606689	0.002005	880	1020	1400	140	440
820.5354	0.400411	0.59959	0.001871	880	1080	1400	200	430

131

Table B.7 Results obtained for pressure difference values at different inlet mass fluxes, inlet qualities and extraction rates

G_1 (kg/s.m²)	G_2/G_1	G_3/G_1	X_1	Measured values					
				P_1 (bar)	P_2 (bar)	P_3 (bar)	ΔP_{12} (bar)	ΔP_{13} (bar)
546.892	0.260056	0.739941	0.001631	390	460	725	70	335
601.492	0.299995	0.700005	0.001483	395	480	735	85	340
656.092	0.324961	0.675039	0.00136	565	645	890	80	325
710.692	0.346091	0.653909	0.001255	540	630	838	90	298
765.292	0.357072	0.642928	0.001166	550	640	838	90	288
819.892	0.353271	0.6467285	0.001088	620	720	935	100	315
547.2678	0.300398	0.699602	0.002317	440	426	835	86	395
601.8678	0.354792	0.645208	0.002106	590	710	990	120	400
656.4678	0.375187	0.624813	0.001931	610	725	1000	115	390
711.0678	0.369413	0.630587	0.001783	660	780	1055	120	395
765.6678	0.385857	0.614143	0.001656	710	835	1200	125	490
820.2678	0.400111	0.599889	0.001546	780	895	1230	115	450

132

Table B.8 Results obtained for homogeneous densities, velocity ratios and void fractions

ρ_{H1} (kg/m³)	ρ_{H2} (kg/m³)	ρ_{H3} (kg/m³)	S_1	S_2	S_3	α_1	α_2	α_3
337.0609	360.4426	324.6952	1.705633	2.280345	1.925303	0.534926	0.436867	0.518713
358.5822	390.0159	341.5854	1.652439	2.142255	1.866131	0.519067	0.421122	0.507432
378.7421	416.9594	357.6466	1.608103	2.033537	1.81506	0.504122	0.406473	0.496632
415.4639	468.5527	384.654	1.53842	1.860322	1.738817	0.476676	0.37758	0.478309
432.2337	492.999	395.9373	1.510543	1.790932	1.71005	0.464045	0.363487	0.470592
357.4433	268.996	422.9996	1.685413	2.541315	1.798787	0.515376	0.516479	0.430255
379.5207	301.1475	438.6391	1.63405	2.332985	1.75667	0.49929	0.498217	0.420384
400.1225	325.4119	456.6322	1.591241	2.203095	1.711792	0.48418	0.484211	0.408918
419.3918	350.459	472.0101	1.555014	2.087929	1.676153	0.469957	0.469547	0.399024
437.454	378.1518	483.6952	1.523959	1.978401	1.65059	0.456547	0.453083	0.391448
454.4189	382.5379	508.1721	1.497043	1.962511	1.600861	0.443881	0.45045	0.375409
293.421	222.4662	354.4075	1.758372	2.540218	1.877298	0.577564	0.579141	0.491751
313.4713	218.8172	416.7494	1.700405	2.423806	1.788275	0.562421	0.595679	0.438027
334.6731	233.8224	451.9065	1.649657	2.291243	1.732531	0.545883	0.588452	0.410638
352.6458	249.3434	470.9379	1.608953	2.195744	1.687172	0.532203	0.578102	0.39849
369.6675	271.4746	482.9027	1.574059	2.078514	1.66049	0.519193	0.563245	0.390783
385.8117	288.9393	497.1132	1.543814	1.998715	1.630471	0.506804	0.551437	0.381559

Table B.8 Results obtained for homogeneous densities, velocity ratios and void fractions

ρ_{H1} (kg/m³)	ρ_{H2} (kg/m³)	ρ_{H3} (kg/m³)	S_1	S_2	S_3	α_1	α_2	α_3
418.731	387.3104	431.0204	1.636472	2.658738	1.751672	0.457938	0.372215	0.428689
441.9846	444.9003	440.7467	1.589543	2.332398	1.727071	0.441553	0.347469	0.422432
463.4372	486.2402	453.2057	1.550431	2.145904	1.697102	0.426301	0.328738	0.414368
483.2904	521.8108	465.118	1.517334	2.009134	1.669954	0.412068	0.311923	0.406606
501.7167	547.8692	479.2926	1.488964	1.920232	1.63941	0.398754	0.299172	0.397304
518.8644	562.1735	497.9113	1.464375	1.874941	1.601938	0.386275	0.292009	0.384974
336.7144	244.4566	401.8308	1.705998	2.65905	1.798922	0.53526	0.537417	0.451869
358.2255	295.824	405.2297	1.652771	2.304123	1.789364	0.519406	0.507713	0.449677
378.3772	326.338	418.4453	1.608407	2.146332	1.75368	0.504464	0.489675	0.441114
397.2945	340.6189	440.2035	1.570865	2.082221	1.699607	0.49036	0.481129	0.426889
415.0873	367.4281	451.9162	1.538681	1.97536	1.672658	0.477023	0.464903	0.419166
431.8531	392.1302	463.1454	1.510787	1.889861	1.648104	0.464393	0.449737	0.411717

134

Table B.9 Results obtained for momentum densities, energy weighted densities, and two-phase flow loss multiplier (ϕ)

ρ_{M1} (kg/m³)	ρ_{M2} (kg/m³)	ρ_{M3} (kg/m³)	ρ_B (kg/m³)	ρ_{E2} (kg/m³)	ρ_{E3} (kg/m³)	$(\phi)_{Sfm}$	$(\phi_{Rsm})_2$	$(\phi_{Rsm})_3$
463.5315	560.5554	479.4525	463.2663	559.6064	478.9547	2.148721	3.159939	2.846547
479.3613	576.4141	490.7492	479.1479	575.7282	490.3351	2.077765	3.021094	2.645948
494.2688	591.122	501.5527	494.0935	590.6065	501.2032	2.015098	2.895115	2.483283
521.6291	620.0468	519.8614	521.5046	619.7425	519.5961	1.909403	2.703655	2.21954
534.2151	634.1275	527.5655	534.1081	633.8889	527.3282	1.864417	2.628259	2.110807
483.0085	480.7623	567.65	482.7701	478.97	567.3612	2.062076	2.096963	3.297501
499.059	499.3269	577.5096	498.8671	498.1323	577.2621	1.995756	2.082417	3.033163
514.1283	513.4748	588.9555	513.9707	512.5786	588.7478	1.937259	2.024449	2.840795
528.3057	528.2327	598.8271	528.1739	527.5574	598.6479	1.885272	1.984525	2.672826
541.6692	544.7544	606.3842	541.5573	544.254	606.2239	1.838761	1.968161	2.517482
554.2877	547.3923	622.3749	554.1915	546.9145	622.2477	1.796901	1.845105	2.45108
421.0369	418.2565	506.3514	420.6968	416.2638	505.9371	2.365588	2.5736	4.099963
436.1674	401.9976	559.921	435.8937	400.3233	559.6364	2.283527	2.217918	4.224146
452.6727	409.4496	587.2292	452.4507	408.1574	587.0057	2.200265	2.079237	4.018522
466.3205	419.9257	599.3519	466.1349	418.8787	599.1659	2.13587	1.997007	3.771773
479.2942	434.9052	607.0396	479.1366	434.1166	606.8737	2.078056	1.978636	3.519625
491.6436	446.7742	616.2381	491.5082	446.1361	616.0931	2.025858	1.933371	3.326318

135

Table B.9 Results obtained for momentum densities, energy weighted densities, and two-phase flow loss multiplier (ϕ)

ρ_{M1} (kg/m³)	ρ_{M2} (kg/m³)	ρ_{M3} (kg/m³)	ρ_{E1} (kg/m³)	ρ_{E2} (kg/m³)	ρ_{E3} (kg/m³)	$(\phi)_{Sfm}$	$(\phi_{Rsm})_2$	$(\phi_{Rsm})_3$
540.2153	624.5123	569.2458	540.0375	622.9336	568.9975	1.843709	2.200129	2.448425
556.5526	649.6059	575.4927	556.4097	648.767	575.2669	1.789588	2.268338	2.247161
571.7543	668.4573	583.5407	571.6369	667.9159	583.3405	1.742007	2.254906	2.101711
585.936	685.3186	591.2843	585.8379	684.9449	591.1058	1.699844	2.225133	1.983381
599.1979	698.0796	600.5622	599.1146	697.7945	600.4061	1.662222	2.1678	1.896457
611.6271	705.2399	612.8556	611.5555	704.9942	612.7246	1.628443	2.079802	1.842059
463.1984	459.6406	546.1315	462.9327	457.3921	545.8283	2.150266	2.147522	3.530036
479.0239	489.9057	548.3227	478.8101	488.7549	548.0296	2.079228	2.296042	3.145195
493.9281	508.1068	556.8755	493.7524	507.3047	556.6185	2.016488	2.270267	2.91104
507.9914	516.7018	571.0752	507.8444	516.0193	570.8673	1.960663	2.14933	2.777716
521.2843	532.9851	578.7815	521.1595	532.4758	578.5957	1.910666	2.123992	2.612392
533.8693	548.1732	586.2116	533.762	547.7802	586.0446	1.865625	2.094197	2.473458

136

Table B.10 Results obtained for single-phase flow loss coefficient, Separated flow model and Reimann and Seeger model pressure difference values

K_{12}	K_{13}	$(\Delta P_{12})_{Sfm}$ (Pa)	$(\Delta P_{13})_{Sfm}$ (Pa)	$(\Delta P_{12})_{Rsm}$ (Pa)	$(\Delta P_{13})_{Rsm}$ (Pa)
1.032545	1.139553	105.6608	225.7379	72.31312	242.8258
1.034234	1.131534	114.1369	256.4242	86.47338	265.9848
1.035872	1.125079	123.0527	288.3739	101.6965	290.2363
1.040425	1.111043	140.987	353.0966	139.4678	334.0798
1.043384	1.103826	150.7645	385.7355	162.656	353.462
1.028738	1.176519	164.0643	183.8038	66.16411	250.9461
1.029692	1.160333	180.0554	205.2876	81.22607	267.5594
1.030399	1.153593	199.0846	230.7787	94.50628	293.5189
1.031552	1.145285	217.6174	255.8637	110.2528	316.6579
1.033778	1.133534	235.0905	278.806	130.7129	332.7418
1.031378	1.146398	262.7069	319.8243	133.6063	392.1107
1.030417	1.153437	202.0796	198.0584	94.53968	273.1428
1.031839	1.143523	252.9373	175.1701	122.7673	286.188
1.033317	1.135672	288.6434	175.2486	145.091	304.1111
1.033588	1.1344	321.6566	195.7392	161.5931	336.9806
1.036186	1.123948	352.6433	212.4056	188.2333	352.0549
1.037524	1.119446	386.134	232.2905	211.3177	377.7437

137

Table B.10 Results obtained for single-phase flow loss coefficient, Separated flow model and Reimann and Seeger model pressure difference values

K_{12}	K_{13}	$(\Delta P_{12})_{Sfm}$ (Pa)	$(\Delta P_{13})_{Sfm}$ (Pa)	$(\Delta P_{12})_{Rsm}$ (Pa)	$(\Delta P_{13})_{Rsm}$ (Pa)
1.031259	1.228634	96.97126	228.1061	36.43924	274.0137
1.028711	1.193235	91.61258	248.361	48.42115	279.9808
1.028868	1.172855	91.8093	273.6164	60.80902	294.9068
1.030053	1.156658	93.63858	300.025	74.9255	310.9517
1.031049	1.148622	98.92481	331.2593	87.93858	335.4192
1.030675	1.151374	108.6181	371.6966	96.14501	376.4396
1.028703	1.192896	177.5487	203.7295	64.54689	284.7811
1.030821	1.150269	184.2839	216.5136	89.93911	272.0142
1.033262	1.135934	200.7856	239.3168	109.2814	286.6367
1.03248	1.139901	224.0727	271.5725	119.0054	327.0013
1.034898	1.128792	241.954	296.2594	140.5906	343.6617
1.037466	1.119635	261.1067	321.9073	163.8462	361.3504

Table B.11 Results of measured pressure difference values at constant inlet mass flux and different inlet qualities

$G_1=547$ (kg/s.m²)			$G_1=602$ (kg/s.m²)			$G_1=656$ (kg/s.m²)			$G_1=711$ (kg/s.m²)			$G_1=765$ (kg/s.m²)			$G_1=820$ (kg/s.m²)		
X_1	ΔP_{12} bar	ΔP_{13} bar	X_1	ΔP_{12} bar	ΔP_{13} bar	X_1	ΔP_{12} bar	ΔP_{13} bar	X_1	ΔP_{12} bar	ΔP_{13} bar	X_1	ΔP_{12} bar	ΔP_{13} bar	$X_1 \times 10^3$	ΔP_{12} bar	ΔP_{13} bar
0.002313	95	390	0.002576	140	425	0.001928	120	375	0.002158	140	400	0.001653	120	450	1.543	115	440
0.002833	125	420	0.00192	100	390	0.002338	155	425	0.001627	110	380	0.002005	140	420	1.871	200	520
0.002114	85	385	0.001483	85	340	0.001762	105	395	0.001255	90	298	0.001511	100	400	1.41	110	430
0.001631	70	335	0.002106	120	400	0.001931	115	390	0.001783	120	395	0.001166	90	288	1.088	100	315
0.002317	86	395				0.00136	80	325				0.001656	125	490	1.546	115	450

Table B.12 Results of measured pressure difference values at constant inlet qualities and different inlet mass fluxes and extraction rates

$X_1 = 0.0024$

G_1 Kg/s.m²	G_2/G_1 Kg/s.m²	G_3/G_1 Kg/s.m²	ΔP_{12} bar	ΔP_{13} bar
601	0.36423	0.63577	140	425
656	0.375563	0.624437	155	425
547	0.300398	0.699602	86	395

$X_1 = 0.0021$

G_1 Kg/s.m²	G_2/G_1 Kg/s.m²	G_3/G_1 Kg/s.m²	ΔP_{12} bar	ΔP_{13} bar
601	0.381719	0.618281	140	425
710	0.377438	0.622562	140	425
547	0.320348	0.679652	85	395
601	0.354792	0.645208	120	400

$X_1 = 0.0018$

G_1 Kg/s.m²	G_2/G_1 Kg/s.m²	G_3/G_1 Kg/s.m²	ΔP_{12} bar	ΔP_{13} bar
656	0.391555	0.608445	120	375
601	0.341185	0.658815	100	390
656	0.350237	0.649763	105	395
656	0.375187	0.624813	115	390
710	0.369413	0.630587	120	390
820	0.400411		200	395

139

Table B.13 Results of the standard deviation of logarithmic ratios between measured and predicted pressure difference values

$X_{12,i} = Ln(\frac{\Delta P_{12,i,meas}}{\Delta P_{12,i,pred}})_{Sfm}$	$X_{13,i} = ln(\frac{\Delta P_{13,i,meas}}{\Delta P_{13,i,pred}})_{Sfm}$	$X_{12,i} = Ln(\frac{\Delta P_{12,i,meas}}{\Delta P_{12,i,pred}})_{Rsm}$	$X_{13,i} = ln(\frac{\Delta P_{13,i,meas}}{\Delta P_{13,i,pred}})_{Rsm}$	$(X_{ln,12,i})^2_{Sfm}$	$(X_{ln,13,i})^2_{Sfm}$	$(X_{ln,12,i})^2_{Rsm}$	$(X_{ln,13,i})^2_{Rsm}$
-0.10636	0.546772	0.272871	0.473803	0.011312	0.29896	0.074459	0.224489
0.204244	0.419314	0.481806	0.382707	0.041715	0.175824	0.232137	0.146465
-0.02512	0.262668	0.165499	0.256231	0.000631	0.068995	0.02739	0.065654
-0.16118	0.242506	-0.15034	0.297868	0.025978	0.058809	0.022603	0.088725
-0.27079	0.131623	-0.34671	0.218999	0.073326	0.017325	0.120204	0.04796
-0.48035	0.751693	0.279294	0.43026	0.230734	0.565042	0.078005	0.185124
-0.5915	0.886332	0.131352	0.39544	0.349871	0.785584	0.017253	0.156373
-0.62177	0.885884	0.066064	0.334696	0.386594	0.78479	0.004364	0.112021
-0.83184	0.714682	-0.14344	0.171439	0.691962	0.51077	0.020575	0.029391
-0.92381	0.895331	-0.29604	0.390042	0.853433	0.801618	0.087639	0.152132
-0.65787	0.80584	-0.05505	0.319613	0.432789	0.649378	0.00303	0.102152
-0.65761	0.739375	0.250513	0.428005	0.432447	0.546675	0.062757	0.183188
-0.58809	0.641735	0.207934	0.376805	0.345855	0.411824	0.043237	0.141982
-0.63977	0.537427	0.105294	0.296944	0.409305	0.288827	0.011087	0.088176
-0.68226	0.395526	-0.0023	0.182349	0.465476	0.156441	5.27E-06	0.033251
-0.8548	0.456259	-0.26783	0.279408	0.730684	0.208172	0.071735	0.078069
-0.87056	0.296013	-0.19442	0.092241	0.757872	0.087624	0.037798	0.008508
-0.32592	0.38432	0.652849	0.200952	0.106223	0.147702	0.426212	0.040382
-0.07492	0.314062	0.562714	0.194225	0.005613	0.098635	0.316648	0.037723
-0.13769	0.172098	0.274289	0.097166	0.018958	0.029618	0.075234	0.009441
-0.03963	-0.00677	0.183315	-0.04254	0.001571	4.59E-05	0.033605	0.00181

140

Table B.13 Results of the standard deviation of logarithmic ratios between measured and predicted pressure difference values

-0.09455	-0.13994	0.023171	-0.15242	0.00894	0.019583	0.000537	0.023232
-0.08267	-0.16551	0.039313	-0.17818	0.006834	0.027392	0.001545	0.03175
-0.7249	0.662093	0.286955	0.327165	0.525477	0.438367	0.082343	0.107037
-0.42899	0.613811	0.288359	0.38561	0.184029	0.376764	0.083151	0.148695
-0.55731	0.488359	0.051006	0.307931	0.31059	0.238494	0.002602	0.094822
-0.62448	0.374657	0.008323	0.188922	0.389974	0.140368	6.93E-05	0.035691
-0.66043	0.50317	-0.11754	0.354748	0.436173	0.25318	0.013815	0.125846
-0.82	0.334984	-0.354	0.2194	0.672395	0.112214	0.125313	0.04136
			$\sum_{i=1}^{n} X^2_{\ln,i} =$	8.90676	8.299019	2.075352	2.548227
			$S_{\ln,i} =$	79.55 %	75.95 %	32.65 %	36.76 %

141

ملخص
" فقدان الضغط الناتج عن جريان ثاني الطور في وصلة ثنائية التفرع (T)"

إعداد
علاء الدين توفيق سليم الحلحولي

المشرف
أ.د. محمود حماد

المشرف المشارك
أ.د. محمود الحسين

خلال هذه الدراسة تم تصميم وبناء جهاز لإجراء تجارب في مجال جريان ثاني الطور خلال
وصلة ثنائية التفرغ (T) . بني هذا الجهاز باستخدام أنابيب مصنوعة من مادة (PVC) بأقطار
داخلية متساوية (٢٥,٤مم) موصلة باتجاه أفقي .

يتضمن جهاز التجربة : مضخة ماء طاردة عن المركز ، ضاغطة هواء، أنابيب، فاصل للماء
عن الهواء ،خلاط ، صمامات ، وصلة ثنائية التفرغ (T) وساعة ضغط.

تم إجراء التجارب على جريان الماء و جريان ثاني الطور في مختبرات الهندسة الميكانيكية في
جامعة مؤتة، من خلال تغيير معدل تدفق الماء و الهواء خلال المدخل و استخدام ضغط نظام
ثابت ابار . وتم قياس معدل جريان الماء و الهواء ، بالإضافة إلى فروق الضغط على طول
المدخل و التفرعات باستخدام أدوات القياس: ساعة ضغط، أدوات لقياس معدل التدفق
.(Rotometers, Pitot tube, Orifice)

تم الحصول على معامل فقدان الطاقة (K) في جريان الماء(single-phase)بالإضافة إلى
فقدان الضغط الناتج عن جريان الماء و جريان ثاني الطور(ماء+هواء) .

أظهرت النتائج أن فقدان الضغط الناتج عن جريان ثاني الطور يعتمد على تدفق ثاني الطور من
المدخل بالإضافة إلى الكمية الموزعة على التفرعات . و من الواضح أن فرق الضغط يزداد
بزيادة أي من هذه العوامل كما أن مقارنة النتائج هذه الرسالة مع دراسات سابقة أظهرت التوافق.